

การสังเคราะห์อิทธิพลเตรียมอะลูมิเนียมคาร์ไบด์ที่มีผลึกขนาดนาโน

โดยวิธีตกตะกอน

นางสาวพรพรรณ หว่านณรงค์

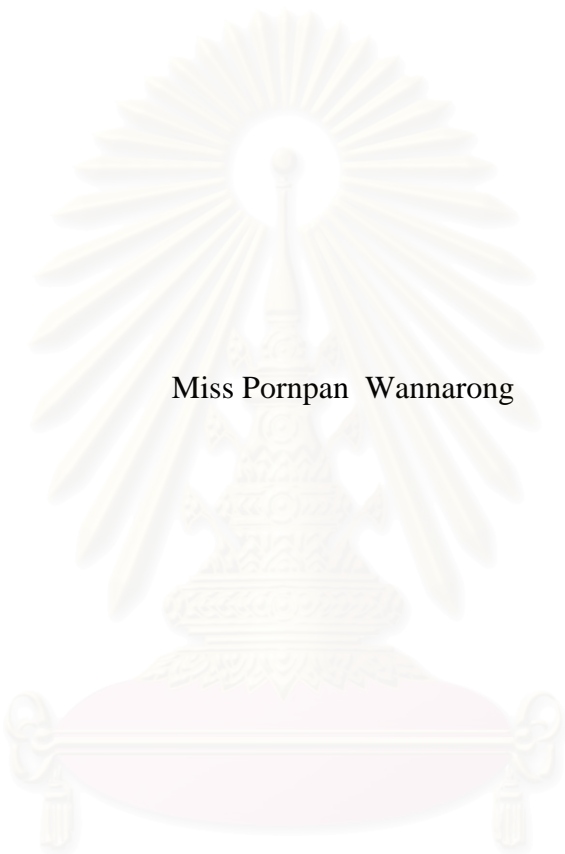
สถาบันวิทยบริการ
วิทยานิพนธ์นี้เป็นส่วนหนึ่งของการศึกษาตามหลักสูตรปริญญาวิศวกรรมศาสตรมหาบัณฑิต
จุฬาลงกรณ์มหาวิทยาลัย
สาขาวิชาวิศวกรรมเคมี ภาควิชาวิศวกรรมเคมี

คณะวิศวกรรมศาสตร์ จุฬาลงกรณ์มหาวิทยาลัย

ปีการศึกษา 2550

ลิขสิทธิ์ของจุฬาลงกรณ์มหาวิทยาลัย

SYNTHESIS OF NANOCRYSTALLITE YTTRIUM ALUMINIUM GARNET BY
PRECIPITATION METHOD



Miss Pornpan Wannarong

สถาบันวิทยบริการ

จุฬาลงกรณ์มหาวิทยาลัย

A Thesis Submitted in Partial Fulfillment of the Requirements
for the Degree of Master of Engineering Program in Chemical Engineering

Department of Chemical Engineering

Faculty of Engineering


Chulalongkorn University

Academic Year 2007


Copyright of Chulalongkorn University


Thesis Title SYNTHESIS OF NANOCRYSTALLITE YTTRIUM
ALUMINIUM GARNET BY PRECIPITATION METHOD
By Miss Pornpan Wannarong
Field of Study Chemical Engineering
Thesis Advisor Assistant Professor Varong Pavarajarn, Ph.D.
Thesis Co-advisor Thanakorn Wasanapiarnpong, Ph.D.

Accepted by the Faculty of Engineering, Chulalongkorn University in Partial
Fulfillment of the Requirements for the Master's Degree


..... Dean of the Faculty of Engineering
(Associate Professor Boonsom Lerdhirunwong, Dr.Ing.)


THESIS COMMITTEE


..... Chairman
(Associate Professor Tawatchai Charinpanitkul, D.Eng.)


..... Thesis Advisor
(Assistant Professor Varong Pavarajarn, Ph.D.)


..... Thesis Co-advisor
(Thanakorn Wasanapiarnpong, Ph.D.)


..... External Member
(Assistant Professor Okorn Mekasuwandumrong, Ph.D.)


..... Member
(Akawat Sirisuk, Ph.D.)

พรพรรณ หว่านฉรงค์ : การสังเคราะห์อิทธิเทียมอะลูมิเนียมการ์เนตที่มีผลึกขนาดนาโน
โดยวิธีตกตะกอน (SYNTHESIS OF NANOCRYSTALLITE YTTRIUM
ALUMINIUM GARNET BY PRECIPITATION METHOD) อ.ที่ปรึกษา : ผศ.ดร.
วงศ์ ปวราจารย์, อ.ที่ปรึกษาร่วม : ดร. ชนากร วาสนาเพชรพงศ์ , 101 หน้า.

ผงอิทธิเทียมอะลูมิเนียมการ์เนตที่มีขนาดผลึกในระดับนาโนเมตรสามารถสังเคราะห์ได้
จากวิธีตกตะกอนร่วมของสารละลายผสมระหว่างอิทธิเทียมไนเตรดกับแอมโมเนียมอะลูมิเนียม
ซัลเฟตโดยใช้แอมโมเนียมไฮโดรเจนคาร์บอเนตเป็นสารตกตะกอน โดยได้ทำการศึกษาปัจจัย
ของอัตราส่วนระหว่างอิทธิเทียมกับอะลูมิเนียม อุณหภูมิระหว่างการทำปฏิกิริยา ค่าความเป็นกรด
ต่างของระบบ ชนิดของกระบวนการตกตะกอน และของระยะเวลาการเผาที่ใช้ ต่อการเกิด
โครงสร้าง และรูปร่างของอิทธิเทียมอะลูมิเนียมการ์เนต พบว่าการเผาตะกอนที่เกิดขึ้นที่อุณหภูมิ
1200 องศาเซลเซียสเป็นเวลา 2 ชั่วโมง ทำให้ได้ผงอิทธิเทียมอะลูมิเนียมการ์เนตทั้งหมด โดยที่เมื่อ
เพิ่มอุณหภูมิการเผาจะทำให้ได้อนุภาคอันดับสองที่เกิดขึ้นจากการผนึกตัวรวมกันของอนุภาคลำดับ
ที่หนึ่ง ซึ่งสามารถทำลายการเกาะกันนี้ได้บางส่วนด้วยการบด กระบวนการตกตะกอนแบบ
ย้อนกลับ ที่กระทำที่อุณหภูมิของการเกิดปฏิกิริยาก่อนข้างต่ำ และอัตราส่วนของอิทธิเทียมต่อ
อะลูมิเนียมที่อัตราส่วนในสูตรโมเลกุลเท่ากับ 3 ต่อ 5 เป็นสภาวะที่เหมาะสมต่อการเกิดอิทธิเทียม
อะลูมิเนียมการ์เนต เมื่อทำการควบคุมค่าความเป็นกรดต่างในระหว่างกระบวนการตกตะกอน
พบว่าเกิดอิทธิเทียมอะลูมิเนียมการ์เนตบริสุทธิ์ที่ปราศจากสารอื่นปะปนจากการเปลี่ยนรูปโดยตรง
ของสารอัญฐานหลังจากเผาที่อุณหภูมิ 900 องศาเซลเซียส หรือมากกว่านั้น นอกจากนี้ได้
ทำการศึกษาปัจจัยต่างๆ ที่มีผลต่อขนาดและการกระจายขนาดของอนุภาคในวิธีตกตะกอน อัน
ได้แก่ ความเร็วในการผสม อัตราการเติม และ ความเข้มข้นของสารตั้งต้น นอกจากนี้ยังได้
ทำการศึกษาเปรียบเทียบความหนาแน่นของชิ้นงานจากอิทธิเทียมอะลูมิเนียมการ์เนตที่สังเคราะห์
ได้ กับอิทธิเทียมอะลูมิเนียมการ์เนตในทางการค้า ชิ้นงานที่ขึ้นรูปได้ถูกเผาผนึกในอากาศที่อุณหภูมิ
1650 องศาเซลเซียส เป็นเวลา 5 ชั่วโมง พบว่าค่าความหนาแน่นของอิทธิเทียมอะลูมิเนียมการ์เนตที่
สังเคราะห์ได้อยู่ในช่วงร้อยละ 91-92 ของความหนาแน่นทางทฤษฎีของอิทธิเทียมอะลูมิเนียมการ์-
เนต

ภาควิชา..... วิศวกรรมเคมี
สาขาวิชา..... วิศวกรรมเคมี
ปีการศึกษา..... 2550

ลายมือชื่อนิสิต จวรสส.ศบ. ๑๖๖๖๖๖๖๖๖๖๖๖
ลายมือชื่ออาจารย์ที่ปรึกษา.....
ลายมือชื่ออาจารย์ที่ปรึกษาร่วม.....

4970455321 : MAJOR CHEMICAL ENGINEERING

KEY WORDS : YTTRIUM ALUMINIUM GARNET, YAG, PRECIPITATION,
NANOPARTICLES

PORNPAN WANNARONG: SYNTHESIS OF NANOCRYSTALLITE
YTTRIUM ALUMINIUM GARNET BY PRECIPITATION METHOD.
THESIS ADVISOR: ASSISTANT PROFESSOR VARONG PAVARAJARN,
Ph.D., THESIS CO-ADVISOR: THANAKORN WASANAPIARNPONG,
Ph.D., 101 pp.

Yttrium aluminium garnet powder with nanocrystallite can be successfully synthesized by co-precipitation method from a mixed solution of yttrium nitrate and ammonium aluminium sulfate using ammonium hydrogen carbonate as a precipitant. Effects of yttrium-to-aluminium ratio, reaction temperature, pH of the reaction, precipitation processes and variation of calcination time on phase formation, structure and morphology of YAG powder were investigated. Generally, it was found that precipitates which were calcined for 2 h at 1200°C would completely become YAG. With the increasing calcination temperature, the secondary particles are formed by the sintering of primary particles which can be partially broken up by milling. The reverse strike process conducting at relatively low reaction temperature with the Y-to-Al molar ratio at stoichiometric ratio of 3:5 is proper to form YAG phase. When the pH is controlled at 7 during the precipitation process, it was found that the pure YAG phase without any intermediate phase occurs by the direct transformation of amorphous to YAG after calcined 900°C or higher. Furthermore, many factors of precipitation condition affect size and size distribution of the powder, including the speed of mixing, the rate of addition and the concentration of precursors. Fabrication of synthesized YAG powder was also investigated and compared with commercial YAG powder. The compacted bodies were sintered at 1650°C for 5 h in air. The relative density of the sintered specimens were in the range of 91-92 % of theoretical density.

Department Chemical Engineering

Field of study Chemical Engineering

Academic Year 2007

Student's signature *Pornpan Wannarong*

Advisor's signature *Varong Pavarajarn*

Co-advisor's signature *Thanakorn Wasanapiarnpong*

ACKNOWLEDGEMENTS

The author would like to express her sincere gratitude and appreciation to her advisor, Assistant Professor Dr. Varong Pavarajarn and her co-advisor, Dr. Thanakorn Wasanapiarnpong for his invaluable suggestions, stimulating, useful discussions throughout this research and devotion to revise this thesis otherwise it can not be completed.

The author is similarly grateful to Mr. Sart Pinkaew for his kind suggestion throughout this work. In addition, the author would also be grateful to Associate Professor Dr. Tawatchai Charinpanitkul, as the chairman, and Associate Professor Dr. Okorn Mekasuwandumrong and Dr. Akawat Sirisuk, as the members of the thesis committee.

Moreover, the author would like to acknowledge to Particle Technology and Material Processing (PTMP) Laboratory, Department of Chemical Engineering and Research Unit of Advanced Ceramics, Department of Materials Science, Chulalongkorn University for equipments support.

The author wishes to thank the members of the Center of Excellence on Catalysis and Catalytic Reaction Engineering, Department of Chemical Engineering, Faculty of Engineering, Chulalongkorn University for their assistance and friendly encouragement.

Finally, the author would like to express her highest gratitude to her parents and her brother who always pay attention to her all the times for suggestions and have provided her support and encouragement. The most success of graduation is devoted to her parents.

CONTENTS

	Page
ABSTRACT (THAI).....	iv
ABSTRACT (ENGLISH).....	v
ACKNOWLEDGEMENTS.....	vi
CONTENTS.....	vii
LIST OF TABLES.....	x
LIST OF FIGURES.....	xi
CHAPTER	
I INTRODUCTION.....	1
II THEORY AND LITERATURE REVIEWS.....	3
2.1 Properties of Yttrium Aluminum Garnet (YAG, $Y_3Al_5O_{12}$).....	3
2.2 Intermediate compounds in Y_2O_3 - Al_2O_3 System Process.....	4
2.2.1 YAG (Yttrium Aluminium Garnet, $Y_3Al_5O_{12}$).....	5
2.2.2 YAP (Yttrium Aluminium Perovskite, $YAlO_3$).....	6
2.2.3 YAM (Yttrium Aluminium Monoclinic, $Y_4Al_2O_9$).....	7
2.2.4 Phase Transformation.....	7
2.3 Synthesis of Ceramic Powder via Precipitation Method.....	10
2.4 Method for Forming of Specimen from Ceramic Powder.....	14
2.4.1 Method for Shape Forming.....	14
2.4.2 Sintering.....	16
2.5 Desirable Powder Characteristics in Ceramics.....	20
III EXPERIMENTAL.....	23
3.1 Chemicals.....	23
3.2 Experimental Procedures.....	23
3.2.1 Synthesis of YAG Powder.....	23
3.2.1.1 Yttrium-to-aluminium ratio.....	25
3.2.1.2 Precipitation processes.....	25

	Page
3.2.1.3 Concentration of both precursors.....	25
3.2.1.4 Speed of mixing or stirring speed.....	26
3.2.1.5 Rate of addition.....	26
3.2.1.6 Reaction temperature.....	26
3.2.1.7 pH value of the reaction system.....	26
3.2.1.8 Calcination temperature.....	26
3.2.1.9 Variation in calcination time.....	27
3.2.2 Fabrication of YAG Specimens.....	27
3.2.2.1 Ball milling.....	27
3.2.2.2 Biaxial hydraulic press.....	27
3.2.2.3 Cold isostatic press.....	27
3.2.2.4 Pressureless sintering.....	28
3.3 Characterizations.....	28
3.3.1 Characterization of the Synthesized Powder.....	28
3.3.1.1 X-Ray Diffraction (XRD).....	28
3.3.1.2 Particle Size Distribution Analysis (PSD).....	28
3.3.1.3 Thermogravimetric Analysis (TGA).....	28
3.3.1.4 Scanning Electron Microscopy (SEM).....	29
3.3.1.5 Transmission Electron Microscopy (TEM).....	29
3.3.1.6 Fourier Transform Infrared spectroscopy (FTIR).....	29
3.3.2 Characterization of Green Specimens.....	29
3.3.3 Characterization of Sintered Specimens.....	30
3.3.3.1 Density of the Sintered specimens.....	30
3.3.3.2 Measurement of grain size of sintered specimens.....	30
IV RESULTS AND DISCUSSION.....	31
4.1 Preliminary Experiments.....	31
4.2 Phase Formation of YAG Powder.....	38
4.2.1 Effects of yttrium-to-aluminium ratio.....	38

	Page
4.2.2 Effects of reaction temperature.....	44
4.2.3 Effects of pH value of the reaction system.....	49
4.2.4 Effect of type of precipitation process.....	55
4.2.5 Effects of calcination time.....	58
4.3 Effects of Preparation Conditions for Precipitation.....	64
4.3.1 Effects of speed of mixing.....	64
4.3.2 Effects of rate of addition.....	66
4.3.3 Effects of reactants concentration.....	67
4.4 Fabrication of YAG Powder.....	70
V CONCLUSIONS AND RECOMMENDATIONS.....	77
5.1 Conclusions.....	77
5.2 Recommendations.....	78
REFERENCES.....	79
APPENDICES.....	83
APPENDIX A: Calculation of concentration of both reactants in precipitation method.....	84
APPENDIX B: Calculation of the crystallite size.....	86
APPENDIX C: Condition for ball mill and dispersion of powder.....	89
APPENDIX D: Density.....	90
APPENDIX E: Particle size distribution.....	92
APPENDIX F: List of publication.....	98
VITAE.....	101

LIST OF TABLES

	Page
4.1 Median diameter of the calcined product prepared by using various stirring speeds.....	64
4.2 Median diameter of the calcined products prepared by using various rates of addition.....	66
4.3 Median diameter of calcined powder prepared via the standard synthesis procedure using various concentration of reactants.....	68
4.4 Median diameter of the calcined powder after ball milled for various period of time.....	71
4.5 Median diameter of commercial YAG powders before and after milling...	72
4.6 Density of the sintered YAG specimen.....	74
4.7 Average grain size of the sintered specimens.....	75
E.1 Median diameter of the calcined product prepared by using various stirring speeds.....	93
E.2 Median diameter of the calcined products prepared by using various rates of addition.....	94
E.3 Median diameter of calcined powder prepared via the standard synthesis procedure using various concentrations of reactants.....	95
E.4 Median diameter of the calcined powder after ball milled for various period of time.....	97

LIST OF FIGURES

		Page
2.1	Chronological development of Y_2O_3 - Al_2O_3 phase diagram.....	4
2.2	Garnet crystal structure.....	5
2.3	Calculated XRD peak positions of YAG.....	5
2.4	Calculated XRD peak positions of orthorhombic YAP.....	6
2.5	Calculated XRD peak positions of hexagonal YAP	6
2.6	Calculated XRD peak positions of YAM.....	7
2.7	Effect of time and temperature on the phase obtained from the heat treatment of amorphous material with composition corresponding to YAG.....	8
2.8	Effect of time and temperature on the phase obtained from the heat treatment of amorphous material with composition corresponding to YAP.....	9
2.9	Parameters affecting property of the precipitate.....	11
2.10	Correlation between green bulk density, final density, and forming pressure of high-purity alumina ceramics.....	14
2.11	Steps of dry pressing operation.....	15
2.12	Formation of a neck during the sintering of two fine particles	17
2.13	Changes in pore shape do not necessarily require shrinkage.....	17
2.14	Density as a function of sintering temperature for reactive alumina powder showing the stages of sintering.....	18
2.15	Development of the ceramic microstructure during sintering.....	19
3.1	Diagram of α -alumina powder preparation by normal route.....	24
4.1	XRD patterns of the powder calcined at various temperatures for 2 h.....	32
4.2	TG/DTA curve of the dried precipitate, which was synthesized with molar ratio for Y:Al of 3:5.....	34
4.3	FTIR spectra of the precipitates and YAG products calcined at different temperatures.....	35
4.4	TEM micrographs of the precipitates (a) and the YAG powder which was calcined at 1000°C (b), 1100°C (c), and 1200°C (d) for 2 h.....	36

	Page
4.5 The particle sizes observed in TEM micrographs and crystallite sizes estimated from XRD pattern using the Scherrer's equation, as a function...	37
4.6 XRD patterns of the powder prepared with Y-to-Al molar ratio of 2:5 and calcined at various temperatures for 2 h.....	39
4.7 XRD patterns of the powder prepared with Y-to-Al molar ratio of 4:5 and calcined at various temperatures for 2 h.....	39
4.8 XRD patterns of the powder prepared with various molar ratios of Y:Al and calcined at 900°C for 2 h.....	40
4.9 DTA/TG curve of the dried powder synthesized with molar ratio for Y:Al of 2:5, 3:5 and 4:5.....	41
4.10 FTIR spectra of the powder synthesis with Y:Al molar ratio of 2:5 and calcined at various temperatures for 2 h.....	42
4.11 FTIR spectra of the powder synthesis with Y:Al molar ratio of 4:5 and calcined at various temperatures for 2 h.....	43
4.12 XRD patterns of the precipitates prepared at 10°C and calcined at various temperatures for 2 h.....	44
4.13 XRD patterns of the precipitates prepared at 50°C and calcined at various temperatures for 2 h.....	45
4.14 TG/DTA curves of the precipitates synthesized at the reaction temperature of 10 and 50°C.....	46
4.15 FTIR spectra of the precipitates prepared at 10°C and calcined at various temperatures for 2 h.....	47
4.16 FTIR spectra of the precipitates prepared at 50°C and calcined at various temperatures for 2 h.....	48
4.17 XRD patterns of the precipitates synthesized at pH 6 and calcined at various temperatures for 2 h.....	49
4.18 XRD patterns of the precipitates synthesized at pH 7 and calcined at various temperatures for 2 h.....	50
4.19 TG/ DTA curves of the precipitates synthesized at pH 6 and 7.....	51

	Page
4.20 FTIR spectra of the precipitates synthesized at pH 6 and calcined at various temperatures for 2 h.....	53
4.21 FTIR spectra of the precipitates synthesized at pH 7 and calcined at various temperatures for 2 h.....	53
4.22 XRD patterns of the precipitated synthesized via the normal strike process and calcined at various temperatures for 2 h.....	55
4.23 TG/DTA curves of the precipitates synthesized by the normal strike process.....	56
4.24 FTIR spectra of the precipitated synthesized via the normal strike process and calcined at various temperatures for 2 h.....	57
4.25 XRD patterns of the powder calcined at 1200°C at various of calcination time.....	59
4.26 XRD patterns of the powder calcined at 1100°C at various of calcination time.....	59
4.27 TEM micrographs of YAG powder which was calcined at various calcination temperatures and calcination times.....	61
4.28 The particle sizes observed in TEM micrographs and crystallite sizes estimated from XRD pattern using the Scherrer's equation, as a function of calcination temperature and calcination time.....	62
4.29 FTIR spectra of the powder which was calcined at various calcination temperatures and calcination times.....	63
4.30 The particle size distributions of the powder prepared via the standard synthesis procedure using various speed of mixing and subsequently calcined at 1200°C.....	65
4.31 The particle size distributions of the powder prepared via the standard synthesis procedure using various rate of addition and subsequently calcined at 1200°C.....	67

	Page
4.32 The particle size distributions of the powder prepared via the standard synthesis procedure using 1 M of AHC solution and ions solution at various concentrations.....	69
4.33 The particle size distributions of the powder prepared via the standard synthesis procedure using 2 M of AHC solution and ions solution at various concentrations.....	69
4.34 SEM images of the commercial powder (a) and synthesized powder (b) the commercial powder which is milled for 72 h.....	71
4.35 Particle size distributions of the synthesized powder calcined at 1200°C milled for various periods of time.....	72
4.36 Particle size distributions of the commercial YAG powder before milling and after milling for 72 h.....	72
4.37 The relative density of YAG specimen, which is fabricated from YAG commercial powder and synthesized powder.....	74
4.38 Microstructures of YAG specimen which is fabricated from YAG commercial powder and synthesized powder.....	76
B.1 The observation peak of α -alumina for calculating the crystallite size.....	87
B.2 The graph indicating that value of the line broadening attribute to the experimental equipment from the α -alumina standard.....	88
E.1 The particle size distributions of the powder prepared via the standard synthesis procedure using various speed of mixing and subsequently calcined at 1200°C.....	93
E.2 The particle size distributions of the powder prepared via the standard synthesis procedure using various rate of addition and subsequently calcined at 1200°C.....	94
E.3 The particle size distributions of the powder prepared via the standard synthesis procedure using 1 M of AHC solution and ions solution at various concentrations.....	95

	Page
E.4 The particle size distributions of the powder prepared via the standard synthesis procedure using 2 M of AHC solution and ions solution at various concentrations.....	96
E.5 Particle size distributions of the synthesized powder calcined at 1200°C and milled for various periods of time.....	97



สถาบันวิทยบริการ
จุฬาลงกรณ์มหาวิทยาลัย

CHAPTER I

INTRODUCTION

$Y_3Al_5O_{12}$ is commonly called as yttrium aluminum garnet (YAG). Its crystal is formed in a cubic garnet structure, which belongs to an isometric crystal system[1, 2]. Due to its homogeneous optical properties and lack of birefringence effects, YAG is widely used for laser and luminescence materials[3, 4].

YAG has been used as an active laser medium in various solid-state lasers. For applications in laser generation, YAG is commonly doped with other elements to obtain specific wavelength. For example, neodymium and erbium are commonly used, yielding YAG:Nd and YAG:Er lasers, respectively. Cerium-doped YAG (YAG:Ce) is used as a phosphor in cathode ray tube and white light-emitting diodes, and as a scintillator. Another application of YAG is in jewelry, as a stimulant for diamond or other gemstone. Colored variants can be achieved by doping elements, for instance chromium (green), cobalt (blue), manganese (red), neodymium (purple). As faceted synthetic gems, they are valued for their clarity, durability, high refractive index and dispersion[5].

Single crystals of YAG have drawn considerable attention since the early 1960s, for fluorescence and solid-state lasers applications. However, more attention has been paid to fabrication of YAG ceramics [6-9] since they have shown better optical and high-temperature mechanical properties. Compared with the single crystal form, the polycrystalline YAG ceramics have excellent possibilities for future application because of many advantages, such as low cost, short preparation time, ease of mass production, etc. [10, 11]. In order to achieve high-density and high-transparency polycrystalline YAG ceramics, highly dispersed ultra-fine YAG powder with narrow size distribution is necessary.

YAG powder has been prepared by many methods, such as solid-state reaction [6, 10], co-precipitation [11-14], sol-gel [9, 15, 16], spray thermal decomposition [17], hydrothermal [18, 19] and solvothermal synthesis [20-22]. The solid-state

reaction method is a simple process for the synthesis of YAG, but high-temperature treatment (higher than 1600 °C) and repeated mechanical mixing are required to obtain pure phase YAG powder. These processes lead to hard agglomeration and contamination of the powder. The sol–gel method also has some disadvantages, such as difficulties in controlling the pH, expensive starting materials and long reaction time, all of which have limited its mass production. The hydrothermal and solvothermal synthesis of YAG powder can avoid the problems described above. However, hydrothermal synthesis requires complicated and expensive facilities due to the high operating temperature and pressure (>400 °C, >30 MPa)[18, 19]. Compared with methods described above, co-precipitation method is one of the most promising techniques because this method requires inexpensive starting materials, a simple synthesis process and commonly available apparatus.

In this research, nanocrystalline YAG powders are synthesized by precipitation method. Effects of various parameters are also investigated to find proper condition for synthesizing nanocrystalline YAG powder, such as yttrium-to-aluminium ratio, rate of addition of one reactant to another, speed of mixing, reaction temperature, pH of the reaction system, calcination temperature and holding time during calcination are also investigated. Moreover, YAG ceramic specimen is fabricated by sintering of the synthesized powder. Correlation between the characteristic of the powder and the density of the sintered specimen is also investigated.

สถาบันวิทยบริการ
จุฬาลงกรณ์มหาวิทยาลัย

CHAPTER II

THEORY AND LITERATURE SURVEY

2.1 Properties of Yttrium Aluminum Garnet (YAG, $Y_3Al_5O_{12}$)

Yttrium aluminium garnet or YAG is a chemical compound of yttrium, aluminium and oxygen with the chemical formula $Y_3Al_5O_{12}$. YAG is a synthetic crystalline material of the garnet group. It is also one of three phases of the yttria-alumina compound, the other two being yttrium aluminum monoclinic (YAM, $Y_4Al_2O_9$) and yttrium aluminum perovskite (YAP, $YAlO_3$). Its crystal is formed in cubic structure, which belongs to an isometric crystal system with lattice parameters $a = 12.004\text{\AA}$.

YAG is an important material in many fields because of its excellent and wide-ranged properties. It has high temperature creep resistance, high melting point at 1950°C , very high hardness of 8.5 (Mohs's hardness), good thermal conductivity, high mechanical strength and excellent chemical stability. Moreover, YAG is fluorescence material and high refractive index with lack of birefringence effect, due to its homogeneous optical properties. Therefore YAG is widely used for laser diode, luminescence material and synthetic gemstone.

YAG is commonly used as a host material in various solid-state lasers. Rare earth elements such as neodymium and erbium can be doped into YAG as active laser ions, yielding Nd:YAG and Er:YAG lasers, respectively. Cerium-doped YAG (YAG:Ce) is used as a phosphor in cathode ray tubes and white light-emitting diodes, and as a scintillator.

2.2 Intermediate Compounds in Y_2O_3 - Al_2O_3 System

According to Y_2O_3 - Al_2O_3 phase diagram, three intermediate compounds are identified. Their existence, stability and formation mechanisms have been long investigated. Chronological development of Y_2O_3 - Al_2O_3 phase diagram is shown in Figure 2.1 and the main difference between them is about the existence and stability range of $YAlO_3$ (YAP) phase [23].

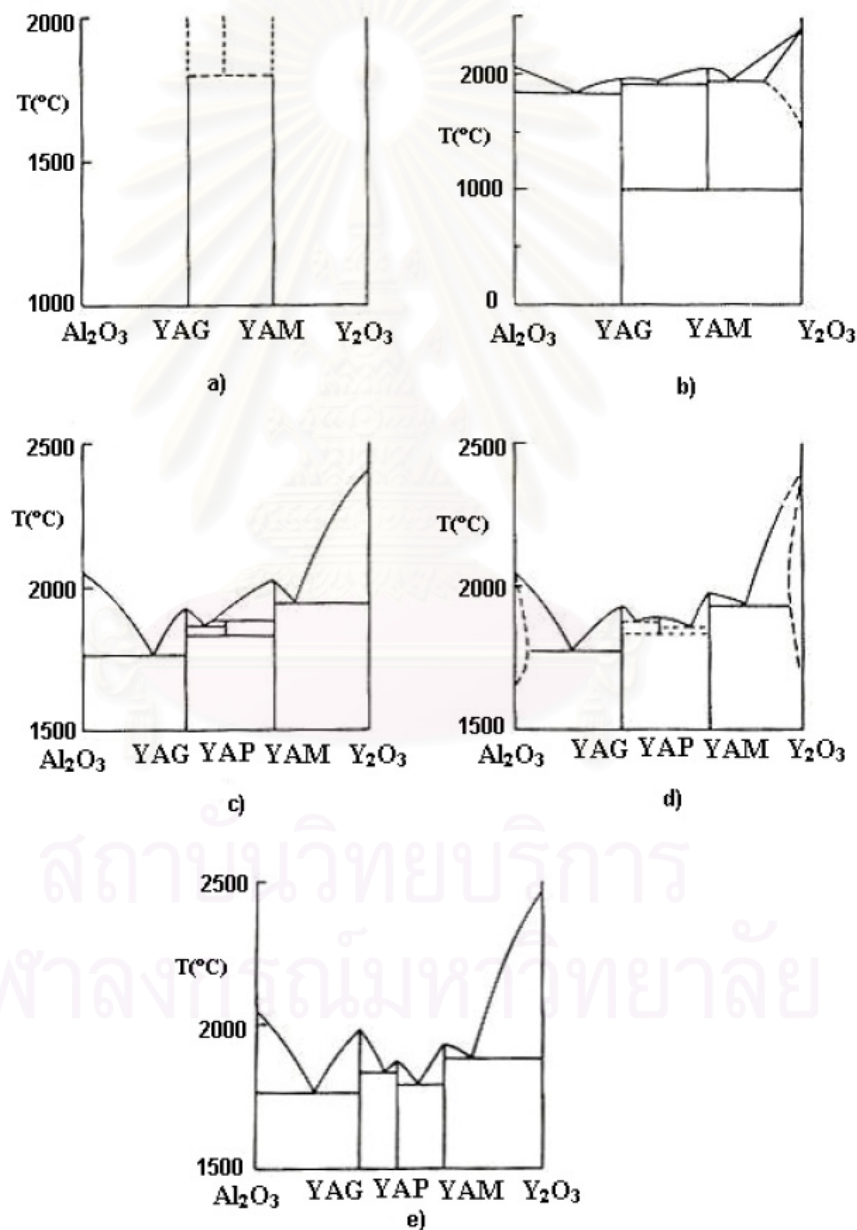


Figure 2.1 Chronological development of Y_2O_3 - Al_2O_3 phase diagram a) Schneider et al. [23] b) Olds et al. [24] c) Toropov et al. [25] d) Mizuno et al. [23] e) Abell et al. [1]

2.2.1 YAG (Yttrium Aluminum Garnet, $Y_3Al_5O_{12}$)

YAG has cubic garnet structure that contains 160 atoms in each unit cell [23]. The garnet crystal structure is shown in Figure 2.2. Calculated X-ray diffraction pattern of YAG is given in Figure 2.3.

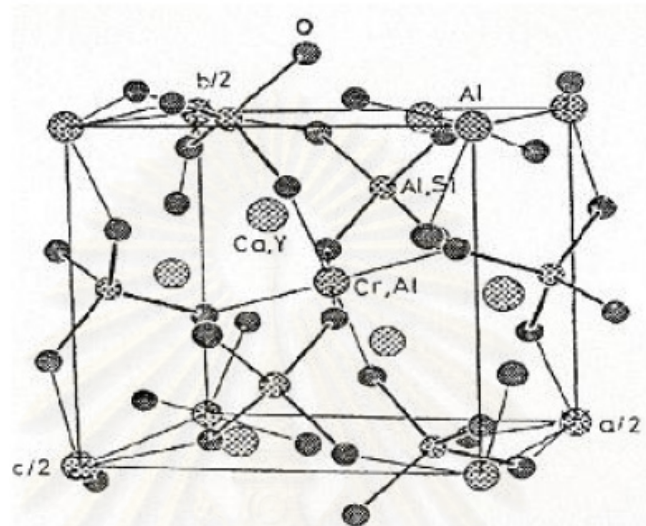


Figure 2.2 Garnet crystal structure [26].

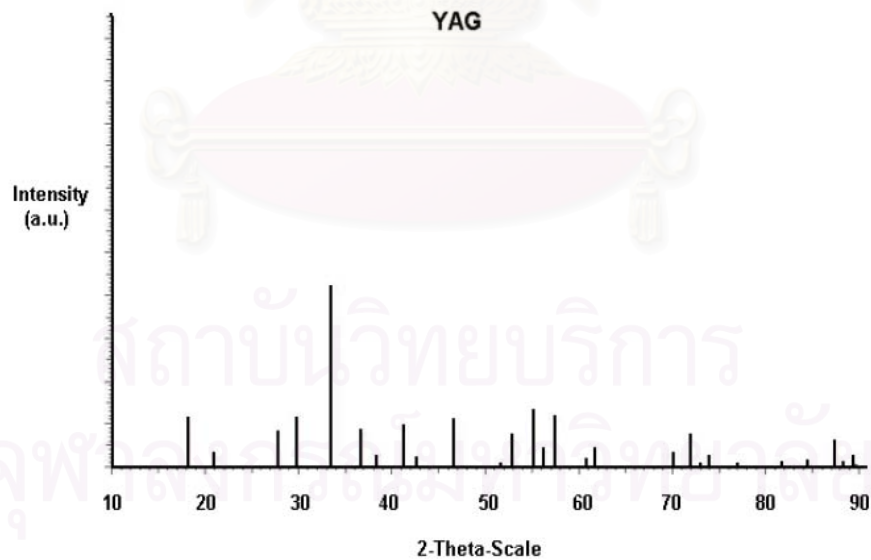


Figure 2.3 Calculated XRD peak positions of YAG.

YAG is one of the stable intermediate phases in the Y_2O_3 - Al_2O_3 binary phase system. Its stability stretches from room temperature to its melting point at 1970 °C [23].

2.2.2 YAP (Yttrium Aluminium Perovskite, $YAlO_3$)

YAP is a dimorphic phase in the binary system. In other words, YAP has two crystal structures. The first one is orthorhombic perovskite structure that has 20 atoms in each unit cell [23] while the second one is hexagonal structure. Figure 2.4 and Figure 2.5 give calculated 2θ values for XRD patterns of YAP.

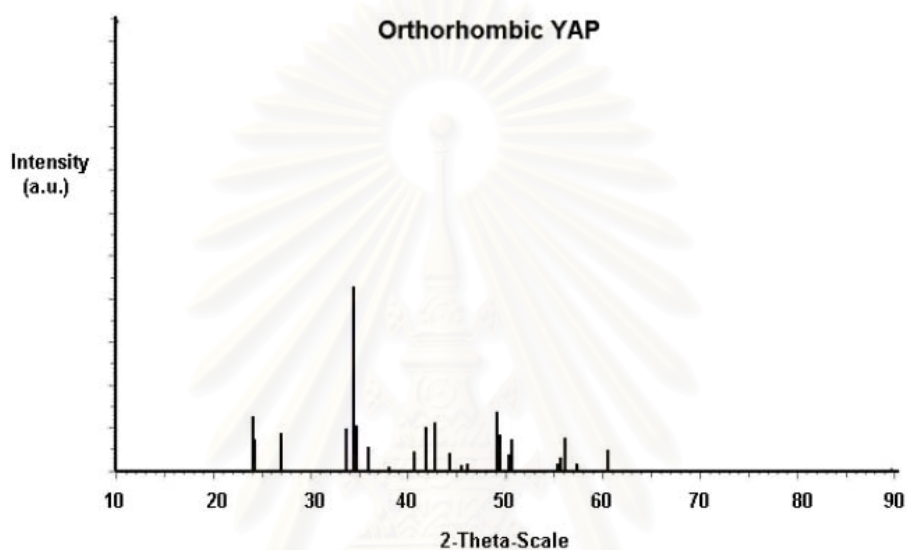


Figure 2.4 Calculated XRD peak positions of orthorhombic YAP.

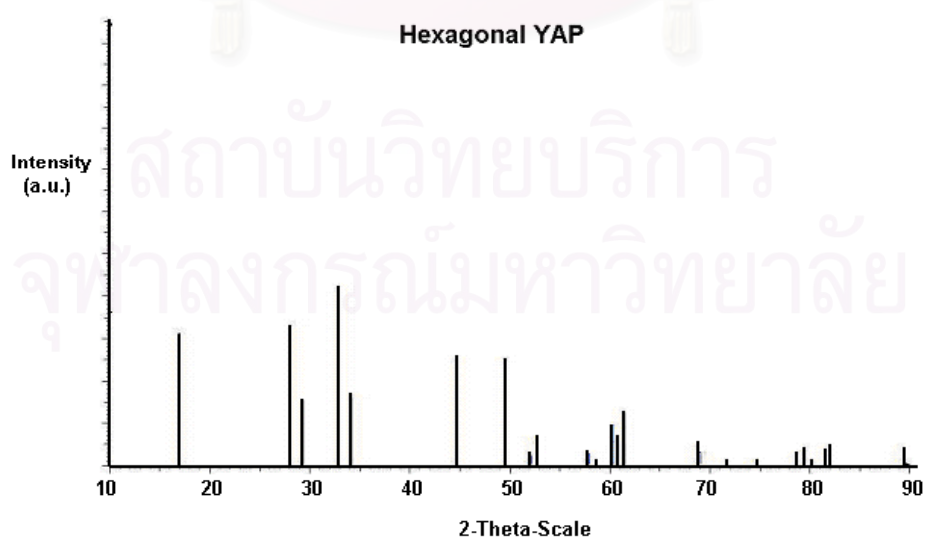


Figure 2.5 Calculated XRD peak positions of hexagonal YAP.

Doubts about existence, stability, crystal structure and composition of YAP are main causes of conflicting results in literatures about Y_2O_3 - Al_2O_3 system. After its production as a single crystal by Czochralski method, it was accepted as a stable phase and shown as such in the Y_2O_3 - Al_2O_3 phase diagram [23].

2.2.3 YAM (Yttrium Aluminium Monoclinic, $Y_4Al_2O_9$)

YAM has monoclinic structure with $\alpha=\gamma=90^\circ$, $\beta=108.8^\circ$, $a=7.4706\text{\AA}$, $b=10.5350\text{\AA}$ and $c=11.1941\text{\AA}$ [27]. YAM melts congruently at 2030°C [2]. Figure 2.6 gives 2θ values of YAM phase.

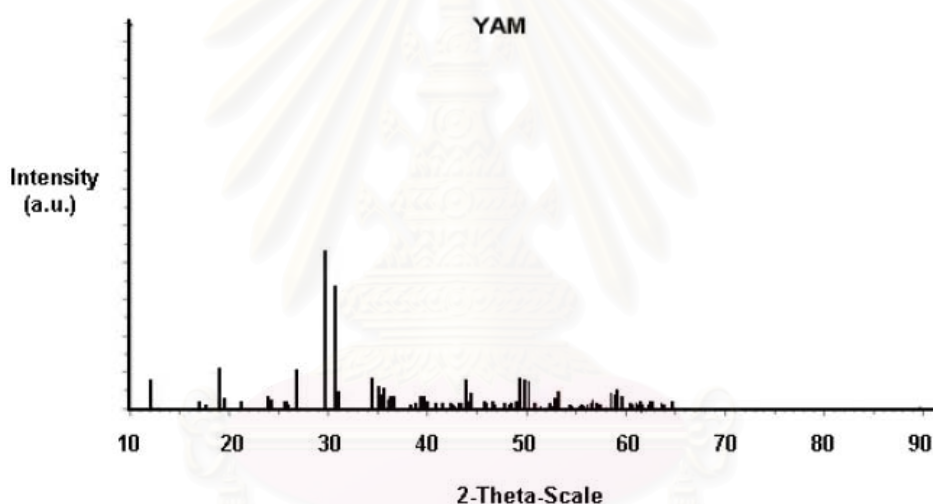


Figure 2.6 Calculated XRD peak positions of YAM.

2.2.4 Phase transformation

Interesting thing about solidification behavior of YAG is that the phase formation and the final phase composition are kinetically controlled. It has been observed that nucleation of solid phase from the melt determines transparency of the sample. Detailed study in Al_2O_3 - Y_2O_3 system has shown that phase transformation incorporated with heterogeneous nucleation during solidification of molten mixture occurs at high temperature because mobility of atoms at high temperature is high enough for the rearrangement into complex structure of YAG phase. On the other hand, for phase transformation with homogeneous nucleation in the molten mixture,

diffusion is the limiting step and mobility of atoms is not sufficient to form the complex YAG phase. Instead, simpler YAP and Al_2O_3 phases with only 20 and 10 atoms per unit cell are formed [23].

Data published by Hess et al. [28] also confirms this conclusion. They studied heat treatment of amorphous oxide products synthesized by the glycine-nitrate process. Composition of the amorphous oxide was adjusted to that corresponding to YAM, YAP and YAG, respectively. Heat treatment for short duration resulted in powder with incomplete crystallization that consisted of a mixture of YAM, YAP, and YAG phases, regardless of the chemical composition of the starting amorphous material. However, heat treatment for longer duration or at higher temperature generated pure-phase of both monoclinic YAM and YAG with the garnet structure, depending on the composition of the starting material. Prolonged heat treatment at high temperature failed to generate pure-phase orthorhombic YAP.

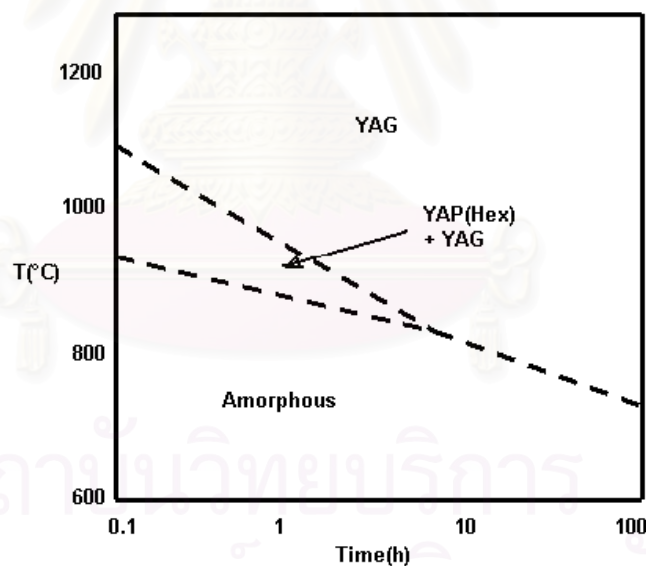
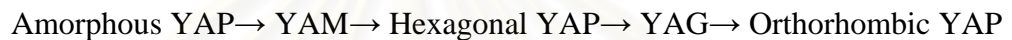


Figure 2.7 Effect of time and temperature on the phase obtained from the heat treatment of amorphous material with composition corresponding to YAG.

Crystallization of YAG, when composition of the starting material was corresponding to YAG stoichiometry, appeared to involve the formation of the intermediate hexagonal YAP, as an intermediate as shown in Figure 2.7. It can be seen that when time is short or temperature is low and fast heating rate is applied,

mixed phase of YAP and YAG is produced. This region is the diffusion limited region. At high temperature and/or long processing time, pure YAG phase is observed. Under such conditions diffusion rate is high and time is long enough for the atoms to arrange themselves in the complex 160-atom unit cells of YAG.

Figure 2.8 shows the effect of time and temperature for the heat treatment of amorphous material with composition corresponding to YAP. They showed that crystallization of YAP involves three intermediate phases: hexagonal YAP, YAG and YAM. Majority of orthorhombic YAP with detectable amount of YAG and YAM were observed at high temperature and long processing time. They suggested the sequence for the crystallization of YAP as followed:



They also suggested that crystallization of YAP could follow different routes, depending on the starting materials and heat treatment procedure [28].

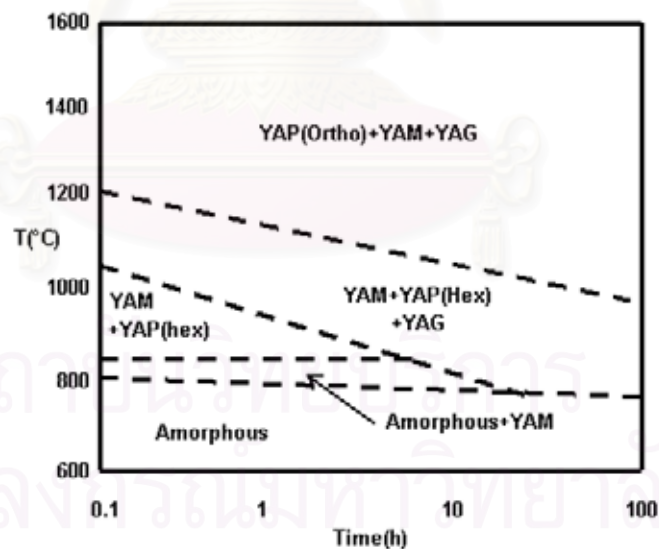


Figure 2.8 Effect of time and temperature on the phase obtained from the heat treatment of amorphous material with composition corresponding to YAP.

When composition of the starting material was corresponding to YAM, after the heat treatment at 1200 °C for 1 hour, orthorhombic YAP phase with YAM phase were observed. Pure YAM phase was obtained after extended heat treatment at 1500 °C. It was explained that the crystallization process of YAM occurred according to the reaction shown below [28].



2.3 Synthesis of Ceramic Powder via Precipitation Method

Precipitation is a formation of solid in liquid-phase solution during a chemical reaction. The solid formed is called precipitate. This phenomena occurs when the solid, i.e. the precipitate, is formed in the solution as an insoluble product from the reaction or when the solution has been supersaturated by a compound. The formation of the precipitate is a sign of change in chemical species. In most situations, the solid forms ("falls") out of the solute phase, and sinks to the bottom of the solution (though it can float if it is less dense than the solvent, or form suspension).

An important stage of the precipitation process is an onset of nucleation. The creation of hypothetical solid particle includes the formation of an interface, which requires energy based on the relative surface energy of the solid and the solution. If this energy is not available, and no suitable nucleation surface is available, supersaturation occurs [5].

The common precipitation method for ceramic powder synthesis usually involves growth of solid crystals from the reaction between reactants in fluid phase. The reactants may or may not be in the same phase before the precipitation takes place. If the reactants are in the same phase, the precipitation is homogeneous, otherwise, it is heterogeneous. The homogeneous precipitation is often preferred because its behavior is more controllable [29].

Basically, all process parameters influence quality of the final product from the precipitation. It is usually desired to get the precipitates with specific properties. These properties may include the nature of the phase formed, chemical composition,

purity, particle size, surface area, pore size, pore volume, and separability from the mother liquor. It may also include demands which are imposed by requirement of downstream processes, such as drying, palletizing or calcinations. It is therefore necessary to optimize the parameters in order to produce the desired material. Figure 2.9 summarizes the parameters which can be adjusted in precipitation processes and the properties which are mainly influenced by these parameters.

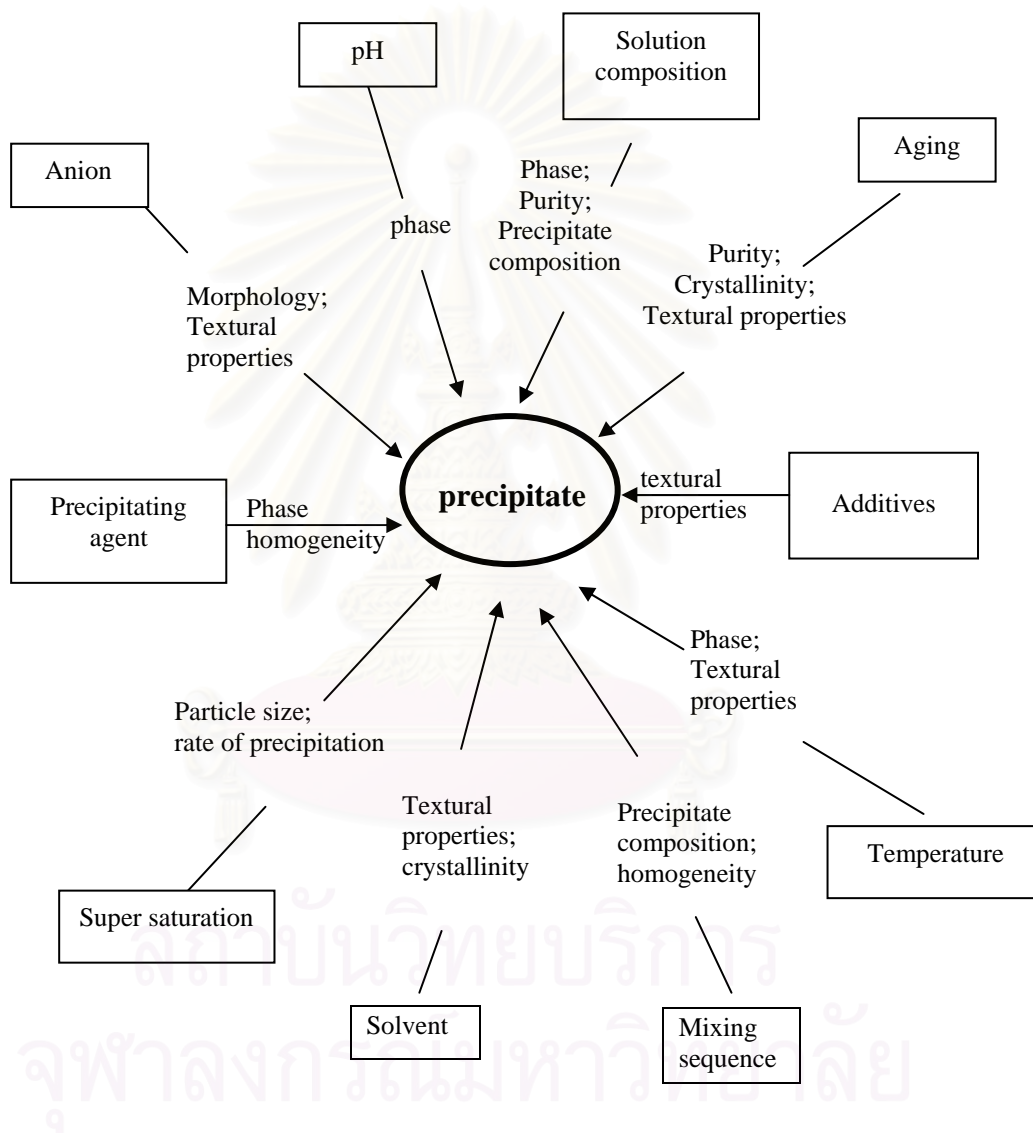


Figure 2.9 Parameters affecting property of the precipitate [30].

In the precipitation method, precursors that can be easily decomposed to volatile products are usually employed. Nitrates of metal as precursors and ammonia or sodium carbonate as the precipitating agent are preferred. Since nucleation rate is extremely sensitive to a change in temperature, precipitation temperature is a decisive

factor in controlling properties of the precipitate such as primary crystallite size, surface area, and phase. However, it is very difficult to state how the precipitation temperature should be adjusted to achieve a product with specific properties. The optimum precipitation temperature is usually a parameter which has to be determined experimentally. In general, most precipitation process is carried out above room temperature, often close to 100°C. Furthermore, pH directly controls the degree of supersaturation, at least in case that hydroxides are precipitated. Therefore, it is also one of the crucial factors in precipitation process. As for many other parameters, the influence of pH is not straight forward and it has to be investigated experimentally for a specific system.

In the previous studies, YAG powder was prepared from yttrium-doped alumina [31]. Ammonium hydrogencarbonate (AHC) and ammonium aluminium sulfate (AAS) were used to synthesize alumina precursor (i.e. ammonium aluminium carbonate hydroxide, AACH) powder via precipitation method. Thermal decomposition of AACH at high temperature yielded alumina powder. However when 10 wt% of yttrium was added to AAS solution, no signal corresponding to any crystalline phase of alumina was observed from sample. Instead, yttrium aluminium garnet (YAG), i.e. $Y_3Al_5O_{12}$, was obtained as the final product from the calcination of precursor at 1200°C. This observation was confirmed by both XRD and FTIR analysis. For the calcination at low temperature (600-800°C), unidentified peaks were detected from the XRD analysis.

Li et al. synthesized YAG powders via co-precipitation from mixed solution of aluminum and yttrium nitrates using ammonia water and ammonium hydrogen carbonate (AHC) as precipitants, respectively [13]. The use of ammonium hydrogen carbonate resulted in better YAG powders, in term of sinter-ability, than ammonia water. When ammonia water was used, a gelatinous hydroxide precursor was produced. The precursor transformed to pure YAG at about 1000°C via YAP intermediate phase. Severe agglomeration caused poor sinterability of the resultant YAG powders. They showed that carbonate precursor of YAG with an approximate composition of $NH_4AlY_{0.6}(CO_3)_{1.9}(OH)_2 \cdot 0.8H_2O$ was synthesized by using ammonium hydrogen carbonate as precipitant. The precursor converted directly to

pure YAG at about 900°C. The precursor was loosely agglomerated after drying and the resultant YAG powders showed good dispersity and sinterability. The most desirable calcination temperature for the carbonate precursor was determined as 1100°C. YAG powder produced at this temperature densified to nearly full density by vacuum sintering at 1500°C for 2 h and the sintered body showed translucency.

Li et al. prepared nano-scaled YAG powders by co-precipitation from mixed solution of aluminum and yttrium nitrates using either urea or ammonium hydrogen carbonate (AHC) as precipitants [14]. The precursor converted directly to pure YAG at about 900 °C without any intermediates. It was found that YAG powder precipitated by using AHC had better sinter-ability than powder precipitated with urea.

From the report of Chiang et al., Ce³⁺ doped yttrium aluminum garnet (YAG:Ce) phosphors were synthesized by four different precipitating processes, in which aluminum nitrate Al(NO₃)₃ or aluminum ammonium sulfate NH₄AlSO₄ was used as the aluminum source [32]. Two different precipitation processes were used, i.e. the normal strike process (NS), which is performed by titrating AHC solution into the ion solution, and the reverse strike process (RS) which is performed by titrating the ions solution into AHC solution. It was found that properties of YAG powder were affected by cation homogeneity of the precursor powder. The intermediate phases, which were identified as YAP (YAlO₃) and YAM (Y₄Al₁₂O₉), appeared when the precursor was calcined at temperature in the range of 800–1300 °C for 2 h.

Li et al. have focused on preparation of nano-crystalline YAG by the co-precipitation method using ammonium hydrogen carbonate [33]. The precursor was converted directly to pure YAG at about 900 °C. The YAG particle size increased with increasing temperature. The resulting YAG powder showed good dispersion and sinterability. Using the nano-crystalline powder, fully transparent YAG ceramic was fabricated under vacuum at 1700 °C for 5 h. It was also found that addition of TEOS (Tetraethyl orthosilicate) was crucial for producing transparency of the YAG ceramic. The results showed that the addition of 0.5 wt% TEOS was optimum. The optical

transmittance of the polycrystalline YAG:Nd ceramic was inferior to that of YAG:Nd single crystal, because of the existence of pores and grain-boundary phases.

2.4 Method for Forming of Specimen from Ceramic Powder

2.4.1 Method for Shape Forming

There are many forming techniques to make ceramics from ceramic powder, for instance, dry pressing, hydrostatic molding, extrusion, injection molding, and hot pressing. The choice of the forming process depends on dimension and shape of parts to be fabricated, quantity of parts, and requirements of the final product. The forming pressure to be applied should be approximately 100 MN/m^2 , but it is usually adaptable in each type of the forming process. Bulk density of the green compacted body, as well as density of the final product after sintering, increases with increasing forming pressure (Figure 2.10). If the forming pressure is too low, the final product will not achieve the full density. On the contrary, excessive pressure, which has the same effect as insufficient plasticization or inhomogeneous distribution of the plasticizer, can lead to defects such as flaws and cracks in the compacted bodies.

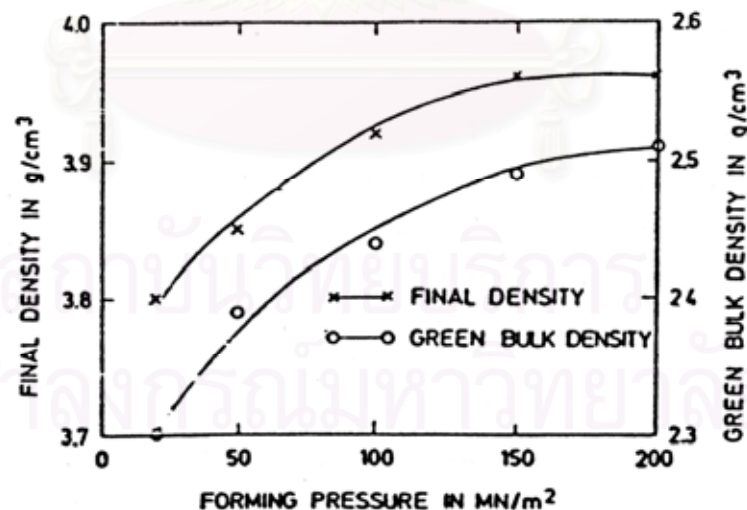


Figure 2.10 Correlation between green bulk density, final density, and forming pressure of high-purity alumina ceramics [34].

The dry-press technique which has advantage in simplicity and low operation cost could provide a green body of ceramic with sufficient physical strength if its

morphology is not so complicated. The method is not suitable to form complicated figure parts. It is restricted, however, to parts with simple shape and to wall thickness greater than 1 mm. Dry pressing is unidirectional. Figure 2.11 illustrates the dry pressing operation using a simple ring, as well as a ring with a flange, under a pressure of 150 MN/m^2 . The procedure is carried out in three basic steps.

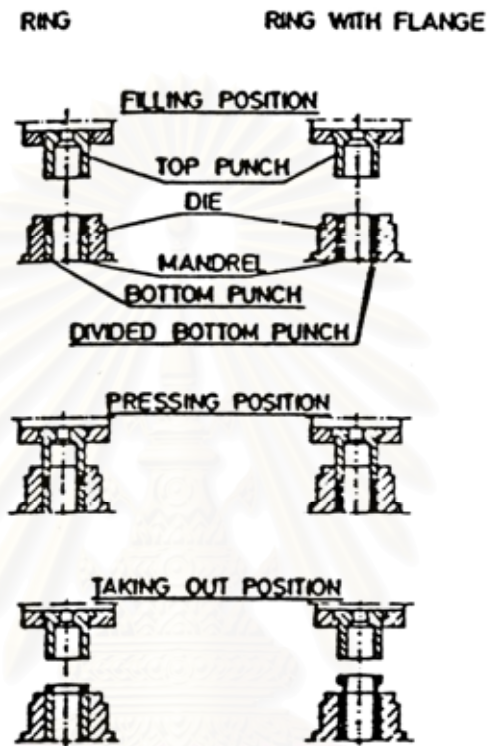


Figure 2.11 Steps of dry pressing operation [34].

1. It is important to get homogeneous distribution of the powder when the die is filled. This can be achieved by using suitably prepared free-flowing powder and by filling the die evenly, for example, by means of a fill shoe.
2. In the pressing position, homogeneous compaction of the powder within the desired shape should be ensured.
3. Removal of the part from the die should be simple, without any risk of damage.

Due to the substantial tool wear caused by the extremely abrasive powder, all parts of the die which are exposed to wear, such as mandrels and punches, are preferably made of cemented carbides.

The isostatic pressing is a process to form ceramic components from dry powder by uniform pressing from all directions. It is also used for other materials, such as metals, plastics, graphite, and carbon. The process is accomplished by enclosing the powder in a deformable mold and then collapsing the mold by using a hydrostatic pressure exerted from fluid medium. For cold isostatic pressing (CIP), the process carried out at or near room temperature.

The general advantages of cold isostatic pressing are:

- Very few size or dimensional limitations, because the uniform application of pressure associated with this process obviates the size limitations of many other processes, particularly the length-to-diameter problems of dry pressing.
- Very uniform pressed compacts, due to the uniform application of pressure, which leads to very consistent density and shrinkage resulting in a reproducible process.
- Generally moderate tooling costs particularly in case of prototype and low-volume production, where the tooling can be quite simple.
- Short overall process time, which do not require long binder burnout or drying period.

2.4.2 Sintering

Sintering is a process by which small particles of material are bonded together by solid-state diffusion during thermal treatment. In the sintering process, particles are coalesced by solid-state diffusion at very high temperatures yet lower than melting point of the compound being sintered. Atomic diffusion takes place between the contacting surfaces of the particles so that they become chemically bonded together. These results are obtained during firing by the transfer of material from one part of the structure to the other; as shown in Figure 2.12 [35]. In ceramic manufacturing, this thermal treatment results in changes in grain size and shape, changes in pore shape and pore size, and compaction of the powder into a dense, coherent product. The kind of change that may occur are shown in Figure 2.13. As the process proceeds, larger particles are formed at the expense of the smaller ones, while the porosity of

the compacts decreases. Finally, at the end of the process, an "equilibrium grain size" is attained.

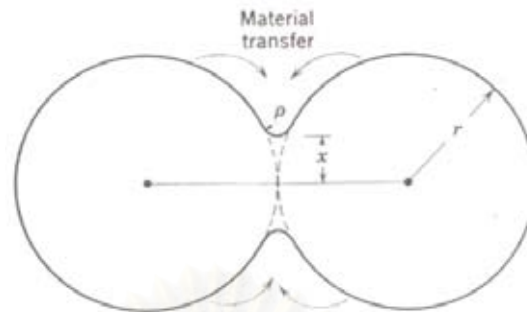


Figure 2.12 Formation of a neck during the sintering of two fine particles [35].

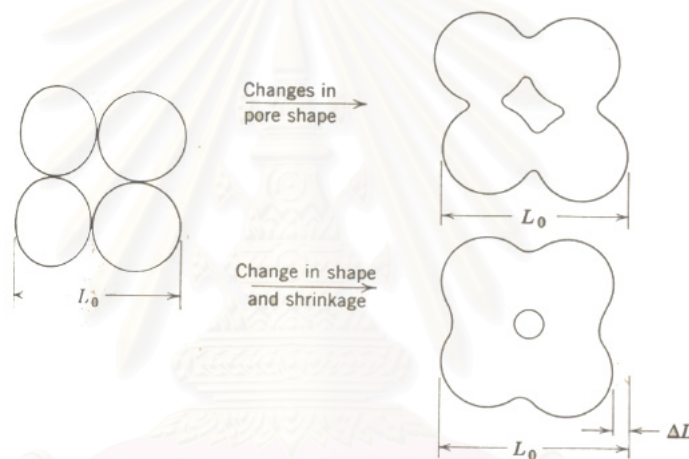


Figure 2.13 Changes in pore shape do not necessarily require shrinkage [35].

Densification, recrystallization, and grain growth occur in the same temperature range. Therefore, strict control of the sintering process as well as small addition of grain growth inhibitor, e.g. TEOS (Tetraethyl orthosilicate), to the YAG powders is essential to achieve a fully dense sintered body with fine-grained microstructure. In the course of sintering, the density increases with the logarithm of time, and the grain size increases with the one-third power of time.

The shrinkage upon sintering of a ceramic component can be monitored by measuring sample size or density as a function of firing temperature and time. A typical plot of density as a function of time is shown in Figure 2.14.

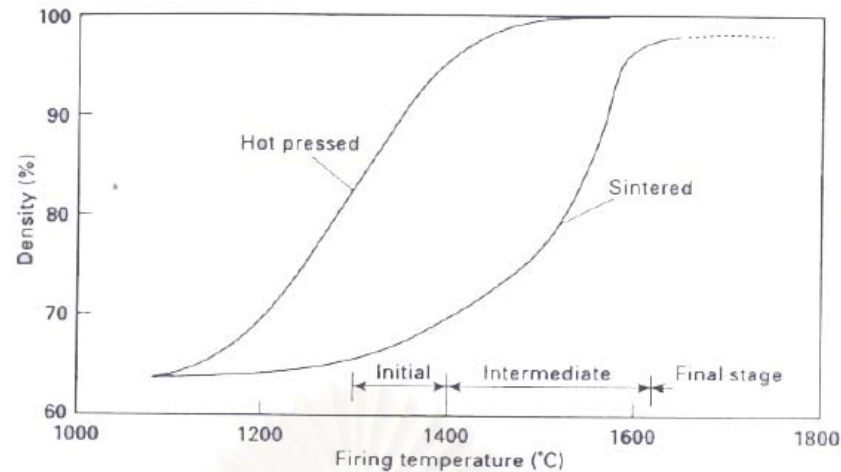


Figure 2.14 Density as a function of sintering temperature for reactive alumina powder showing the stages of sintering [35].

Figure 2.15 illustrates development of the ceramic microstructure during sintering. The procedure is carried out in three basic steps.

1. Initial sintering involves rearrangement of the powder particles and formation of a strong bond or neck (Figure. 2.15(b)) at contact points between particles. Relative density of the compact may increase from 0.5 to 0.6 due mostly to the increased packing of the particles.

2. Intermediate sintering is where the size of the necks grows, the amount of porosity decreases substantially and particles move closer (Figure. 2.15(c)) leading to shrinkage of the component. Grain boundaries (and grains) are formed and move so that some grains grow at the expense of others. This stage continues while pore channels are connected (open porosity) but this stage is considered over when the pores are isolated (closed porosity). Majority of the shrinkage of the ceramic component occurs during intermediate sintering and relative density at the end of this stage may be about 0.9.

3. In final stage of sintering, the pores become closed and are slowly eliminated generally by diffusion of vacancies from the pores along grain boundaries with only little densification of the component. The diffusion along grain boundaries is more rapid. Grain size increases during this stage (Figure. 2.15(d)).

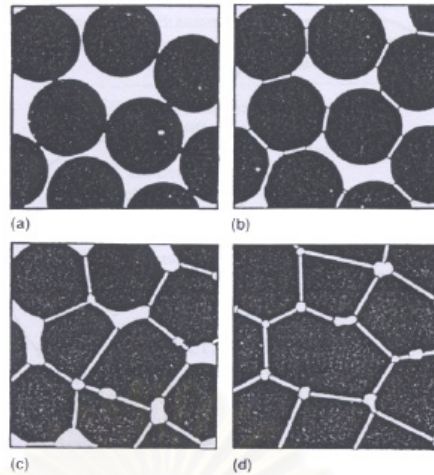


Figure. 2.15 Development of the ceramic microstructure during sintering: (a) loose powder particles, (b) initial stage, (c) intermediate stage and (d) final stage [36].

Nature of the sintering atmosphere may influence the rate of sintering and the residual porosity. Many additives besides temporary binders have been used in sintering process for several purposes, such as crystal growth repression, crystal growth acceleration, acceleration of sintering or shrinkage rate, reduction in maturing temperature, porosity alteration, changes in physical or chemical properties, and removal of impurities. Many researchers have studied effects of sintering additives on the sintering process in order to improve properties of the material obtained. The choice of sintering temperature, which is usually between 1600 and 1800°C, depends on surface energy, grain size distribution, and the additives of the YAG powder. The sintering time and particularly the heating rate should be adapted to the size and the wall thickness of the body to be sintered. Larger parts require a longer sintering time and slower rate of heating-up. Smaller parts can be heated up more quickly, allowing much shorter sintering time.

In the previous studies, a fully transparent YAG ceramic was fabricated under vacuum at 1700 °C for 5 h [33]. It was also found that addition of TEOS (Tetraethyl orthosilicate) was crucial for producing transparency of the YAG ceramic. The results showed that the addition of 0.5 wt% TEOS was optimum. The average grain size of the YAG ceramic obtained was about 2–3 μm. The transmittance of the YAG ceramic increased as the sintering temperature and wavelength increased. The optical transmittance was about 55% in visible range, and reached almost 70% in infrared

region. The optical transmittance of the polycrystalline YAG:Nd ceramic was inferior to that of YAG:Nd single crystal, because of the existence of pores and grain-boundary phases.

From the report of Wen et al., which employed yttria powder and a commercial ultrafine Al_2O_3 powder as starting material, fully transparent YAG ceramics was fabricated by vacuum sintering at 1700 °C for 4 h through a solid-state reaction method [37]. It was found that the addition of 0.5 wt.% tetraethyl orthosilicate (TEOS) was suitable for the fabrication of transparent YAG ceramics. If the amount of TEOS is less than 0.05 wt.%, abnormal grain growth occurred, and pores were entrapped in the grains. If the amount of TEOS was higher than 3 wt.%, large amount of liquid phase was yielded, leaving some residual inclusions at grain boundaries. These were detrimental for the transparency of YAG ceramics.

2.5 Desirable Powder Characteristics in Ceramics

Traditional ceramics generally require less specific property than advanced ceramics. They can be chemically inhomogeneous and can have complex microstructures. Unlike the case of advanced ceramics, chemical reaction during firing is often a requirement for traditional ceramics. On the other hand, for advanced ceramics, very specific property requirements must be met. Therefore, chemical composition and microstructure must be well controlled.

For advanced ceramics, the important powder characteristics are the size, size distribution, shape, state of agglomeration, chemical composition, and phase composition. The structure and chemistry of the surface are also important. The most profound effect of the particle size, however, is on the sintering. The rate at which the body densifies increases strongly with a decrease in particle size. Normally, if other factors do not cause severe difficulties during firing, a particle size of less than $\approx 1 \mu\text{m}$ allows the achievement of high density within a reasonable time. Whereas powder with a wide distribution of particle size may lead to higher packing density in the green body, this benefit is usually vastly outweighed by difficulties in the control of the microstructure during sintering. A common problem is that the large grains

coarsen rapidly at the expense of the smaller grains, making the attainment of high density with controlled grain size impossible. Homogeneous packing of the powder with narrow size distribution (i.e., neatly monodispersed powder) generally allows greater control of the microstructure. A spherical or equiaxial particle shape is beneficial for controlling the uniformity of the packing.

Agglomerates lead to heterogeneous packing in the green body, which in turn leads to differential sintering (different regions of the body sintering at different rates) during the firing stage. This can cause serious problems such as the development of large pores and voids in the fired body. Furthermore, the rate at which the body densifies is roughly similar to that for a coarse-grained body with a particle size equivalent to that of the agglomerates. An agglomerated powder therefore has serious consequences for the fabrication of ceramics when high density coupled with a fine-grained microstructure is desired. Agglomerates are classified into two types : soft agglomerates in which the particles are held together by weak van der Waals forces and hard agglomerates in which the particles are chemically bonded together by strong bridges. The ideal situation is the avoidance of agglomeration in the powder. However, in most cases this is not possible. In such cases, we would prefer to have soft agglomerates rather than hard agglomerates. Soft agglomerates can be broken down relatively easily by mechanical method (e.g., pressing or milling) or by dispersion in a liquid. Hard agglomerates cannot be easily broken down and therefore must be avoided or removed from the powder.

Surface impurities may have a significant influence on the dispersion of the powder in a liquid, but the most serious effect of variations in chemical composition and microstructure is encountered in the firing stage. Impurities may lead to the presence of a small amount of liquid phase at the sintering temperature, which causes selected growth of large individual grains. In such case, the achievement of a fine uniform grain size would be impossible. Chemical reactions between incompletely reacted phases can also be a source of problems. We would therefore like to have no chemical change in the powder during firing. For some materials, polymorphic transformation between different crystalline structures can also be a source of severe difficulties for microstructure control. To summarize, the desirable powder characteristics for the fabrication of advanced ceramics are listed in Table 2.1.

Table 2.1 Desirable powder characteristics for advanced ceramics

Powder characteristic	Desired property
Particle size	Fine ($< 1 \mu\text{m}$)
Particle size distribution	Narrow
Particle shape	Spherical or equiaxial
State of agglomeration	No agglomeration or soft agglomerates
Chemical composition	High purity
Phase composition	Single phase



สถาบันวิทยบริการ
จุฬาลงกรณ์มหาวิทยาลัย

CHAPTER III

EXPERIMENTAL

This chapter describes experimental system and procedures for yttrium aluminium garnet synthesis (YAG) as well as fabrication of YAG specimen. It is divided into three parts, i.e. used chemicals, preparation of samples and characterization of the obtained products, respectively.

3.1 Chemicals

All chemicals used in this work are listed as following:

1. Ammonium aluminum sulfate (99 %+) ($\text{NH}_4\text{Al}(\text{SO}_4)_2 \cdot 12\text{H}_2\text{O}$) available from Univar.
2. Ammonium hydrogen carbonate (98%) (NH_4HCO_3) available from Unilab.
3. Acetic acid (99%+)(CH_3COOH) available from CARLO ERBA REAGENT.
4. Yttrium (III) nitrate hexahydrate (99.9%) available from Aldrich.
5. Yttrium aluminium oxide (99%) available from Aldrich.
6. Ethanol (99%+) available from MERCK.
7. Ammonia solution (~25%) available from MERCK.
8. Tetraethyl orthosilicate (98%) available from Sigma-Aldrich.

3.2 Experimental Procedures

3.2.1 Synthesis of YAG Powder

Yttrium aluminium garnet nano-sized powder was synthesized from mixed solution of aluminum precursor (ammonium aluminum sulfate: AAS) and yttrium nitrates via the co-precipitation method using ammonium hydrogen carbonate (AHC) as precipitating agent. The procedure for synthesis YAG powder is shown in Figure 3.1

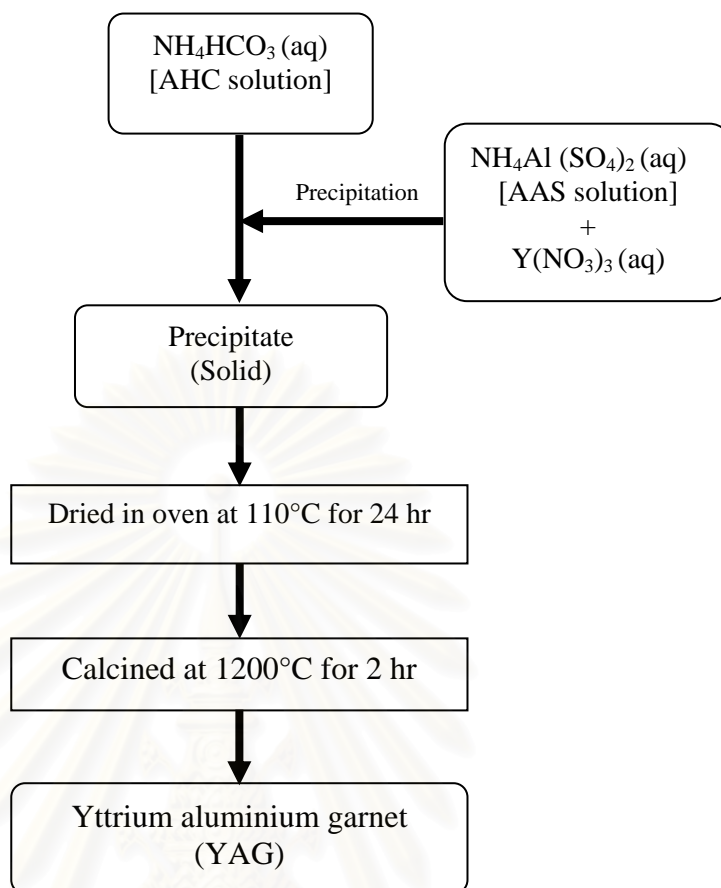


Figure 3.1 Diagram of YAG powder preparation by normal route.

In this work, ammonium aluminium sulfate (AAS) and yttrium nitrate ($\text{Y}(\text{NO}_3)_3$) with molar ratio for Y : Al of 3:5 were dissolved into deionized water to obtain 250 ml of ion solution. Ammonium hydrogen carbonate (AHC) was also dissolved into deionized water to obtain 100 ml of precipitant solution. In order to form two different precipitation processes were used. The first one is the normal strike process (NS), which was performed by titrating precipitant solution into the ion solution, while the other is the reverse strike process (RS) which was performed by titrating the ion solution into AHC solution. The ion solution was gradually added to the precipitant solution with concentration ratio of AAS to AHC of 0.2:2.0 mol/l at the room temperature. The addition rate of the ion solution into the precipitant solution was controlled 5 ml/min. The mixture was constantly stirred using magnetic stirrer rotating at 500 rpm. The pH of the mixture during the reaction was not controlled. After the reaction, the mixed solution was left for 15 minutes to allow

complete reaction. The white precipitates formed were collected, washed with deionized water and methanol, separated from the solution by centrifugation, then dried in the oven at 110°C overnight.

The dried precipitate was calcined in air in a box furnace. The precipitate was heated at a rate of 10°C /min to the desired temperature, in the range of 800-1200°C, and held at that temperature for different holding time. The obtained powder was found to be YAG phase.

The procedures described above are considered as the standard synthesis route. Several modifications were made on this set of procedure, in order to investigate effects of various factors on particle size of the obtained powder as well as properties of the sintered articles. Such modifications are listed as followed.

3.2.1.1 Yttrium-to-aluminium ratio

The yttrium-to-aluminium ratio of the ion solution was varied from 2:5, 3:5 and 4:5.

3.2.1.2 Precipitation processes

Two different precipitation processes were investigated. One was the normal strike process (NS), which was performed by titrating AHC solution into the ion solution, and the other was the reverse strike process (RS) which was performed by titrating the ion solution into AHC solution.

3.2.1.3 Concentration of both precursors

The concentration of both precursors was varied from 1.0 and 2.0 mol/l for ammonium hydrogen carbonate solution (precipitant solution) and 0.1, 0.2, 0.3, mol/l for ammonium aluminum sulfate solution (AAS solution).

3.2.1.4 Speed of mixing or stirring speed

Magnetic stirrer was used for mixing with controlled speed. The stirring speed was varied from 0, 300 and 500 rpm for each batch of reaction.

3.2.1.5 Rate of addition

The ion solution of ammonium aluminum sulfate premixed with yttrium nitrate was added to the solution of ammonium hydrogen carbonate in dropwise fashion at different rate of addition. The adding rate was varied from 5, 10 ml/min and pour the whole ion solution directly into the precipitant solution.

3.2.1.6 Reaction temperature

The range of reaction temperature was varied from 30-35 (room temperature), 5-15 and 45-55°C by using water bath for maintaining temperature at desired value.

3.2.1.7 pH value of the reaction system

The precipitate was synthesized at different pH value of the reaction system. For the first system, the pH value of reaction system was kept constant at 5, 6 and 7 by adding acetic acid or ammonia solution. The pH value was monitored continuously with pH meter. For another system, the pH value of the mixture during the reaction was not controlled. The final pH value of the solution was found to be 5.7.

3.2.1.8 Calcination temperature

The precipitate was heated at a rate of 10°C/min to the desired temperature, in the range of 800-1200°C.

3.2.1.9 Variation in calcination time

The precipitate was synthesized according to the normal synthesis procedure and calcined at 1100-1200°C, using two methods with various holding times. For the first method, the precipitate was heated up from room temperature to 1200°C at rate of 10°C /min, and was held at 1200°C for various holding time, i.e. 30, 60 and 120 minutes respectively. For the second method, the precipitate was put into the oven when oven temperature was around 1140°C. The system was further heated up to 1200°C and held at that temperature for 30 minutes.

3.2.2 Fabrication of YAG specimens

In order to fabricate YAG specimens, the following steps were followed.

3.2.2.1 *Ball milling*

The synthesized YAG powder was mixed with TEOS in the amount of 0.5 wt.% in polypropylene bottle (125 ml), using ethanol as solvent. Alumina balls were used as grinding media. The powder was milled for 72 h (see Appendix C) and subsequently dried in an oven at 110°C for 24 h to eliminate residual ethanol and moisture.

3.2.2.2 *Biaxial hydraulic press*

The milled powder was pressed into a pallet of 19 mm in diameter by biaxial hydraulic press with pressure of 20 MPa.

3.2.2.3 *Cold isostatic press*

After powder was pressed into a pallet by biaxial hydraulic press, the pallet was further undergone cold isostatic press under the pressure of 300 MPa for 2 minute. The green compact was dried in the oven at 110°C for 2 h.

3.2.2.4 Pressureless sintering

The dried green bodies were sintered at 1650°C for 5 h in air under atmospheric pressure.

3.3 Characterizations

3.3.1 Characterization of the Synthesized Powder

3.3.1.1 X-Ray Diffraction (XRD)

The X-ray diffraction (XRD) analysis of powder was performed by a SIEMENS D5000 X-ray diffractometer, using Ni-filtered CuK α radiation. The scan was performed over the 2 θ range from 10° to 80°, using step size of 0.020°.

The crystallite size of the powder was estimated from the XRD line broadening according to the Scherrer equation. The value of shape factor, K , was taken to be 0.9 and α -alumina was used as an external standard.

3.3.1.2 Particle Size Distribution Analysis (PSD)

The particle size and particle size distribution were analyzed by using laser scattering particle size distribution analyzer (Mastersizer S model) at the Center of Excellence on Particle Technology, Faculty of Engineering, Chulalongkorn University.

3.3.1.3 Thermogravimetric Analysis (TGA)

The powder samples were subjected to a differential thermal analysis (Diamond Thermogravimetric and Differential Thermal Analyzer, STA 4094) to determine the temperature of possible decomposition and phase change in the range of 20-1000°C. The analysis was performed at a heating rate of 10°C/min under 50 ml/min flow of air.

3.3.1.4 Scanning Electron Microscopy (SEM)

Morphology of the sample was observed on JSM-5410LV scanning electron microscope. The SEM was operated using the secondary electron mode at 15 kV at the Research Equipment Center, Faculty of Science, Chulalongkorn University.

3.3.1.5 Transmission Electron Microscopy (TEM)

Morphology and size of primary particles of the samples were observed by transmission electron microscope (TEM) model JEM-100SX at the Scientific and Technological Research Equipment Center, Chulalongkorn University (STREC)

3.3.1.6 Fourier Transform Infrared spectroscopy (FTIR)

Functional groups in the samples were identified by using an infrared spectroscopy (Nicolet Impact 400). Before measurement, the sample was mixed with KBr and formed into a thin pellet.

3.3.2 Characterization of Green Specimens

Diameter and thickness of green specimens were measured using vernier caliper and the bulk density was calculated by the following equation.

$$\text{Bulk density } (\rho) = \frac{M}{V} \quad (3.1)$$

Where M is the mass of green pellet and V is the volume of green pellet.

3.3.3 Characterization of Sintered Specimens

3.3.3.1 *Density of the sintered specimens*

The sintered densities were measured by the Archimedes method (see Appendix D), using water as an immersion medium. The relative densities were calculated with respect to the theoretical density of $Y_3Al_5O_{12}$ (4.5 g/cm^3).

3.3.3.2 *Measurement of grain size of sintered specimens*

The microstructure of the specimens was observed by JSM-5410LV scanning electron microscope. The SEM was operated using the secondary electron mode at 30 kV at the Research Equipment Center, Faculty of Science, Chulalongkorn University. The specimens were polished to get mirror-like surface with SiC abrasive paper grit number 600 followed by diamond paste ($6 \mu\text{m}$). Before observing by SEM, the specimens were thermally etched at the sintering temperatures for 15 minutes.

CHAPTER IV

RESULTS AND DISCUSSION

In this chapter, the experimental results and discussion are presented. The chapter can be divided into 4 sections as follows:

Section 4.1 presents results from preliminary experiments of standard synthesis procedure. The phase formation, morphology and particle size of YAG powder are reported.

Section 4.2 describes the effects of yttrium-to-aluminium ratio, reaction temperature, pH of the reaction, precipitation processes and variation of calcination time on phase formation, structure and morphology of YAG powder.

Section 4.3 discusses particle size distribution of YAG powder prepared from different conditions in precipitation methods. Further investigation on effects of various factors such as concentration of precursors, speed of mixing and dropping rate on morphology of powder synthesized by the precipitation method are also investigated.

Section 4.4 discusses results for the fabrication of synthesized YAG powder into YAG ceramics, including relative density and structure of the fabricated YAG specimen. The results are compared with those obtained from commercial YAG powder.

4.1 Preliminary Experiments

In the preliminary experiments, 250 ml of ammonium aluminium sulfate (AAS) and yttrium nitrate ($Y(NO_3)_3$) solution with molar ratio for Y:Al of 3:5 was gradually added to 100 ml of ammonium hydrogen carbonate (AHC) solution with the concentration ratio of AAS to AHC of 0.2:2.0 mol/l at the room temperature. The addition rate of the ion solution into the precipitant solution was controlled at 5 ml/min. The mixture was constantly stirred using magnetic stirrer rotating at 500 rpm. For these experiments, pH of the mixture during the reaction was not controlled.

After the precipitation was finished, the completeness of the reaction was confirmed by further adding the ions solution into the clear liquid of the precipitation system that had been centrifuged to remove the precipitate. It was found that the precipitation was already completed since there was no more precipitation taking place. The completeness of the reaction may be further confirmed by investigating the cation content remaining in the liquid by the ICP (Inductively Coupled Plasma) technique. The XRD patterns of the as obtained precipitates as well as that of the powder calcined at different temperatures are shown in Figure 4.1.

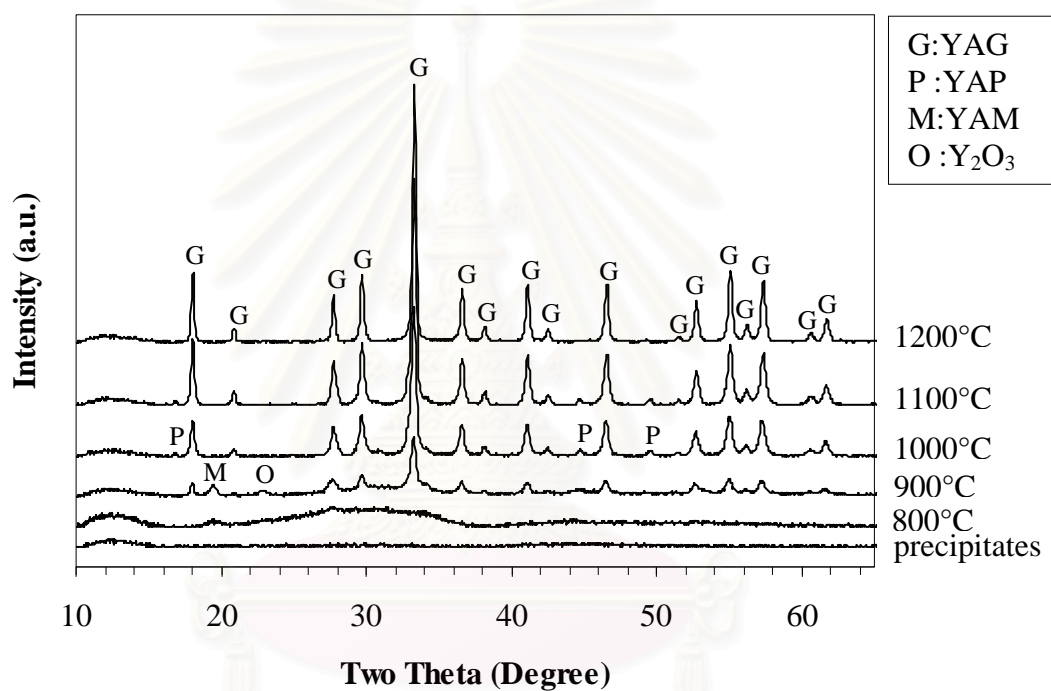


Figure 4.1 XRD patterns of the powder calcined at various temperatures for 2 h.

Figure 4.1 shows XRD patterns of YAG precursor (i.e. the precipitate) and powders which were calcined at 800-1200°C for 2 h. No obvious diffraction peak is observed from the powder calcined at temperature of 800°C. It is indicated that the precipitate powders remain amorphous until this temperature. From the previous work by Su et al. [38], it revealed that Y³⁺ usually precipitates as basic salt of approximate formula Y₂(OH)₅·X·nH₂O (where X is NO₃⁻ or Cl⁻ depending on the type of starting salts, and n = 1-2), thus it can be supposed that the approximate formula of the precipitate is Al(OH)₃·0.3[Y₂(OH)₅(NO₃)_x·nH₂O]. All of the characteristic XRD peaks for YAG phase start to appear when at 900°C. When the precipitates are

calcined at 900 to 1100°C, intermediate phases are detected and identified as YAP (YAlO_3), YAM ($\text{Y}_4\text{Al}_2\text{O}_9$) and yttrium oxide (Y_2O_3). The precursor powder initially crystallizes into YAG mixed with YAM phase and yttrium oxide phase at 900°C. The higher calcination temperature, the higher intensity of diffraction peaks of YAG observed. As the calcination temperature is increased to 1000°C, YAP phase is still remain while the YAM and yttrium oxide phase are disappeared. At 1100°C, the diffraction peaks of YAG become sharper and stronger in intensity, while the intensity of peaks of YAP phase is decreased. It is indicated that strong cubic YAG phase is formed. The precursor is converted to pure phase of YAG without any other intermediate after calcined at 1200°C.

The results from TG-DTA analysis in oxygen atmosphere, using heating rate of 10°C/min, of the precipitate powder obtained from the standard synthesis procedure are shown in Figure 4.2. The TG curve indicates an overall weight loss of approximately 40%. Many of this weight loss take place at temperature up to 600°C. The broad endothermic peak in DTA curve at temperature about 200°C accompanied by the weight loss is due to the evaporation of water. Broad exothermic peak and the gradual weight loss appear from 200 to 600°C, which can be attributed to decomposition of ammonia and carbonate. Two broad and slightly exothermic peaks at 806 and 898°C can be attributed to the crystallization of small amount of intermediate phases which are identified as yttrium oxide, YAM and YAP. Then, the sharp weight loss starting at temperature of 900°C, which is accompanied by a sharp exothermic peak at about 950°C in DTA curve, can be attributed to crystallization and crystal growth of the product. It can be seen that phase transformation observed by XRD analysis is consistent with DTA observations.

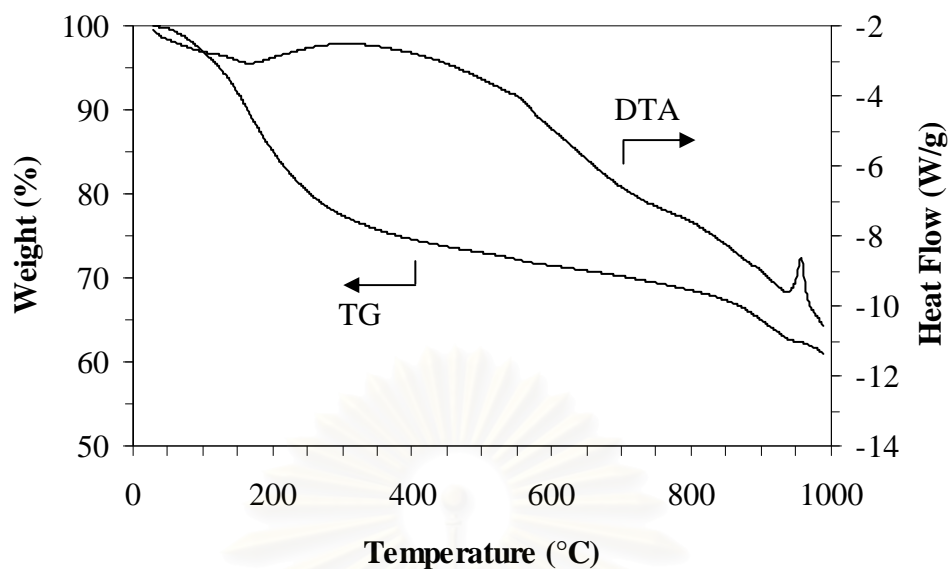


Figure 4.2 TG/DTA curve of the precipitate, which was synthesized with molar ratio for Y:Al of 3:5.

The FTIR spectra of the as-obtained precipitates as well as that of the powder calcined at different temperatures are shown in Figure 4.3. FTIR spectra of the precipitates and powder calcined at 800-1200°C show the wide band between 3200 to 3500 cm^{-1} , and a band at 1640 cm^{-1} , which can be attributed to the O-H stretching vibration of all hydroxyl groups including moisture absorbed on the surface of the sample [39]. After calcined at 900°C, new absorption bands appear at 770 and 625 cm^{-1} which represent the characteristic bands of Al-O vibration [40]. Moreover the absorption bands positioned at wavenumber of 708 and 551 cm^{-1} , which represent the characteristic bands of Y-O vibration [40], are also detected. These bands become sharper with the increasing calcination temperature. These results indicate the decomposition of the starting organics and suggest the formation of compound containing Y, Al and O. Furthermore it also indicates that the formation of Y-O and Al-O bonding within the sample increases with the increasing calcination temperature. Unidentified absorption bands at wavenumber approximately in the range of 1100-1500 cm^{-1} are detected in the powder calcined at 800-1200°C. The pattern of these bands is changed as the sample is calcined at 1200°C. Similar behavior is also observed for unidentifiable absorption bands in the range of 2200-2400 cm^{-1} , which occur in the powder calcined at 900°C. These bands disappear after the calcination temperature is increased. Furthermore, the unidentified band at

2345cm^{-1} appears at 800°C . It shifts to the wave number of 2360 cm^{-1} as the powder is calcined at $1000\text{-}1200^\circ\text{C}$. The attempt to identify functional groups associated with all of these bands was unsuccessful.

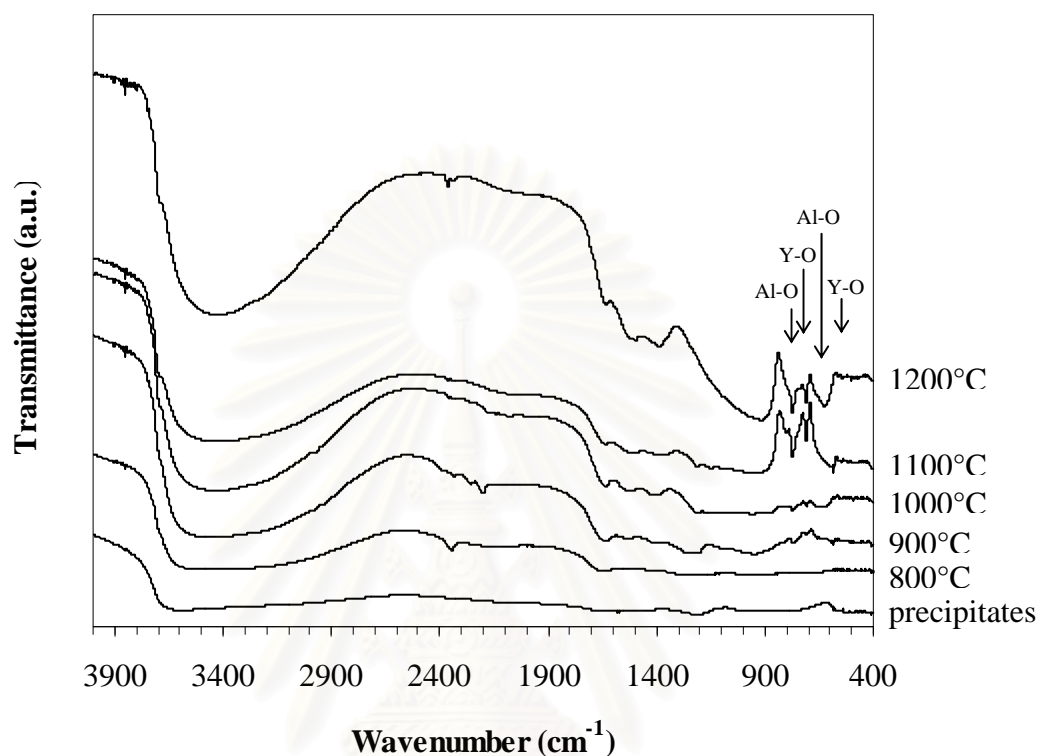


Figure 4.3 FTIR spectra of the precipitates and YAG products calcined at different temperatures.

Figure 4.4 shows TEM micrographs of the precipitates and the YAG powders calcined at 1000 , 1100 and 1200°C , respectively. The micrographs indicate that all particles are fairly uniform. The mean particle size was estimated from both width and length of large number of particles observed in TEM micrographs. The average particle size of the sample calcined at 1000°C (Figure 4.4b) is in the range of $20\text{-}30$ nm. The particle size is increased with the increasing calcination temperature. Particles calcined at 1100°C are about $30\text{-}50$ nm in size and the particle size increases up to around $60\text{-}80$ nm when the calcination temperature is increased to 1200°C . Beside the particle size, the average size of YAG nano-crystallites was also estimated from the broadening of XRD diffraction peaks, using the Scherrer's equation (Appendix B). The average crystallite sizes of all samples are in the range of $20\text{-}70$

nm. The crystallite size is increased with the increasing calcination temperature, as shown in Figure 4.5.

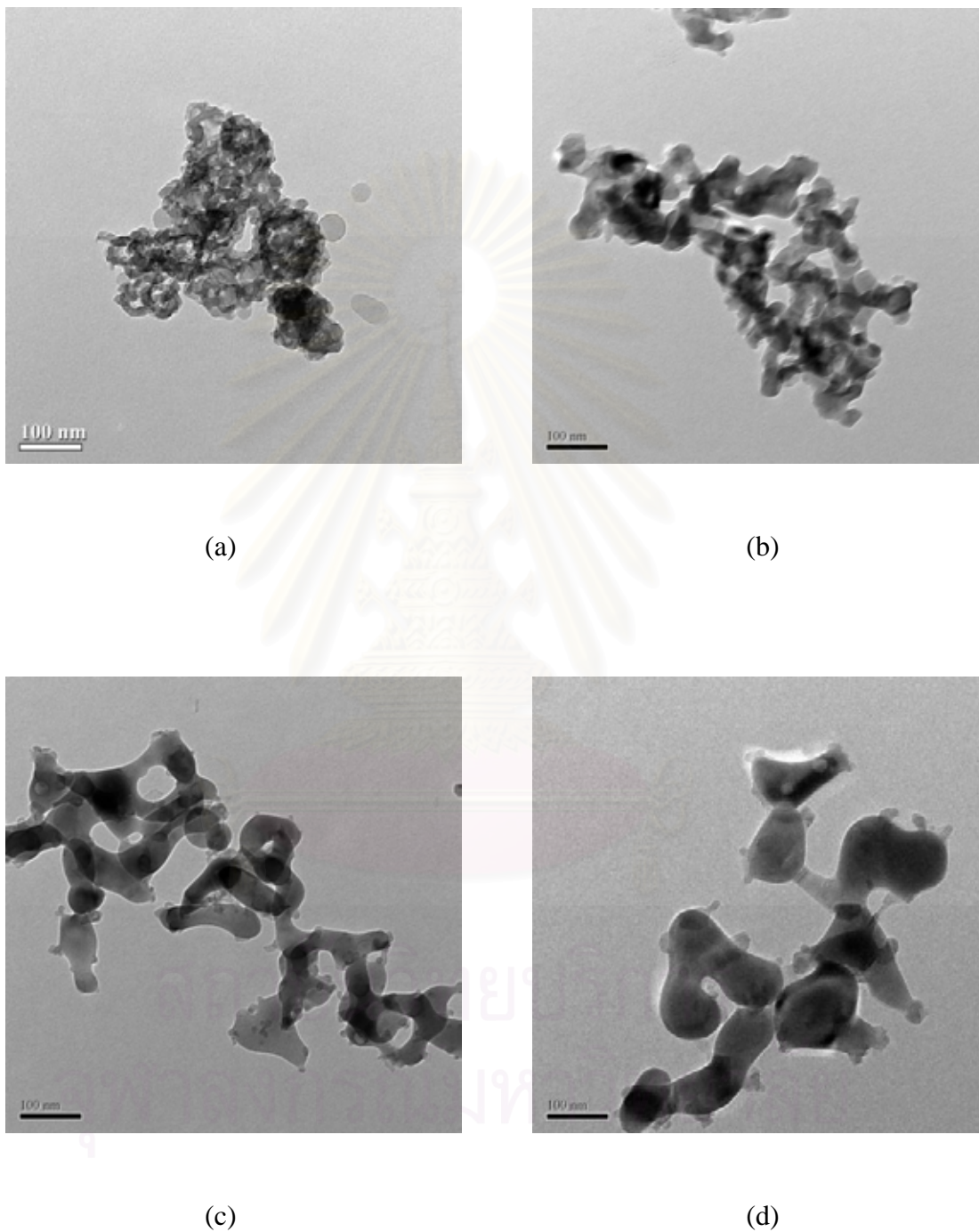


Figure 4.4 TEM micrographs of the precipitates (a), the YAG powder which was calcined at 1000°C (b), 1100°C (c), and 1200°C (d) for 2 h.

Figure 4.5 exhibits the crystallite size and mean particle size of the YAG powder as a function of calcination temperature. It is found that, for the powder calcined at 1000 and 1100°C, the particle sizes observed in TEM micrographs are only slightly larger than the crystallite sizes, indicating that the calcined powder is mostly single crystals. As the calcination temperature is increased from 1000 to 1100°C, the graphs showing the increase in both crystallite size and particle size have almost the same slope. These results suggest that the crystal growth of the powder occurs from the direct transformation from amorphous precipitates to YAG phase with small effect from sintering during the calcination in the range of 1000-1100°C. As the calcination temperature is increased to 1200°C the particle size becomes much larger than the crystallite size. Moreover, the increase in particle size occurs more rapidly than the crystallite size, since the crystal growth and the sintering among particles take place simultaneously. These results are consistent with the TEM images (Figure 4.4), which show that the secondary particles are formed from the sintering of small primary particles. The extent of the sintering increases upon the increase in calcination temperature and calcination time. Furthermore, it can be observed that size of the primary particles is increased by grain growth, while size of the secondary particles is also increased by sintering.

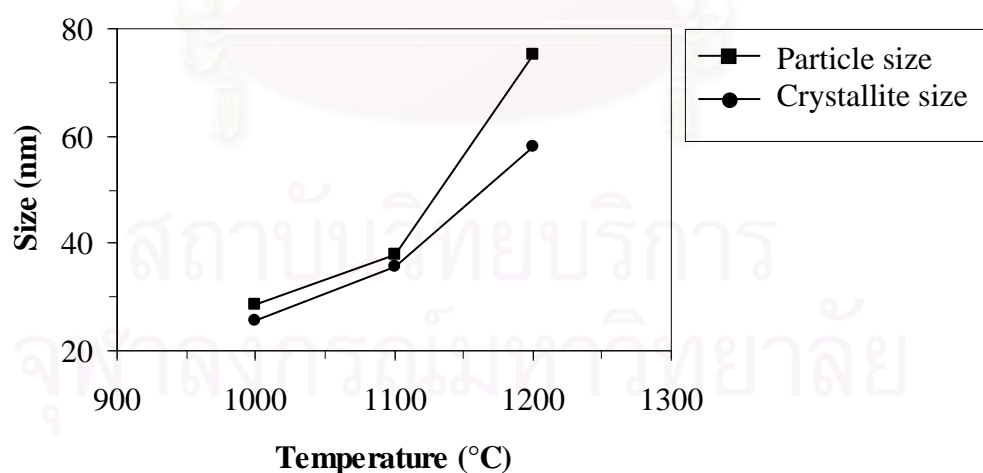


Figure 4.5 The particle sizes observed in TEM micrographs and crystallite sizes estimated from XRD pattern using the Scherrer's equation, as a function of calcination temperature.

4.2 Phase Formation of YAG Powder

In this section, the effects of yttrium-to-aluminium ratio, reaction temperature, pH of the reaction, precipitation processes and variation of calcination time on phase formation, structure and morphology of YAG powder are presented.

4.2.1 Effects of Yttrium-to-Aluminium Ratio

In this work, the yttrium-to-aluminium ratio of the ion solution was varied from 2:5, 3:5 and 4:5. It is indicated that the content of yttrium has significant effect on phase formation of YAG powder as shown in the Figure 4.6-4.8. Figure 4.6 shows the XRD patterns of the powder prepared with Y-to-Al molar ratio of 2:5 and calcined at 800-1200°C for 2 h. It is found that no diffraction peak appears at 800°C, indicating that the precipitate powder is amorphous until this temperature. When the sample is calcined at 900°C, small amount of YAM and yttrium oxide are observed. At 1000°C, the diffraction peaks of YAP appear together with those of YAG, while YAM and yttrium oxide phase disappear. With the increase in calcination temperature to 1100°C, the diffraction peaks of YAG become sharper and the intensity becomes higher. The precursor converts to pure phase of YAG after calcination at 1200°C.

The XRD patterns of the powder prepared with Y-to-Al molar ratio of 4:5 and calcined at 800-1200°C for 2 h are shown in Figure 4.7. It is indicated that the precipitates remain in amorphous phase until about 800°C. At 900°C, the small diffraction peaks of YAG appear with the presence of small peaks of intermediate phase, which are identified as YAM and yttrium oxide. At 1000°C, the YAM and yttrium oxide phases disappear while the small diffraction peaks of YAP phase appear instead. The higher the calcination temperature, the higher intensity of YAG and the lower intensity of YAP observed. Only YAG phase is detected without the formation of any intermediate phase at 1200°C. The XRD patterns of the powder synthesized with various Y-to-Al molar ratios and calcined at 900°C (i.e. transition point for YAG formation) for 2 h are compared in Figure 4.8.

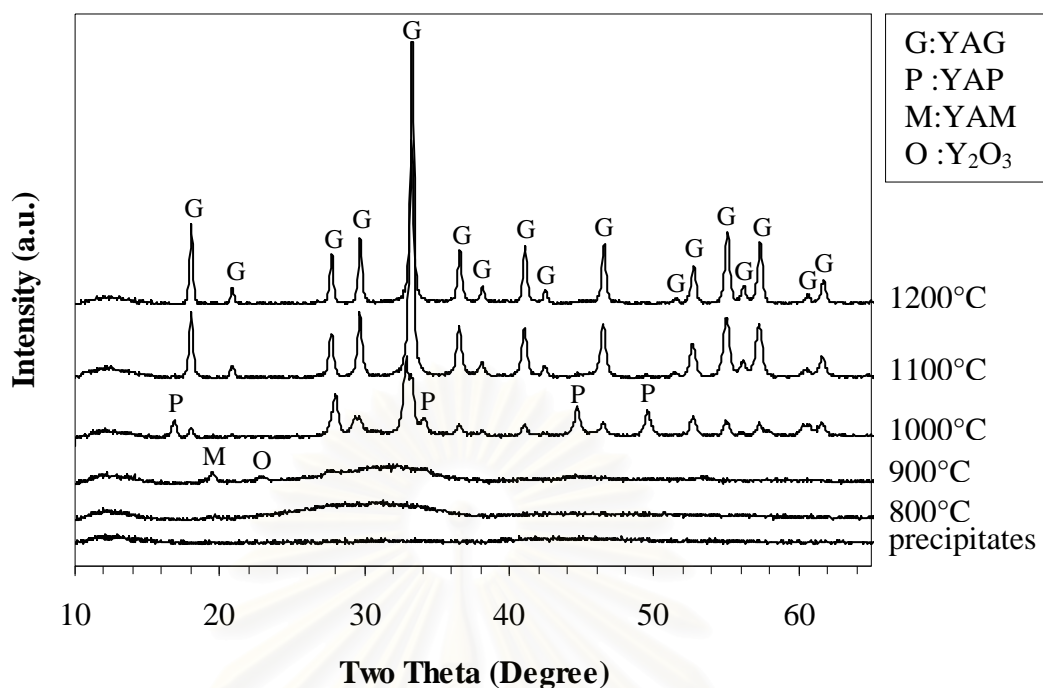


Figure 4.6 XRD patterns of the powder prepared with Y-to-Al molar ratio of 2:5 and calcined at various temperatures for 2 h.

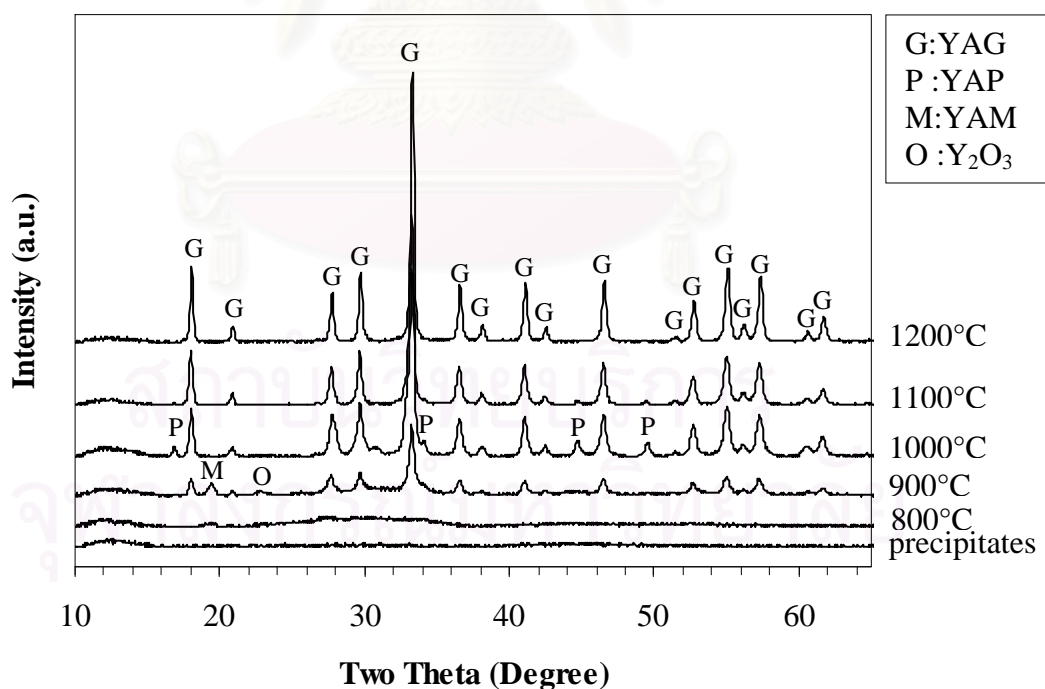


Figure 4.7 XRD patterns of the powder prepared with Y-to-Al molar ratio of 4:5 and calcined at various temperatures for 2 h.

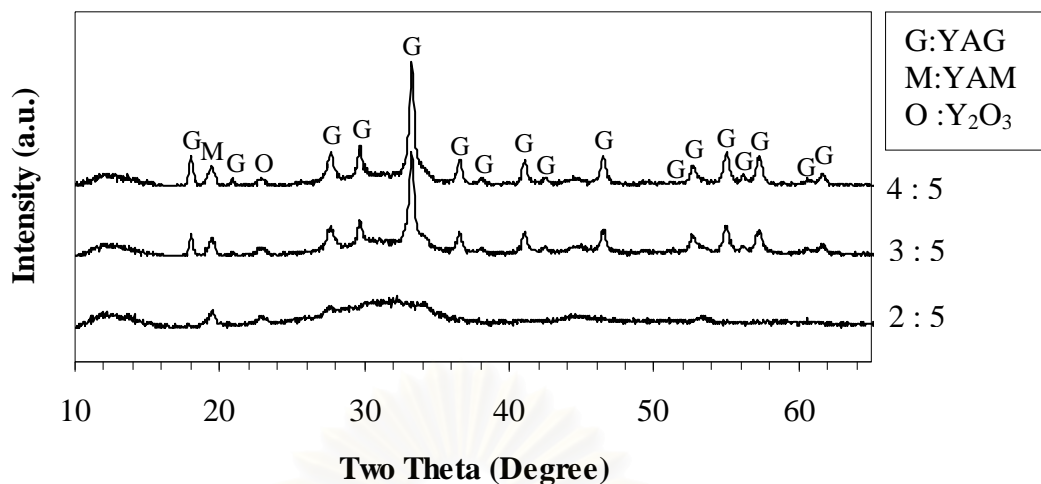


Figure 4.8 XRD patterns of the powder prepared with various molar ratios of Y:Al and calcined at 900°C for 2 h.

With the molar ratio of 2:5, no obvious diffraction peaks of YAG are observed when the sample is calcined at 900°C. In case of the sample with low yttrium content, it requires higher calcination temperature to form YAG phase. At the same calcination temperature of 900°C, clear diffraction peaks of YAG are already observed for the samples with Y:Al ratio of 3:5 and 4:5. The results for the phase formation of these two samples are the same. According to these results, it is indicated that, when the molar ratio of Y:Al is lower than the stoichiometric ratio of 3:5, it requires higher energy to form YAG phase. However, with the increasing Y:Al molar ratio to the level higher than the stoichiometric ratio, the YAG phase forms at the same temperature as in case of the sample with stoichiometric ratio. These results are confirmed by the results from TG/DTA analyses of the precipitates synthesized with various Y:Al molar ratio, as shown in Figure 4.9.

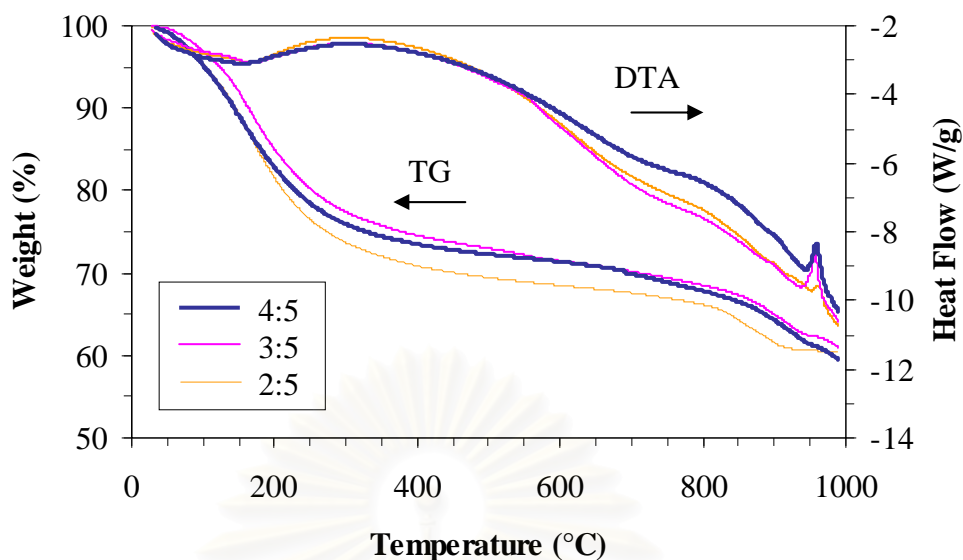


Figure 4.9 TG/DTA curves of the precipitates synthesized with the Y-to-Al molar ratio of 2:5, 3:5 and 4:5.

The TG curves demonstrate that the majority of weight losses for all samples, i.e. about 40%, occurs up to the temperature of 600°C. The endothermic peaks at 200°C occur due to the removal of bound water. The broad exothermic peaks in the DTA curve accompanied with the weight loss in the TG curve at temperature in the range of 200-600°C indicates the combustion or decomposition of organic groups within the precipitates. Two broad exothermic peaks are observed at about 800 and 900°C on all three samples, which indicate the formation of intermediates before the formation of YAG phase. The first one is the broad exothermic peak which can be attributed to the crystallization of YAM and yttrium oxide phase. The followed one is the slightly broad exothermic peaks which can be attributed to the crystallization of YAP phase. These results are consistent with the phase transformation observed by XRD observations. The sharp exothermic peaks are detected at 960, 957 and 959°C for the sample with Y:Al molar ratio of 2:5, 3:5 and 4:5 respectively. These peaks can be attributed to crystallization of YAG. The exothermic energy associated with the formation of YAG phase can be estimated from the area under these exothermic peaks. For the sample with Y:Al molar ratio of 2:5, 3:5 and 4:5, the energy determined is 19.36, 103.10 and 114.20 J/g, respectively. It shows that the exothermic energy for the sample with Y:Al ratio of 3:5 is similar to that of the sample with the ratio of 4:5, while the energy for the sample with Y:Al ratio of 2:5 is the least. Since

the exothermic energy recorded is the energy released after the formation of YAG phase, small amount of the energy released indicates that there is small amount of YAG in the sample. The sharp exothermic peak for the sample with Y:Al ratio of 2:5 starts at higher temperature than the sample with Y:Al molar ratio of 3:5 and 4:5. Therefore, when Y:Al molar ratio is lower than the stoichiometric ratio (e.g. Y:Al = 2:5), the formation of YAG phase requires higher energy for the crystallization and crystal growth of YAG than the case of sample with the ratio equal to or higher than the stoichiometric ratio.

The FTIR spectra of the powder synthesized with Y:Al molar ratio of 2:5 and 4:5 and calcined at various temperatures for 2 h are shown in Figure 4.10 and 4.11, respectively.

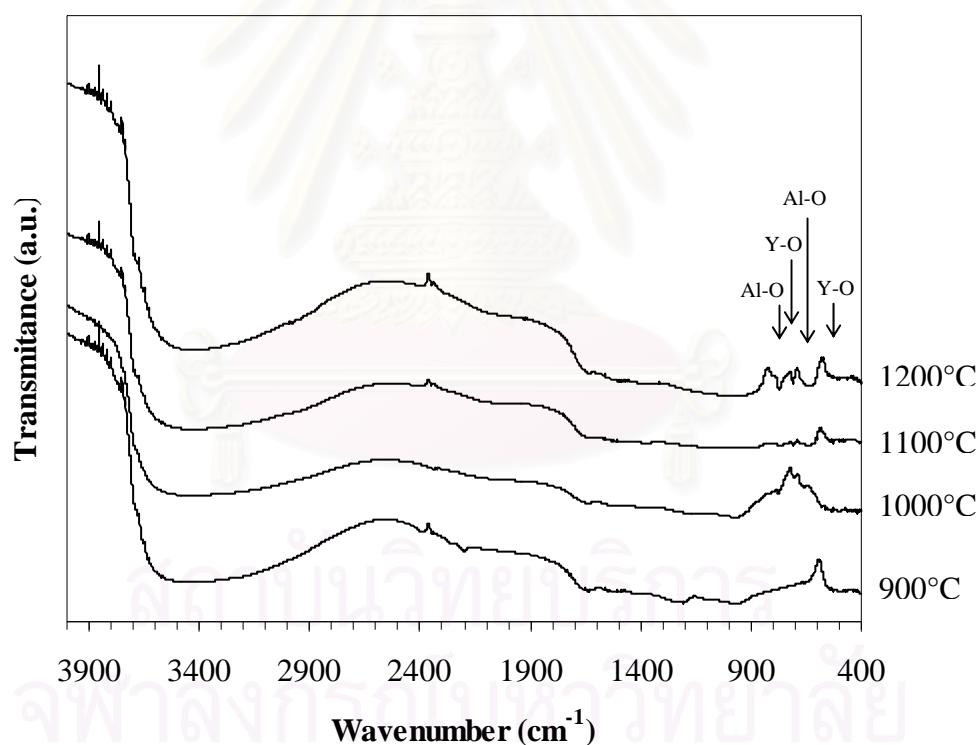


Figure 4.10 FTIR spectra of the powders synthesized with Y:Al molar ratio of 2:5 and calcined at various temperatures for 2 h.

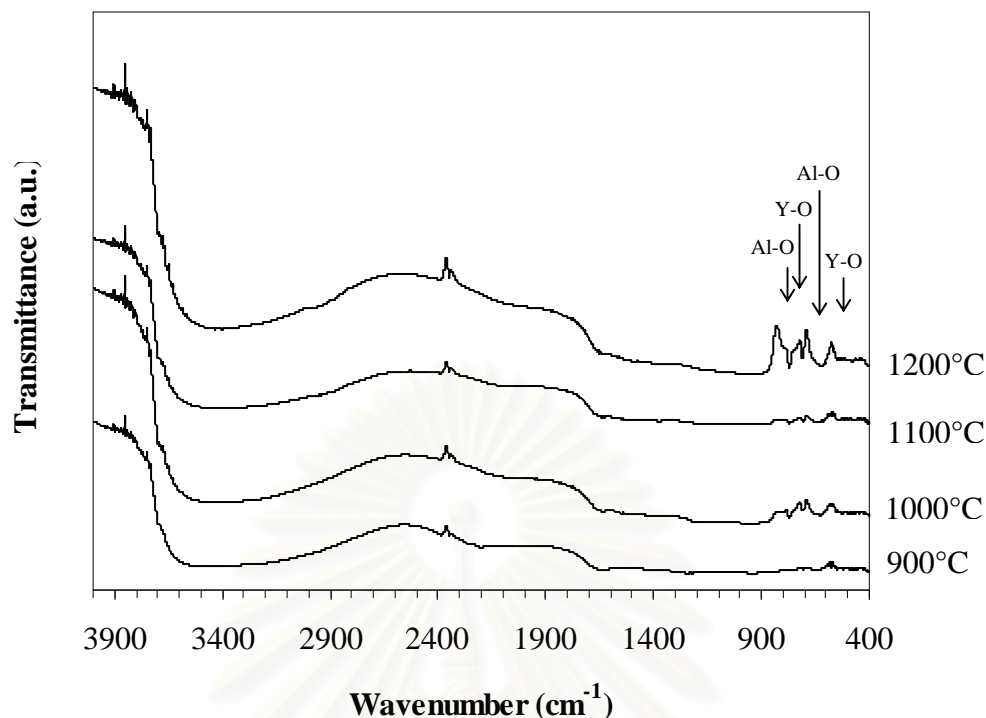


Figure 4.11 FTIR spectra of the powders synthesized with Y:Al molar ratio of 4:5 and calcined at various temperatures for 2 h.

When the precursor is calcined at 900 to 1200°C, the samples show absorption bands at wavenumber between 3200 to 3500 cm^{-1} and 1640 cm^{-1} , which can be assigned to the O-H stretching vibration of hydroxyl groups of water absorbed on the surface of sample [39]. The peaks at about 770 and 625 cm^{-1} represent the characteristic bands of Al-O vibration, while the peaks at about 708 and 551 cm^{-1} represent the characteristic bands of Y-O vibration [40]. These characteristic peaks become sharper with the increase in the calcination temperature, which indicates the higher amount of bonding of Y-O and Al-O formed in the sample. The figure shows that the absorption bands for the sample with Y:Al ratio of 3:5 is similar to that of the sample with Y:Al ratio of 4:5. On the contrary, for the sample with Y:Al ratio of 2:5, no absorption band of Al-O and Y-O vibration are detected when the sample is calcined at 900°C. Therefore, when the molar ratio of Y:Al is less than the stoichiometric ratio, it requires higher energy to form YAG phase. It can be seen that the FTIR results are in good agreement with XRD and TG/DTA observations. It should be noted that very slight unidentified absorption bands between 1100-1500 cm^{-1} and clear absorption band at about 2360 cm^{-1} , which appear in the sample with

Y:Al ratio of 3:5, are also detected for the sample with Y:Al ratio of 2:5 and 4:5 after calcined at 900-1200°C. Similar behavior is also observed for unidentifiable absorption bands in the range of 2200-2400 cm^{-1} , which occur in the powder calcined at 900°C. These bands disappear after the calcination temperature is increased. Nevertheless, the attempt to identify the functional groups associated with these absorption bands was not successful.

4.2.2 Effects of Reaction Temperature

In this section, the reaction temperature was varied from 30 (room temperature), to 5-15 and 45-55°C by using water bath for maintaining temperature at desired value. It is indicated that the reaction temperature has significant effect on phase formation of YAG powder as shown in Figure 4.12-4.13, which show the XRD patterns of the precipitates synthesized at 10 and 50°C, respectively, and subsequently calcined at 800, 900, 1000, 1100 and 1200°C.

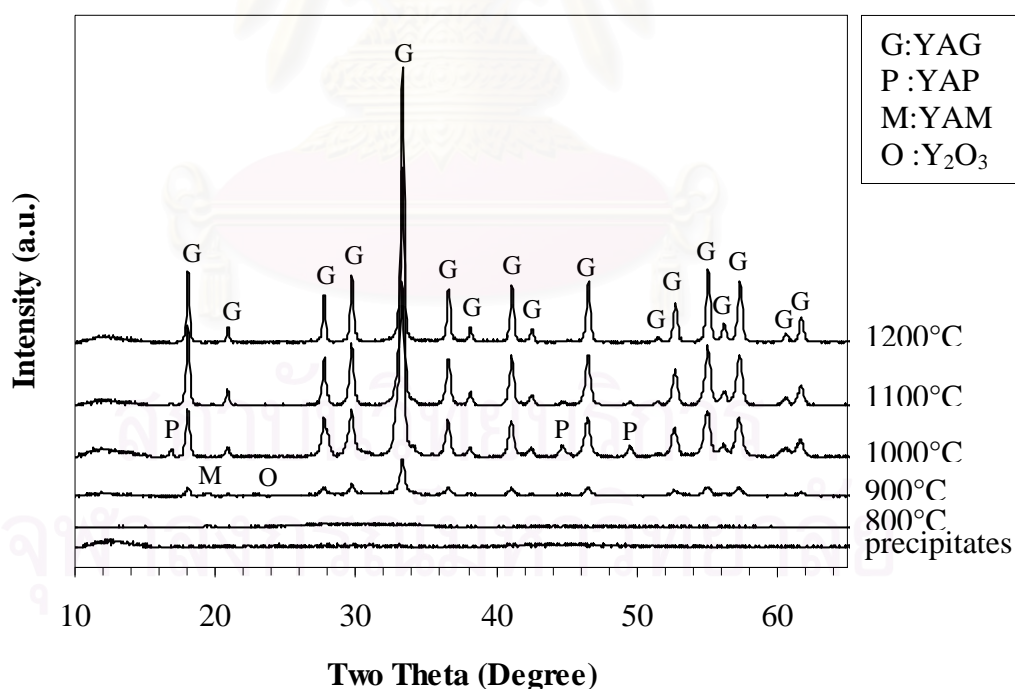


Figure 4.12 XRD patterns of the precipitates prepared at 10°C and calcined at various temperatures for 2 h.

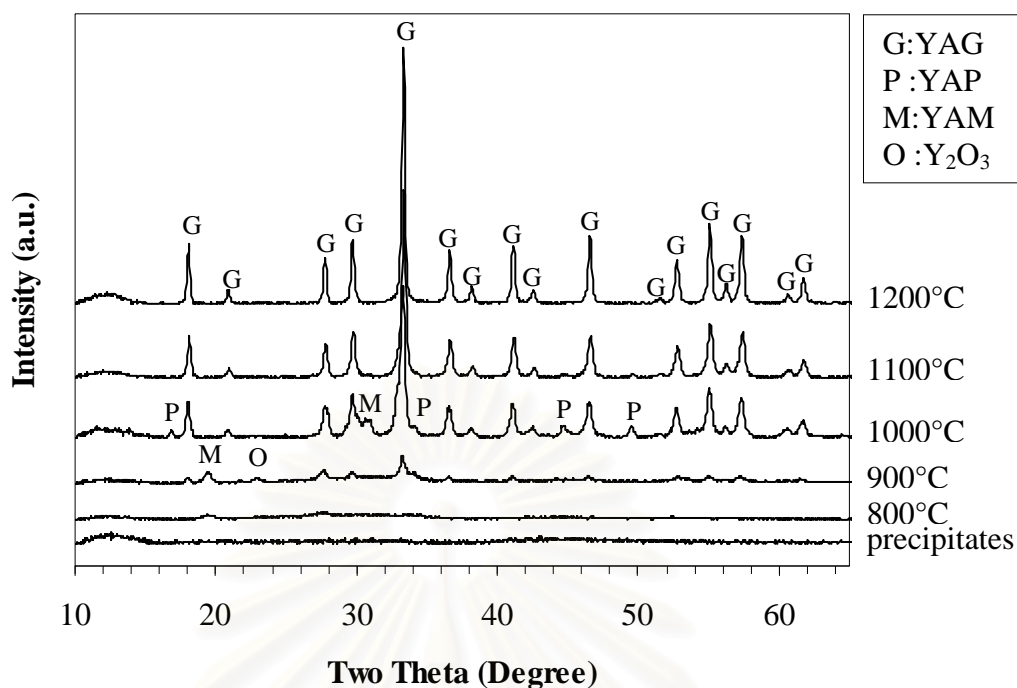


Figure 4.13 XRD patterns of the precipitates prepared at 50°C and calcined at various temperatures for 2 h.

After calcined at 800°C, the powders precipitated at both 10 and 50°C are still amorphous. Generally, the results for increasing the calcination temperature to 900–1200°C from the precipitates synthesized at both 10 and 50°C are similar. The only difference is observed from the calcination at 1000°C whereas the XRD pattern of the precipitates synthesized at 50°C shows the presence of YAM phase. The precipitates synthesized at both 10 and 50°C convert to YAG phase almost completely as the calcination temperature is raised up to 1100°C. Only small amount of YAP phase has remained in the samples. After calcination at 1200°C, pure YAG is the only phase detected in diffraction peaks. The decomposition of the reactants, especially AHC, occurs when the reaction temperature is increased, as witnessed from the increased number of bubbles formed in solution, even before the reaction. As the result, distribution of Al^{3+} and Y^{3+} during the precipitation process is not uniform and therefore brings about non-homogeneity of the precipitates such that the local deviation of Y-to-Al molar ratio may occur. Consequently, intermediate phases will appear when this precipitate is calcined. The results of YAG formation from XRD are confirmed by the results of TG /DTA as shown in Figure 4.14.

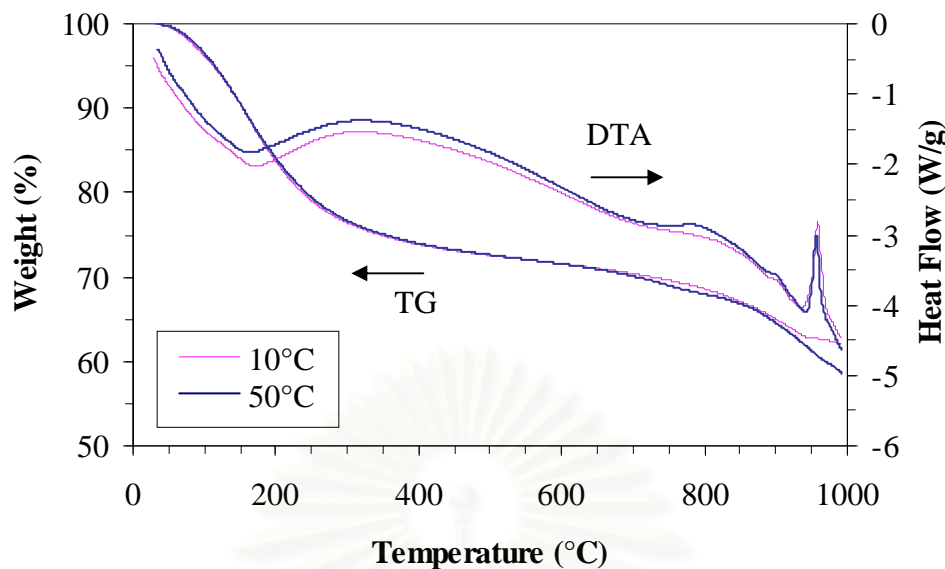


Figure 4.14 TG/DTA curves of the precipitates synthesized at the reaction temperature of 10 and 50°C.

In Figure 4.14 the TG/DTA curves of the precipitates prepared at different reaction temperatures are reported. It shows the similar features of previously described for Figure 4.2 and 4.9. In the same manner as the results presented in the preliminary section, two broad exothermic peaks are observed at about 800 and 900°C on all three samples, which indicate the formation of intermediates before the formation of YAG phase. Then, the sharp exothermic peak at about 958, 957 and 956°C is observed from the sample precipitated at 10, 30 (room temperature) and 50°C, respectively. These three samples also show different amount of exothermic energy released after the YAG formation, which is calculated from the area under this exothermic curve. The sample synthesized at the temperature of 10, 30 and 50°C reveals the exothermic energy of 122.6, 103.10 and 84.70 J/g, respectively. When the reaction temperature is increased, lower energy is released. The premature decomposition of the reactants, especially AHC, by high reaction temperature decreases the formation of precipitates, leading to small amount of YAG formed in the sample. Nevertheless, it was observed that the change in the reaction temperature have less effect on the reaction rate than the decomposition of reactants since the reaction between the ions solution and the AHC solution to form precipitates takes place instantaneously. White precipitates can be observed immediately after the ions

solution is titrated into the AHC solution. It can be confirmed by the result of DTA that the precipitates synthesized at 10°C release the highest amount of energy to form the highest amount of YAG among all three samples investigated. The decomposition of the reactants has the effect on the formation of intermediate after calcination as well.

Figure 4.15 and 4.16 show the FTIR spectra of the precipitates prepared at 10 and 50°C and subsequently calcined at 900-1200°C.

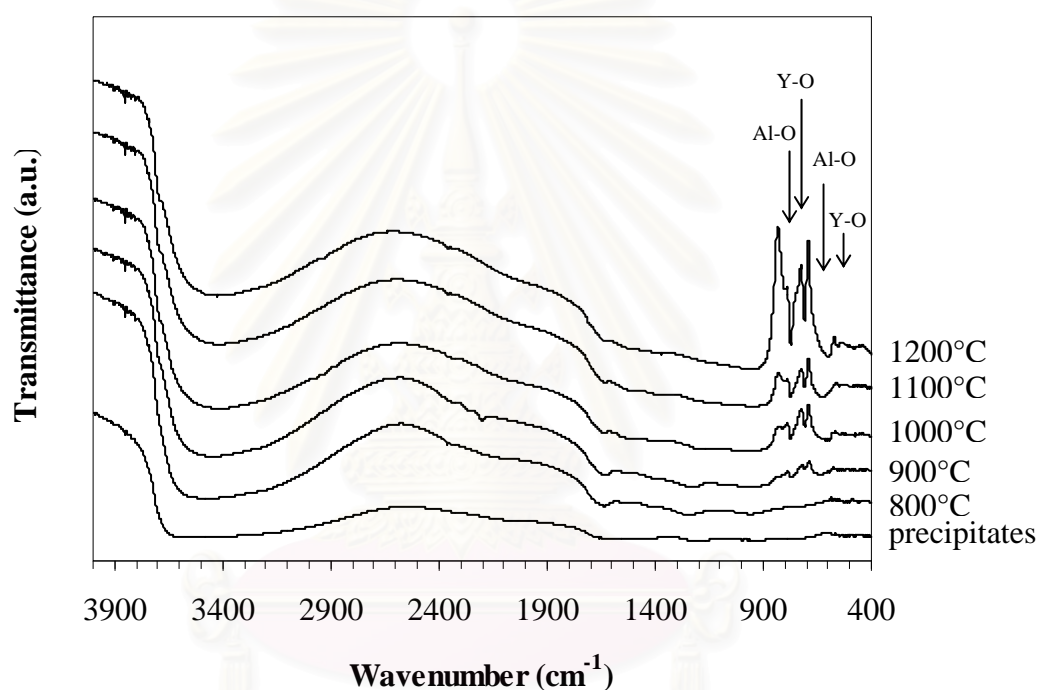


Figure 4.15 FTIR spectra of the precipitates prepared at 10°C and calcined at various temperatures for 2 h.

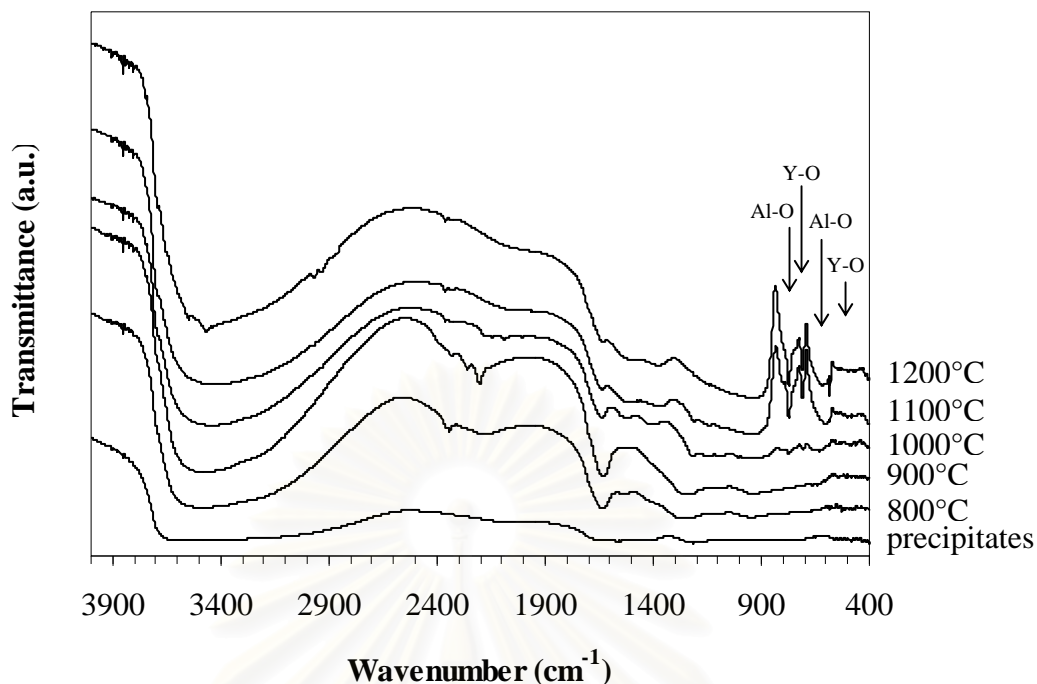


Figure 4.16 FTIR spectra of the precipitates prepared at 50°C and calcined at various temperatures for 2 h.

The FTIR spectra in Figure 4.15 and 4.16 reveal similar set of absorption bands as those reported for sample precipitated at room temperature, except that the intensity of the characteristic absorption bands for Al-O and Y-O vibration from the precipitates synthesized at 50°C and calcined at 900°C is much lower than observed earlier. It is indicated that the amount of Al-O and Y-O bonds within such sample is low because the reactants has already been decomposed by high reaction temperature. The bands become sharper as the calcination temperature is increased, which shows that the formations of these bond are increased. It is noted that very slight unidentified absorption bands between 1100-1500 cm^{-1} and at 2360 cm^{-1} are found from the precipitates prepared at 10°C at all calcination temperatures. In addition, very slight absorption bands between 2200-2400 cm^{-1} are also detected when the sample is calcined at 900°C. In contrast, these absorption bands are distinct for the precipitates prepared at 50°C at all calcination temperatures.

4.2.3 Effects of pH of the Reaction System

Controlling pH at a constant value during the precipitation process is very important for obtaining pure YAG phase. In this section, pH of the reaction system was kept constant at 5, 6 and 7 by adding acetic acid or ammonia solution. The XRD patterns of the resulting powders that have been calcined at various temperatures for 2 h are shown in Figure 4.17 and 4.18.

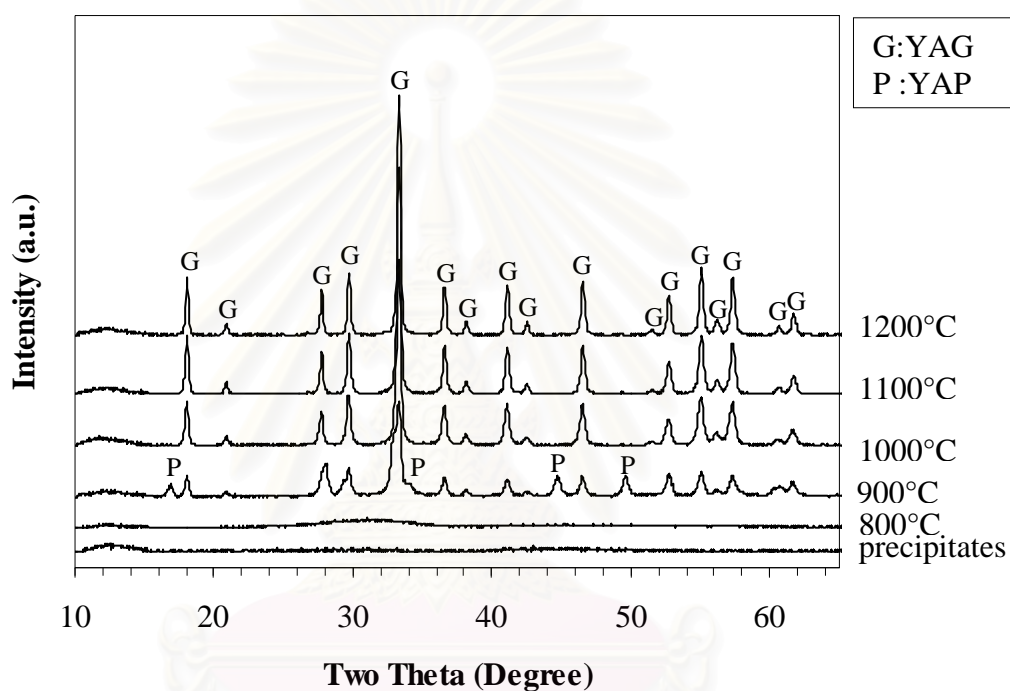


Figure 4.17 XRD patterns of the precipitates synthesized at pH 6 and calcined at various temperatures for 2 h.

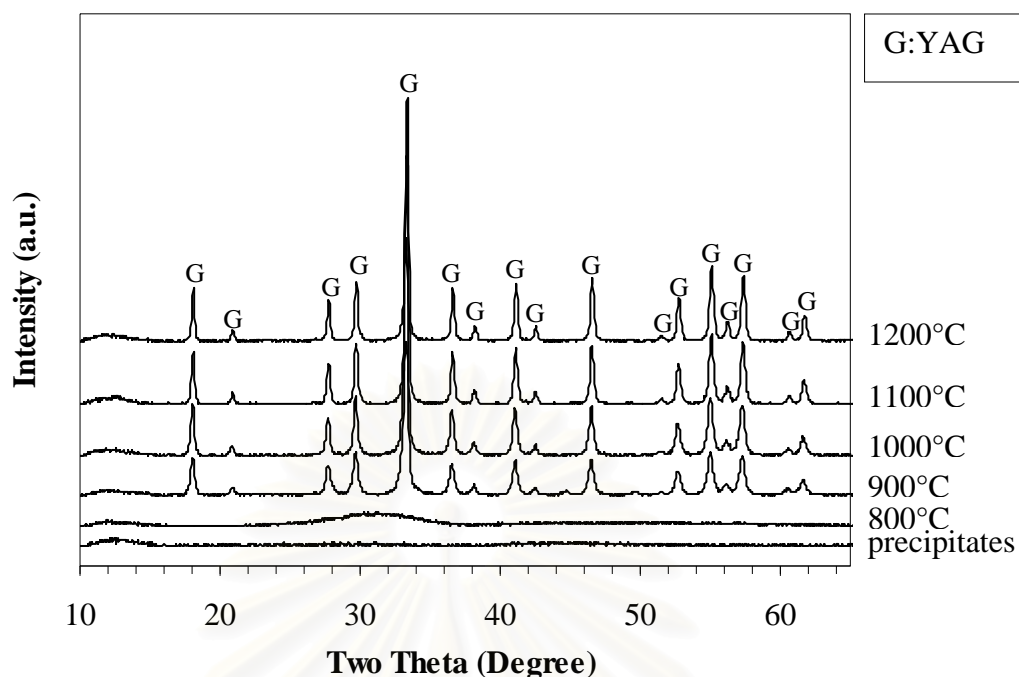


Figure 4.18 XRD patterns of the precipitates synthesized at pH 7 and calcined at various temperatures for 2 h.

When pH of the reaction system is adjusted to 5 by adding acetic acid, the reaction does not proceed because H^+ from the acid reacts with the reactants, resulting in no the precipitate formed. For the powders synthesized by controlling pH of the reaction system at 6 and 7, they are found to be amorphous upon the calcination at temperature up until about 800°C, above which crystallization take place. For the powder synthesized at pH 6, YAG phase crystallizes at 900°C together with the presence of small fraction of YAP phase. The YAP disappears after the calcination temperature is increased to 1000°C, leaving YAG as the only phase presented in the sample. On the other hand, the sample prepared at pH 7 shows no sign of any intermediate phase throughout the calcination process. YAG is the only crystalline phase formed at the calcination temperature of 900°C. Above 900°C, continuous refinement of shape and intensity of the XRD peaks are observed, indicating crystallite growth of the YAG powder as temperature increases.

These results indicate that controlling pH at a constant value is very important for obtaining pure YAG phase. The native pH value of the ions solution and the precipitant (i.e. AHC solution) is 2.6 and 7.8, respectively. If pH value of the mixture

is not controlled, pH of the mixture fluctuates intensively during the addition of the ions solution into the AHC solution. Therefore, hydroxides of Al^{3+} and Y^{3+} are exposed to the precipitant at different pH values, which results in the non-uniform distribution of Al^{3+} and Y^{3+} as well as the deviation of the local Y-to-Al ratio from the stoichiometric value of 3:5. As the result, intermediate phases will appear when this precipitate is calcined. For the controlled pH value of 7, the pH of the mixture is kept in the range between 7.5 to 7.9 so that the pH system is not changed dramatically from the pH of AHC solution.

TG/ DTA curves of the precipitates produced by controlling pH of the reaction system at 6 and 7 are given in Figure 4.19.

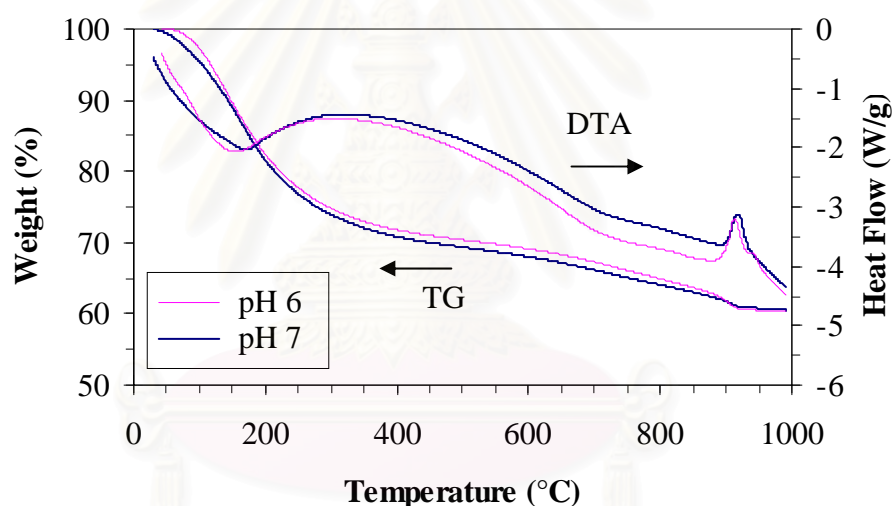


Figure 4.19 TG/ DTA curves of the precipitates synthesized at pH 6 and 7.

The TG/DTA curves of two samples synthesized with controlled pH value show similar features as previously described for Figure 4.2, except that there are no broad exothermic peaks at 800 and 900°C which are associated with the formation of intermediate phases as seen in the previous section. However, the sharp exothermic peaks of two samples appear at almost the same temperature. For the precipitates synthesized at pH 6, the sharp exothermic peak presents at 913°C which is followed by a broad and slight exothermic peaks at 942°C. These exothermic peaks are associated with the crystallization of YAG, as previously proposed by Yamaguchi et

al [42]. It can be described that the first sharp exothermic peak is associated with the crystallization of YAP, whereas the second slightly exothermic peak at higher temperature can be attributed to the transformation from the hexagonal YAP phase to YAG phase identified by XRD analysis (Figure 4.17). The formation of YAP (hexagonal) in the precipitates prepared at pH 6 is the result of the deviation of pH of the system from the pH of AHC solution, which consequently causes non-uniform distribution of Al^{3+} and Y^{3+} as well as the deviation of the Y-to-Al ratio from the value of 3:5 at local point in the system during the precipitation process. On the other hand, only one sharp exothermic peak at 918°C is observed from the precipitates synthesized at pH 7, which is corresponding to the crystallization of YAG phase. It indicates that pH 7 is proper value to form precipitates suitable for later transformation to YAG phase.

From these results, it is indicated that the formation of YAG phase can occur in two ways. The first one can be described as the direct transformation of amorphous precipitates to YAG phase, which occurs at wide range of temperature from 900 to 1200°C . The second way is the transformation through a series of the intermediates. It can be seen that these phenomena occur simultaneously when the calcination temperature is increased above 800°C . The higher the calcination temperature, the higher the intensity peaks for YAG phase which is the result of crystallization of YAG phase from both routes.

FTIR spectra of the powder synthesized at pH 6 and 7 and subsequently calcined at various temperatures for 2 h are shown in Figure 4.20 and 4.21, respectively.

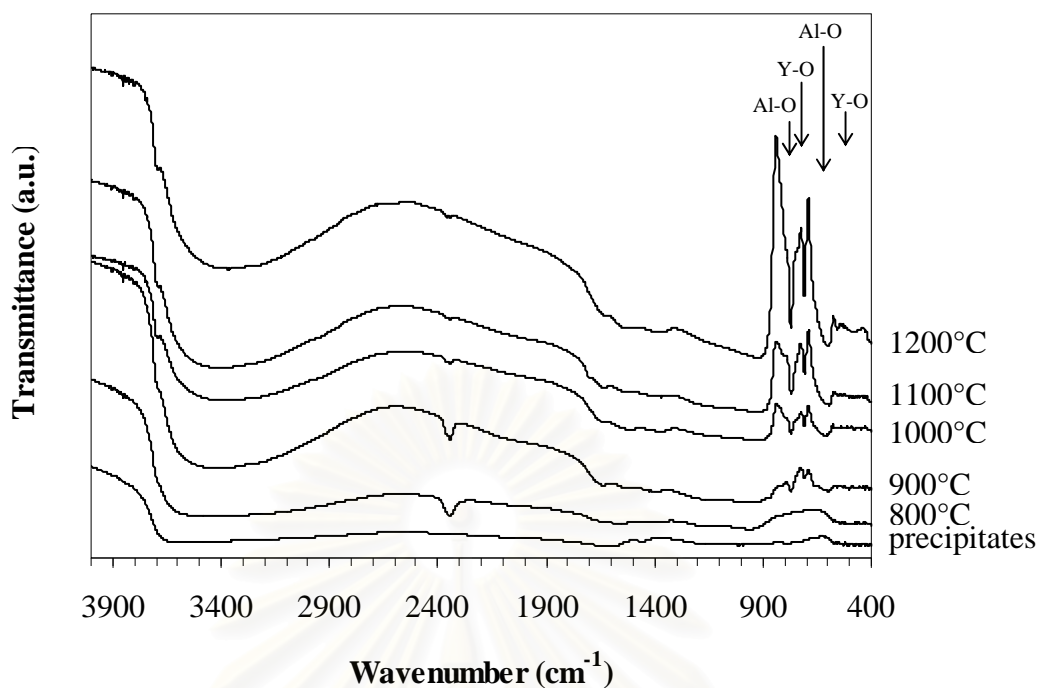


Figure 4.20 FTIR spectra of the precipitates synthesized at pH 6 and calcined at various temperatures for 2 h.

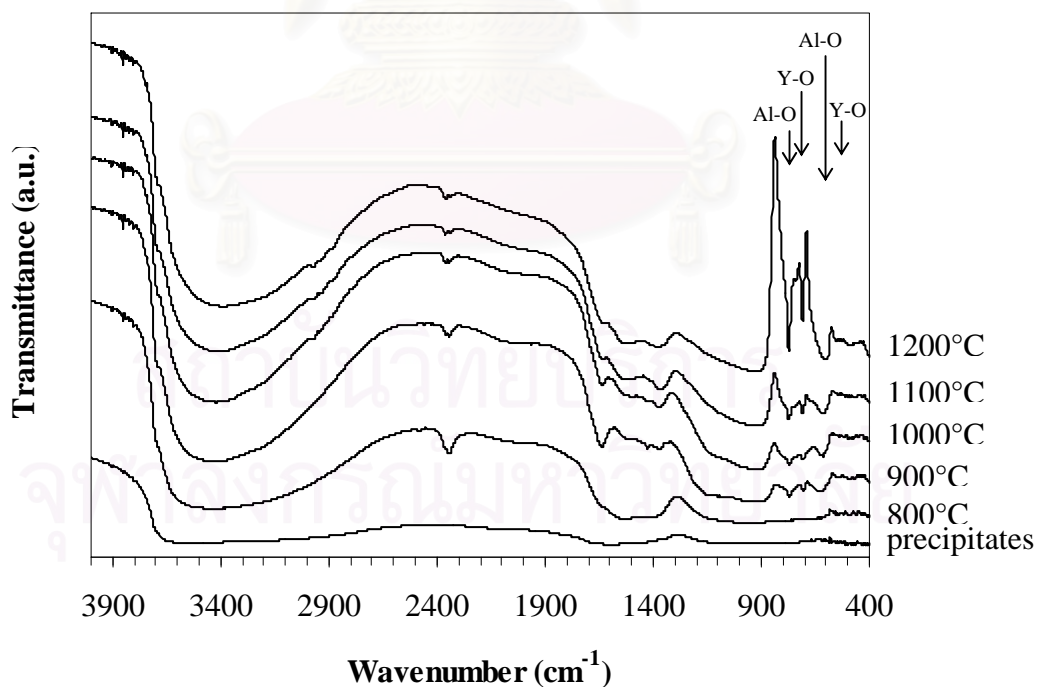


Figure 4.21 FTIR spectra of the precipitates synthesized at pH 7 and calcined at various temperatures for 2 h.

The absorption bands corresponding to Al-O bonding (i.e. 770 and 625 cm^{-1}) and those corresponding to Y-O vibration (i.e. 708 and 551 cm^{-1}) are clearly observed when the powders are calcined at 900°C or higher. Unidentified absorption bands at wavenumber approximately in the range of 1100-1500 cm^{-1} are detected in the powders calcined at 800-1200°C. The intensity of these bands is quite low for the precipitates synthesized at pH 6, but they become noticeable for the precipitates synthesized at pH 7. Furthermore, an unidentified band at 2342 cm^{-1} appears for the precipitates synthesized at pH 6 and calcined at 800-1200°C. In contrast, for the precipitates synthesized at pH 7, this band shifts to the wavenumber of 2360 cm^{-1} as the powder is calcined at 900-1200°C. Nevertheless, the attempt to identify functional groups associated with all of these bands was unsuccessful.

The higher the calcination temperature, the higher the intensity of the sharp absorption bands observed. This observation is attributed to the formation of compound containing Y, Al and O bonds in greater extent. If the transformation through intermediates is only process to form YAG phase, the intensity of the absorption bands should remain unchanged after the calcination temperature has reached the intermediates-to-YAG crystallization point. However, the intensity of the absorption bands is still increased with the increased calcination temperature, even when the sample does not contain any form of intermediate (e.g. the case of the precipitates synthesized at pH 7). Therefore it confirms that the formation of YAG occurs not only by the transformation of the intermediates, but also the direct transformation from the amorphous precipitates occurring at a wide range of temperature. It can be seen that, for precipitates synthesized at pH 6, the formation of YAG phase through the transformation of the intermediates takes place more than the direct transformation from amorphous to YAG, as confirmed by TG/DTA analyses (Figure 4.19). On the contrary, for precipitates synthesized at pH 7, the formation of YAG phase occurs from the transformation from amorphous to YAG phase directly more than from the transformation of the intermediates (Figure 4.19). It can be concluded that when part of the precipitates have the Y-to-Al molar ratio deviated from the value of 3:5, the formation of YAG phase occurs from the transformation of the intermediates.

4.2.4 Effect of Type of Precipitation Process

Two different types of precipitation process were investigated in this work. For the standard synthesis procedure, the precipitation was done by the reverse strike process (RS), in which the ions solution was titrated into AHC solution. In this section, the precipitation was conducted by the normal strike process (NS), in which the AHC solution was titrated into the ions solution. All of the operating conditions for the normal strike process were the same as those for the standard synthesis procedure.

The XRD patterns of the powder synthesized via the normal strike process and calcined at 800-1200°C for 2 h are shown in Figure 4.22.

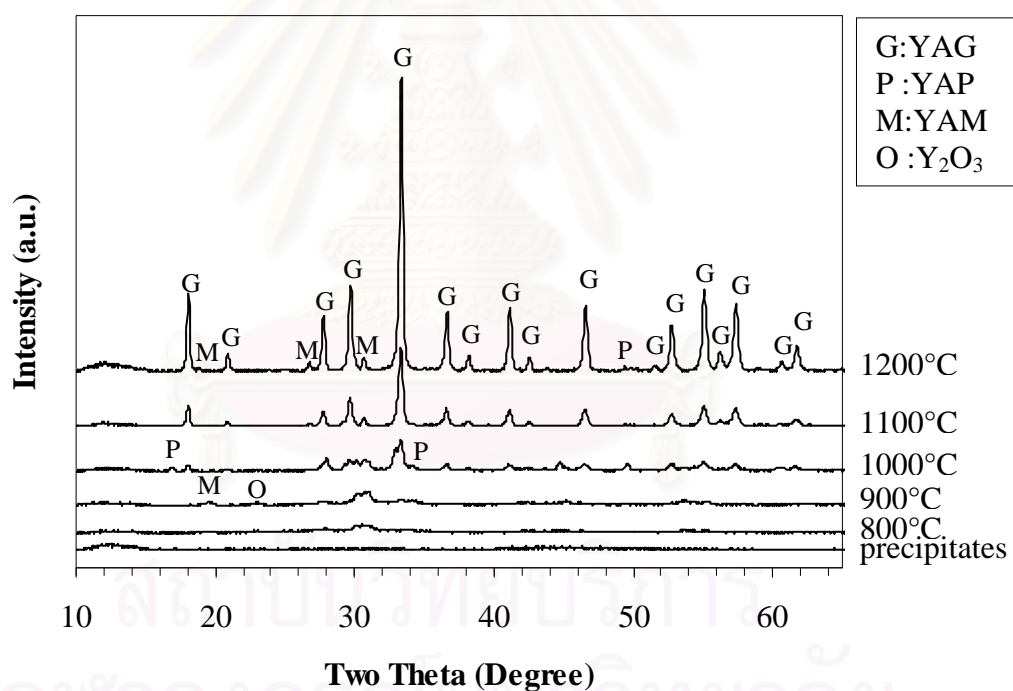


Figure 4.22 XRD patterns of the precipitated synthesized via the normal strike process and calcined at various temperatures for 2 h.

The powder prepared by the normal strike process and calcined at 800°C is mostly amorphous with small amount of YAM presented. When the precipitate is calcined at 900°C, yttrium oxide appears as in addition to YAM and YAP. As the calcination temperature is raised to 1000°C, YAP, YAM and yttrium oxide exist with

very small amount of YAG phase. The sample still contains intermediate phase, i.e. YAP and YAM, even after calcination at 1200°C. The intensity of the diffraction peaks of YAG phase becomes higher with increasing calcination temperature.

Results from the XRD analysis show that although the calcination temperature is increased up to 1200°C, the product from the normal strike process still contains the intermediate phases. On the contrary, the product from the reverse strike process is pure YAG without any intermediate phase when it is calcined at 1200°C. The main difference between these two methods is the complete reaction of the ions solution when it is dropped into AHC solution for the reverse strike process. In contrast, for the normal strike process, in which the AHC solution was titrated into the ions solution, it is found that the reaction of the ions solution is not thoroughly completed. Parts of the ions solution remain unreacted, resulting in non-uniform distribution of Al^{3+} and Y^{3+} during precipitation process. In addition, the non homogeneity of the precipitates in term of the local Y-to-Al molar ratio occurs. As the result, the intermediate phases are formed after calcined. These results are consistent with previous study which has reported that, for multi-cations materials, the reverse strike process has the advantage of better cation homogeneity in the precursor [13].

Figure 4.23 shows the TG/DTA curves of the powder prepared by the normal strike process.

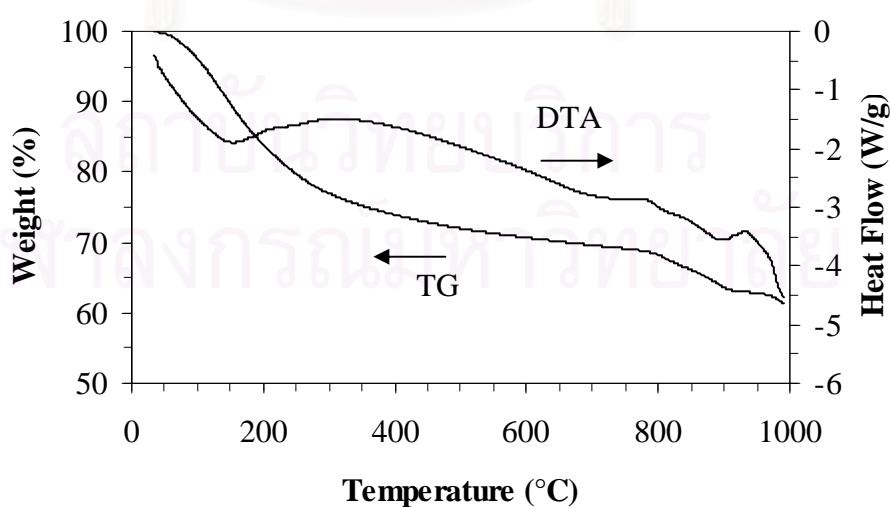


Figure 4.23 TG/DTA curves of the precipitates synthesized by the normal strike process.

Besides the endothermic peak at around 200°C, the DTA curve exhibits three exothermic peaks, i.e. the first weak and broad peak at 783°C, the second weak and broad peak at 842°C and a strong and sharp peak at 937°C, respectively. Considered with the results from XRD analyses (Figure 4.22), it is suggested that the first two exothermic peaks are corresponding to the crystallization of the intermediate phases i.e. YAM for the first peak, and YAP and yttrium oxide for the second peak, while the third sharp peak is corresponding to the formation of YAG phase.

The FTIR spectra of the powder synthesized by the normal strike process and calcined at 800-1200°C are shown in Figure 4.24.

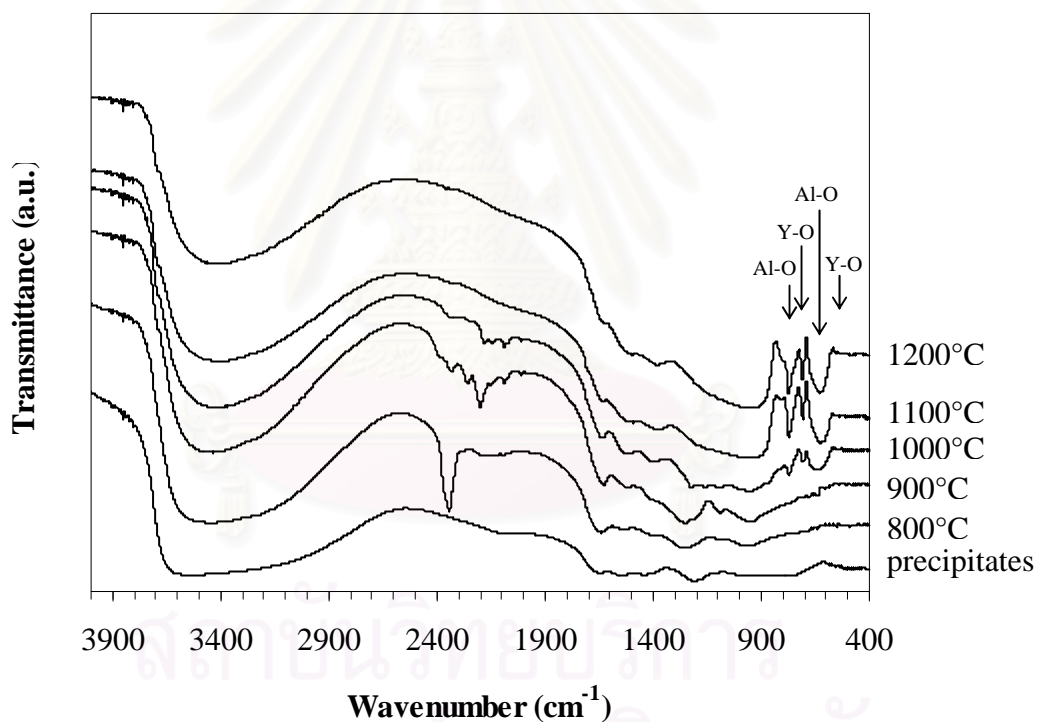


Figure 4.24 FTIR spectra of the precipitates synthesized via the normal strike process and calcined at various temperatures for 2 h.

No absorption bands at 770 and 625 cm^{-1} ; and at 708 and 551 cm^{-1} , which are the characteristic bands of Al-O and Y-O vibration respectively, appear in the sample calcined at 800°C. These characteristic peaks appear very faintly after the sample is calcined at 900°C. The bands become sharper as the calcination temperature is

increased. The fact that no absorption bands associated with Al-O and Y-O vibration appear at 800°C, contrast with the result from XRD analyses. It may be suggested that the bonding between Y, Al and O may not be fully developed, or the surrounding amorphous structure may hinder the vibration signals of the formed bands. When the results from XRD, TG/DTA and FTIR analyses are considered together, it is suggested that almost all of the intermediate phases found in the product synthesized via the normal strike process are formed by the direct transformation from amorphous, which occurs at wide range of calcination temperature in similar manner to the formation of YAG phase. Furthermore, unidentified absorption bands at wavenumber approximately in the range of 1100-1500 cm^{-1} are clearly detected in the powder calcined at 800-1200°C which is similar to the standard synthesis procedure (reverse strike). Similar behavior is also observed for unidentifiable absorption bands in the range of 2200-2400 cm^{-1} , which occur in the powder calcined at 900 and 1000°C. These bands disappear after the calcination temperature is increased. On the contrary, these absorption bands for product synthesized by the reverse strike process are detected only at 900°C and disappear at higher calcination temperature. For the product prepared by the normal strike process and calcined at 800°C, the distinct unidentified band appears at 2342 cm^{-1} . This band shifts to wave number of 2360 cm^{-1} while its intensity is decreased when the powder is calcined at 1100-1200°C.

4.2.5 Effects of calcination time

In this part, the precipitate was synthesized according to the standard synthesis procedure and calcined at 1100-1200°C for various periods of time, using two calcination methods. For the first method, the precipitate was heated up from room temperature to the desired temperature (1100 or 1200°C) at a rate of 10°C/min, and held at that temperature for various periods of time, i.e. 30, 60 and 120 minutes, respectively. For the second method, the precipitate was put into the furnace when the furnace temperature was around 1100°C. The system was further heated up to the desired temperature and held at that temperature for 30 minutes. After that, the calcined powder was immediately brought out of the furnace and cooled down to room temperature. The XRD patterns of powder calcined at 1000 and 1200°C using two calcination methods are shown in the Figure 4.25-4.26.

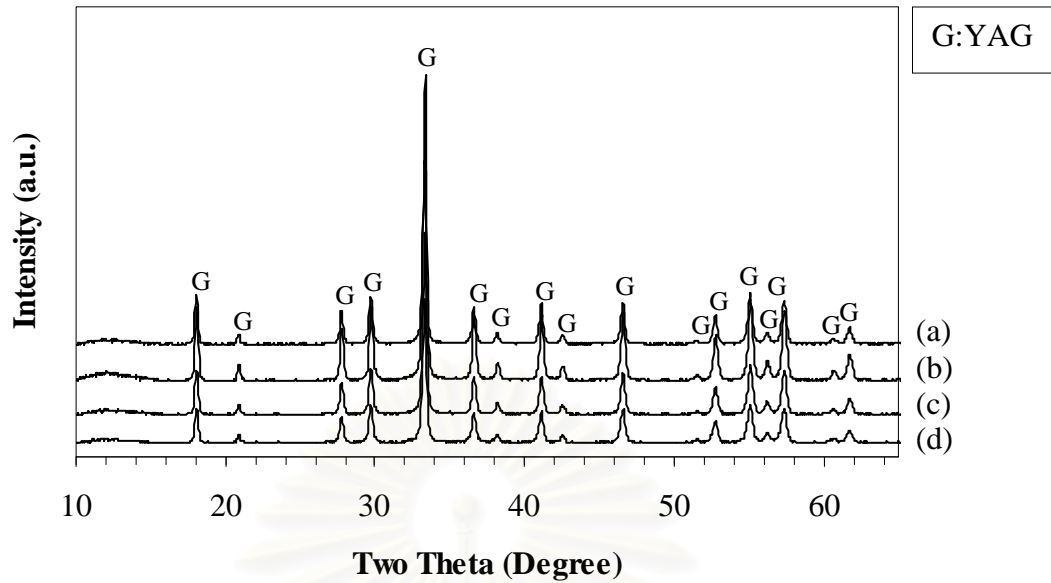


Figure 4.25 XRD patterns of the powder calcined at 1200°C for 120 (a), 60 (b) and 30 minutes (c) when the sample was heated from room temperature at the rate of 10°C/min, compared with that of the sample put into the furnace when the temperature was around 1100°C and held at 1200°C for 30 minutes (d).

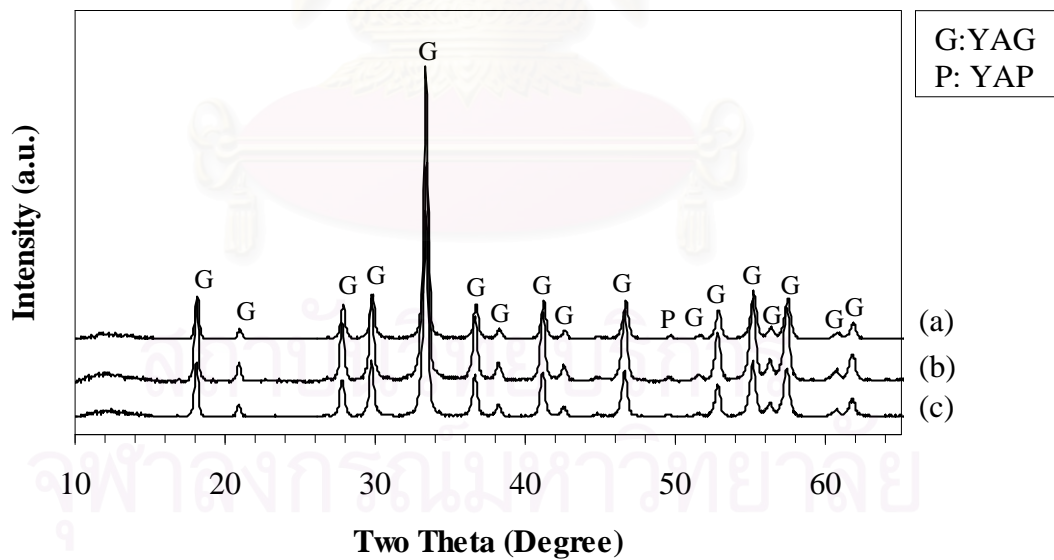


Figure 4.26 XRD patterns of the powder calcined at 1100°C for: (a) 120 minutes; (b) 60 minutes and (c) 30 minutes. Noted that the sample was heated from room temperature at the rate of 10°C/min.

The powders that are calcined at 1200°C by heating from room temperature and held at 1200°C for 30, 60 and 120 minutes are all YAG phase without any intermediate phase (Figure 4.25 a-c). The same result was obtained for the precipitate that was put into the furnace after the furnace had reach 1100°C and held at 1200°C for 30 minutes (Figure 4.25d). On the other hand, the samples that were heated from room temperature and held at 1100°C for 30, 60 and 120 minutes, contain very small amount of YAP as intermediate in addition to the YAG phase (Figure 4.26).

Analysis of the width of XRD diffraction using the Scherrer's equation gives the average crystallite size of the sample. It can be observed that the powders calcined for various periods of time have different average crystallite sizes. For the samples calcined at 1200°C for all of the holding periods investigated, the average crystallite sizes are in the range of 50-60 nm. It is also shown that the crystallite size is increased with increasing calcination time. For the precipitate that was put into the furnace at high temperature and held at 1200°C for 30 minutes, it is found that the average crystallite size is about 45 nm. This value is similar to the average crystallite size of the powder heated from room temperature when the holding period is also 30 minutes. When the calcination is done at 1100°C, the average crystallite size is in the range of 25-35 nm.

In addition, the mean particle size was estimated from TEM micrographs of a large number of particles as shown in Figure 4.27. It can be seen that the powders calcined for various periods of time have different particle sizes. After calcined at 1100 and 1200°C, the particle size is in the range of 20-50 and 30-80 nm, respectively. The comparison between the crystallite size and the particle size as a function of calcination time are shown in Figure 4.28.

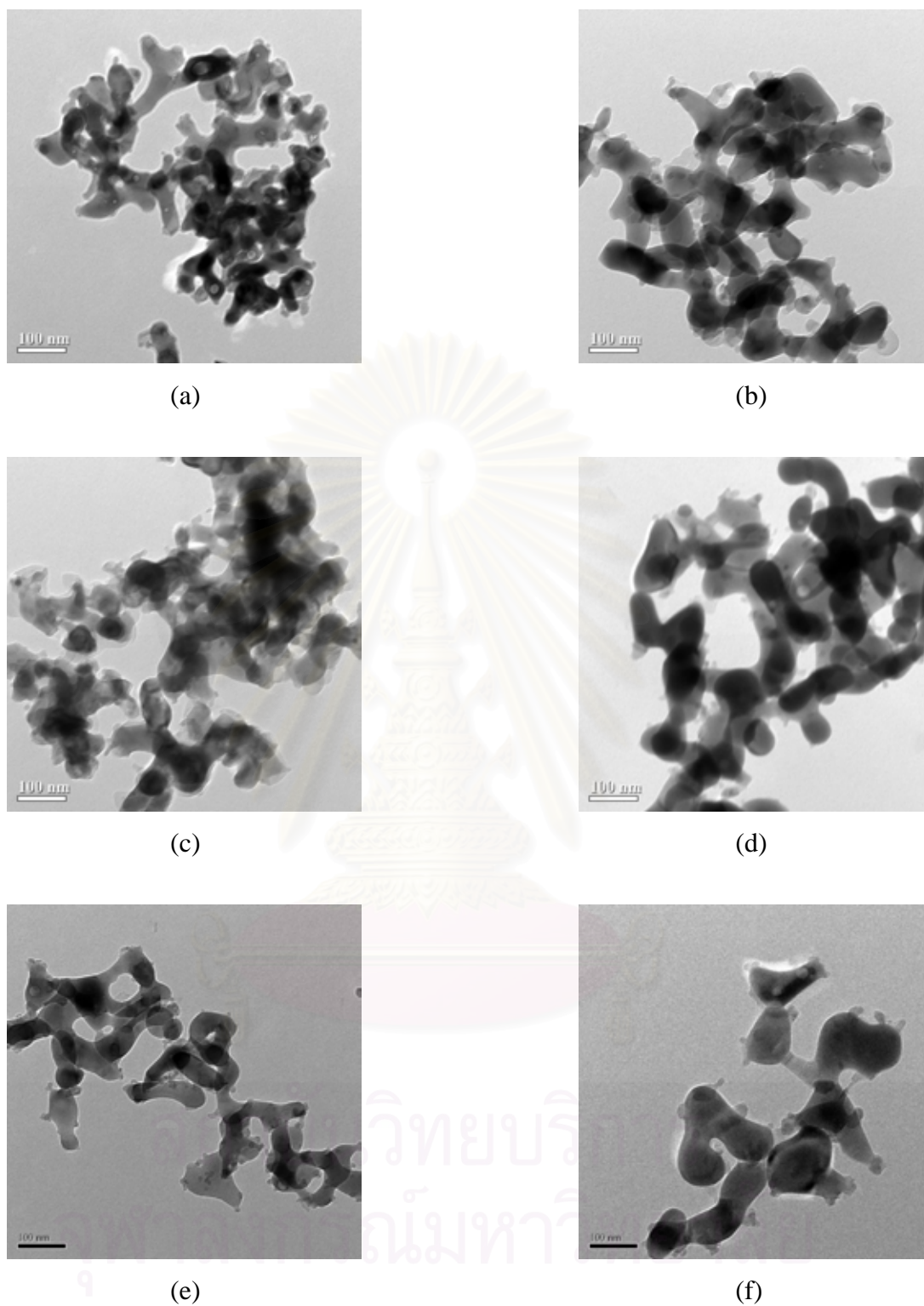


Figure 4.27 TEM micrographs of YAG powder which was calcined at various calcination temperatures and calcination times: (a) 1100°C for 30 minutes, (b) 1200°C for 30 minutes, (c) 1100°C for 60 minutes, (d) 1200°C for 60 minutes, (e) 1100°C for 120 minutes and (f) 1200°C for 120 minutes.

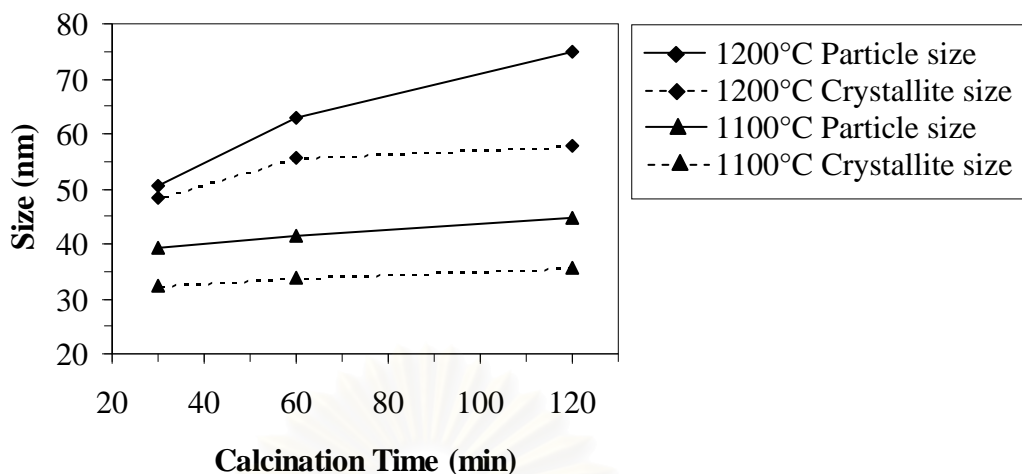


Figure 4.28 The particle sizes observed in TEM micrographs and crystallite sizes estimated from XRD pattern using the Scherrer's equation, as a function of calcination temperature and calcination time.

According to Figure 4.28, the crystallite size and the particle size are increased with the increasing calcination time. It is found that, for all periods of calcination time, the particle sizes observed in TEM micrographs are larger than the crystallite sizes, indicating that the primary particle of calcined powder is polycrystalline. When the powder is calcined at 1100°C, the increases in both crystallite size and particle size with respect to the calcination period are similar. It indicates that the crystallite growth from the direct transformation of amorphous precipitates to YAG phase occurs as the holding time is prolonged. Nevertheless, according to TEM micrographs in Figure 4.27, the sintering of small particles has already taken place even after only 30 minutes of calcination. When the calcination temperature is raised up to 1200°C, the increasing rate in both crystallite size and particle size are no longer constant throughout the of holding period. The crystallite size is increased more quickly in the first 30-60 minutes than during the later holding period. In addition, the particle size is much larger than the crystallite size after the calcination at 1200°C for 120 minutes, since the crystals form serious agglomeration after the holding time is pronged to 120 minutes or longer. This phenomenon is mainly caused by the sintering of smaller primary particles and form into larger secondary particle. When the crystals grow, the attractive force between them is increased, and the sintering among the particles occurs [41]. Therefore, it can be concluded that the secondary particle is formed by

the sintering of small primary particles as calcination progresses, which is consistent with the observation by TEM micrographs (Figure 4.27).

The FTIR spectra of the powder calcined at 1100 and 1200°C for 30, 60 and 120 minutes are shown in Figure 4.29. It reveals similar set of absorption bands as those reported for calcined powder with standard synthesis procedure. All absorption bands shown in this Figure are the same. It indicates that the change in calcination time in the range of 30-120 minutes, for the calcination at 1100-1200°C, has no effect on bond structure of the sample. Nevertheless, the longer the period of calcination at high temperature, the higher the intensity of absorption bands representing Al-O and Y-O vibrations observed.

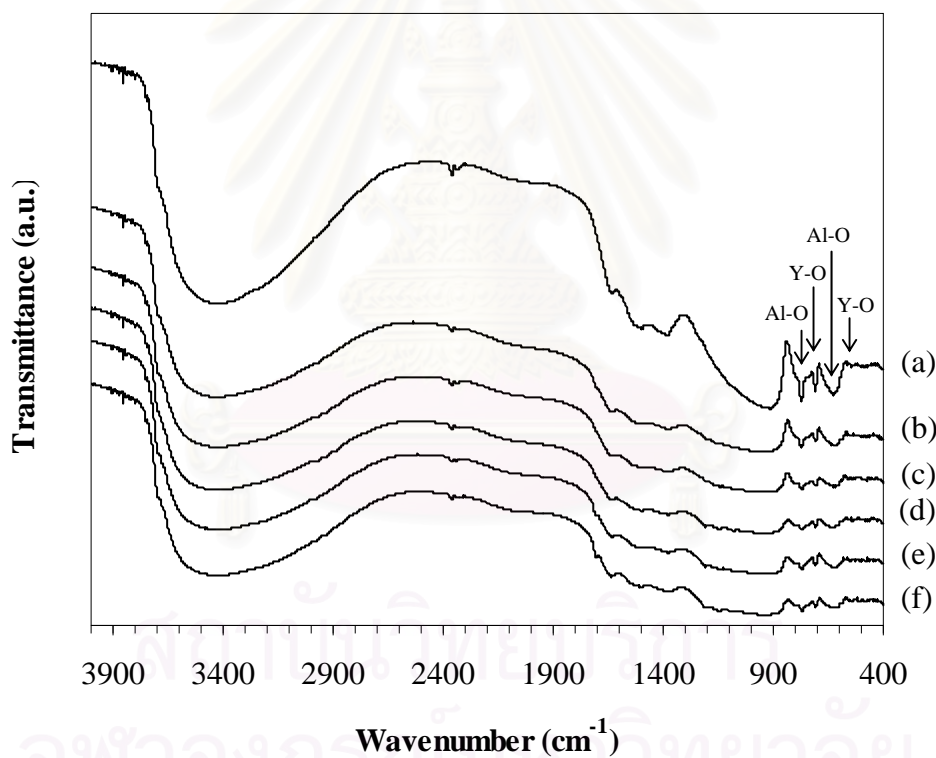


Figure 4.29 FTIR spectra of the powder which was calcined at various calcination temperatures and calcination times: (a) 1200°C for 120 minutes, (b) 1200°C for 60 minutes, (c) 1200°C for 30 minutes, (d) 1100°C for 120 minutes, (e) 1100°C for 60 minutes, (f) 1100°C for 30 minutes.

4.3 Effects of Preparation Conditions for Precipitation

The detailed study on the effect of preparation conditions on the formation of precipitates is investigated. The concerned factors include the speed of mixing, the rate of addition of ions solution into the reaction system and the concentration of both reactants. It should be noted that the particle size measurement was done after the calcination of the powder at 1200°C for 2 h. The precipitate has been converted to pure phase of YAG without any other intermediate phase. The results from XRD, TG/DTA and FTIR analyses done on the powders synthesized in this section are the same as described in the previous chapter and therefore omitted.

4.3.1 Effects of Speed of Mixing

In this work, speed of mixing or stirring speed in the precipitation system was varied from 100, 300 and 500 rpm. The phase formation which is observed by XRD pattern of 100 and 300 rpm are the same as the phase formation of the standard synthesis procedure with stirring speed of 500 rpm. It indicates that the speed of mixing affects both average particle size and size distribution of the obtained product as shown in Table 4.1 and Figure 4.30.

Table 4.1 Median diameter of the calcined product prepared by using various stirring speeds.

Stirring speed (rpm)	Median diameter (μm)
100	0.83
300	0.77
500	0.65

Table 4.1 reports the median diameter of the powder prepared by using various speed of mixing and subsequently calcined at 1200°C. When the stirring speed was varied from 100 to 500 rpm, the median diameter of the product varies in the range of 600-800 nm. The higher speed of mixing, the smaller median diameter of the product appears.

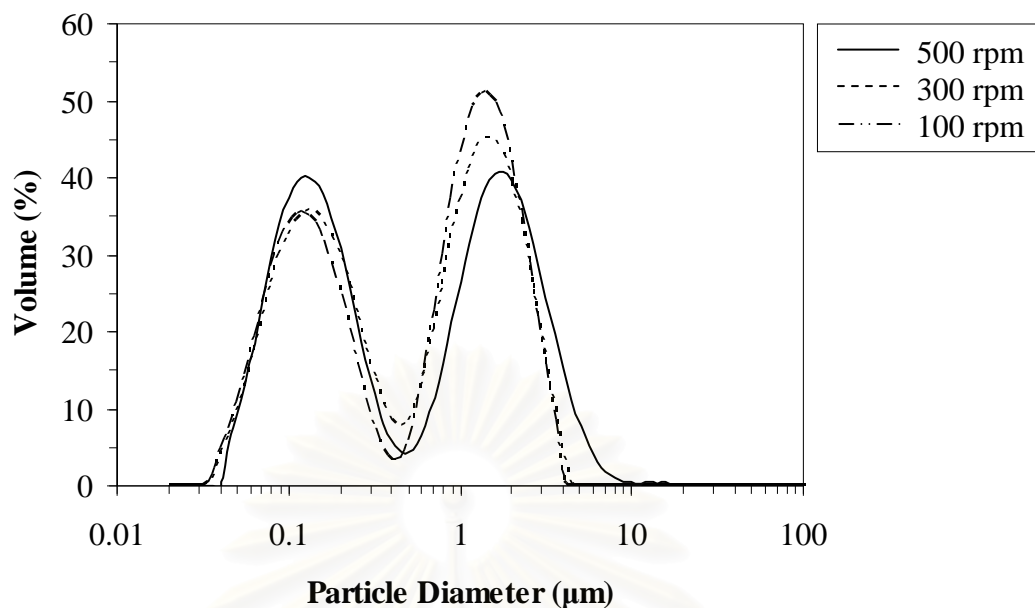


Figure 4.30 The particle size distributions of the powder prepared via the standard synthesis procedure using various speed of mixing and subsequently calcined at 1200°C.

Figure 4.30 shows the size distributions of the calcined products obtained by the Laser particle size distribution analyzer under volume basis. According to Figure 4.30, the particle size distribution apparently splits into bimodal distribution. The first peaks has maxima located around 0.12 μm , while the second peak appears at about 1.5 μm . As the mixing speed is increased, the heighten in the intensity of the first peaks is observed, while the intensity of the second peak is lowered. It indicates that small particles are more dispersed with the increase in stirring speed. Since the reaction between AHC solution and ions solution to form the precipitates take place immediately after the ions solution is mixed with AHC solution, high mixing speed prevents the agglomeration of the precipitates.

During the particle size distribution measurement, the powder was mixed with the dispersant solution. It is found that, without the dispersant, the particle size distribution curve is unimodal distribution with higher average size than reported in Figure 4.30. On the contrary, with the aids of the dispersant, the particle size distribution curve splits into bimodal distribution. It is indicated that the particles synthesized in this work are easily agglomerated. Size of the particle within the first

peak of the particle size distribution is comparable to the primary particles and small secondary particles, indicating that the first peak is corresponding to lightly aggregated particles. On the contrary, the second peak represents particles that are heavily agglomerated, which is the result from the agglomeration of the precipitates and the sintering among the primary and secondary particles. It can be suggested that the high speed of mixing reduces the agglomeration of the precipitates during the precipitation procedure and therefore partially prevents hard agglomeration via the sintering of particles during calcination.

4.3.2 Effects of Rate of Addition

In this section, the powder was prepared by the standard synthesis procedure using rate of addition of ions solution into AHC solution at 5, 10, 15 ml/min, respectively. The rate of addition was controlled with a peristaltic pump. The results were also compared with the synthesis by directly pouring all of the ions solution into the AHC solution. All experiments were conducted using the stirring speed of 500 rpm. The effect of addition rate to particle size distribution and median diameter can be clearly observed as shown in Table 4.2 and Figure 4.31.

Table 4.2 Median diameter of the calcined products prepared by using various rates of addition

Adding rate (ml/min)	Median diameter (μm)
5	0.65
10	0.87
15	1.19
pour directly	3.70

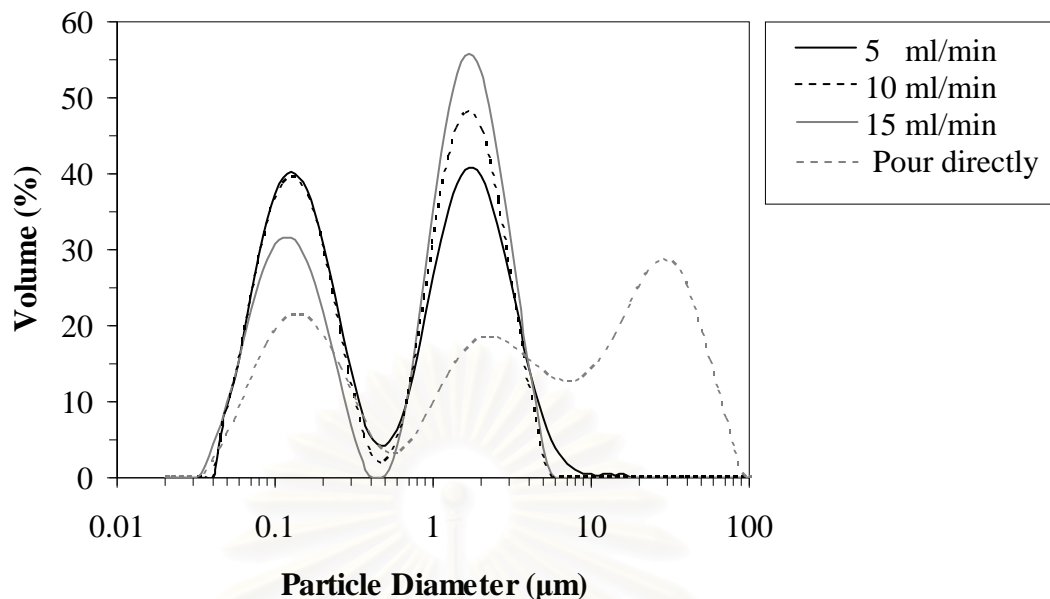


Figure 4.31 The particle size distributions of the powder prepared via the standard synthesis procedure using various rate of addition and subsequently calcined at 1200°C.

The results shown in Table 4.2 and Figure 4.31 indicate the same phenomena as observed from varying the stirring speed. The lower the addition rate, the smaller the particles become. On the contrary, when the ions solution is pour into AHC solution directly, the particle size is quite large and their distribution is trimodal, which is undesirable. Since the ions solution is acidic (pH=2.6), while the AHC solution is basic (pH=7.8), sudden pouring of the ions solution into AHC solution causes rapid fluctuation and nonuniformity in pH value of the system. Some regions in the system may be acidic, which results in undesired product in precipitates. On the other hand, at low rate of addition, the stirring in the system is capable of quick dispersion of the ions solution within the system and therefore homogenizing pH of the system.

4.3.3 Effects of Reactants Concentration

In this section, concentration of both reactants, i.e. the AHC solution and the ions solution are varied. It is varied from 1.0 and 2.0 mol/l for ammonium hydrogen carbonate solution (AHC solution) and 0.1, 0.2, 0.3 mol/l for ammonium aluminum

sulfate solution (AAS solution). The median diameters of all obtained powders synthesized from the solution with different concentrations are shown in Table 4.3. It should be noted that the particle size measurement was done after the calcination of the powder at 1200°C.

Table 4.3 Median diameter of calcined powder prepared via the standard synthesis procedure using various concentrations of reactants.

Concentration of AHC solution	Median diameter at various concentration of ion solution (μm)		
	0.1 M	0.2 M	0.3 M
1 M	0.26	0.52	0.82
2 M	0.24	0.64	0.76

Table 4.3 reports the median diameter of the powder prepared from solution with various concentrations after calcination at 1200°C. It shows that the median diameter increases with the increase in the concentration of the ions solution. On the contrary, when the concentration of the AHC solution is increased, there is no effect on the median diameter and the particle size distribution of the calcined powder. Figure 4.32 and 4.33 show the particle size distribution of powders prepared from the reaction between the ions solution at various concentrations and AHC at the concentration of 1 and 2 M, respectively.

สถาบันวิทยบริการ
จุฬาลงกรณ์มหาวิทยาลัย

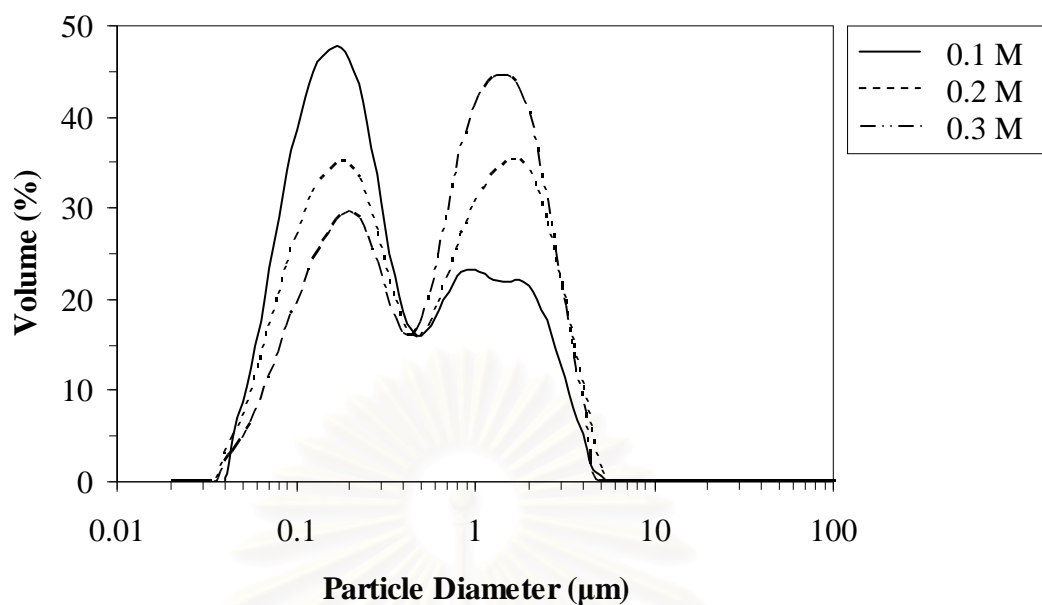


Figure 4.32 The particle size distributions of the powder prepared via the standard synthesis procedure using 1 M of AHC solution and ions solution at various concentrations.

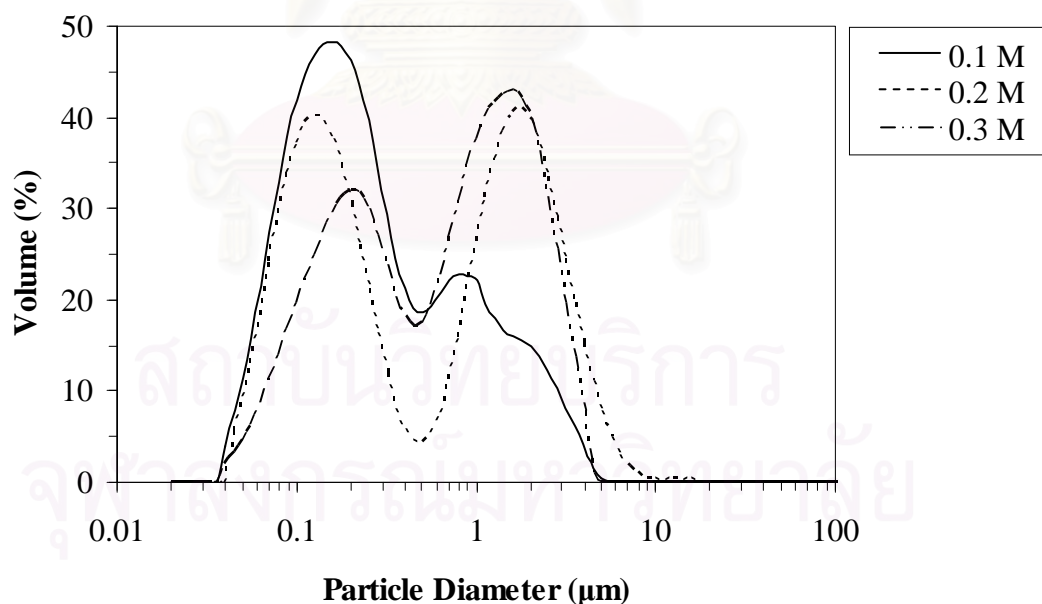


Figure 4.33 The particle size distributions of the powder prepared via the standard synthesis procedure using 2 M of AHC solution and ions solution at various concentrations.

From the particle size distribution curve in Figure 4.32, where the concentration of AHC solution is fixed at 1 M, it is found that the curve apparently splits into bimodal distribution. The intensity of the peak corresponding to large particles is increased at high concentration of the ions solution. The same behavior is also observed when the concentration of AHC solution is increased to 2 M, as shown in Figure 4.33, in which the distribution curve also splits into bimodal mode and the amount of agglomerated particle is increased at high concentration of the ions solution.

When the concentration of the ions solution is fixed and the concentration of the AHC solution is varied, it is found that the median diameter and the particle size distribution curves remain almost the same. In the other words, the concentration of the AHC solution has no effect on the median diameter as well as the particle size distribution. This is attributed to the fact that the reaction during the precipitation process is rapid. White precipitates are formed immediately after a drop of the ions solution reaches the AHC solution. Therefore, for the reverse strike process, the growth as well as the agglomeration of the precipitates are mainly associated with concentration of the ions solution. Low concentration of the ions solution provides lower degree of agglomeration for the precipitates.

4.4 Fabrication of YAG Powder

The particle size, size distribution and state of agglomeration of powder are important factors for fabrication of advanced ceramic, as mentioned earlier. To ensure homogeneity of the starting material, soft agglomeration powders are broken up by ball milling to decrease the particle size as well as control the size distribution into narrow range. The proper milling time depends upon the nature of powder. In this study, the optimum milling time was determined by ball milling the powders calcined at 1200°C in the range of 0 to 96 h. The samples were periodically take out for particle size measurement.

The morphology of calcined powder and commercial powder including before milled and after milled for 72 h are also shown in Figure 4.34. Moreover, the median

diameter and particle size distribution of powder milled at various milling time as well as those of the commercial YAG powder are shown in Table 4.4- 4.5 and Figure 4.35-4.36, respectively.

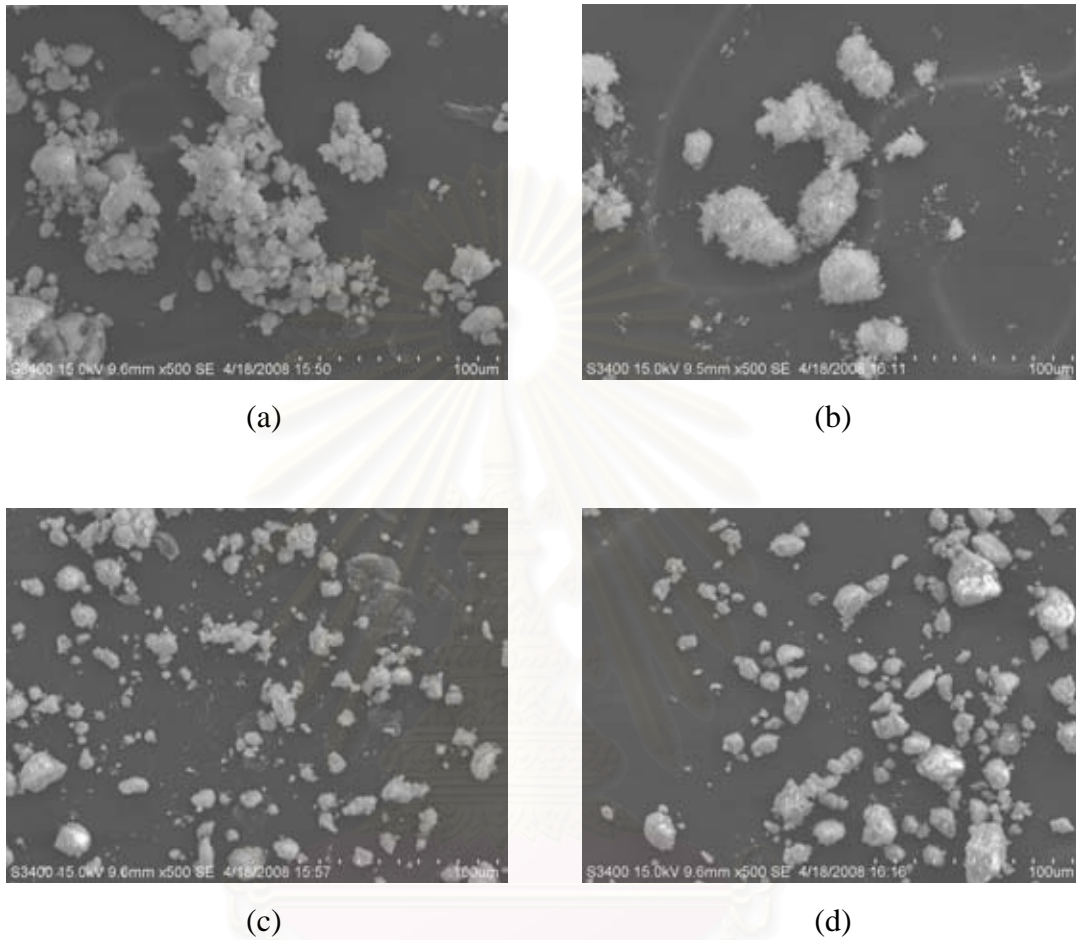


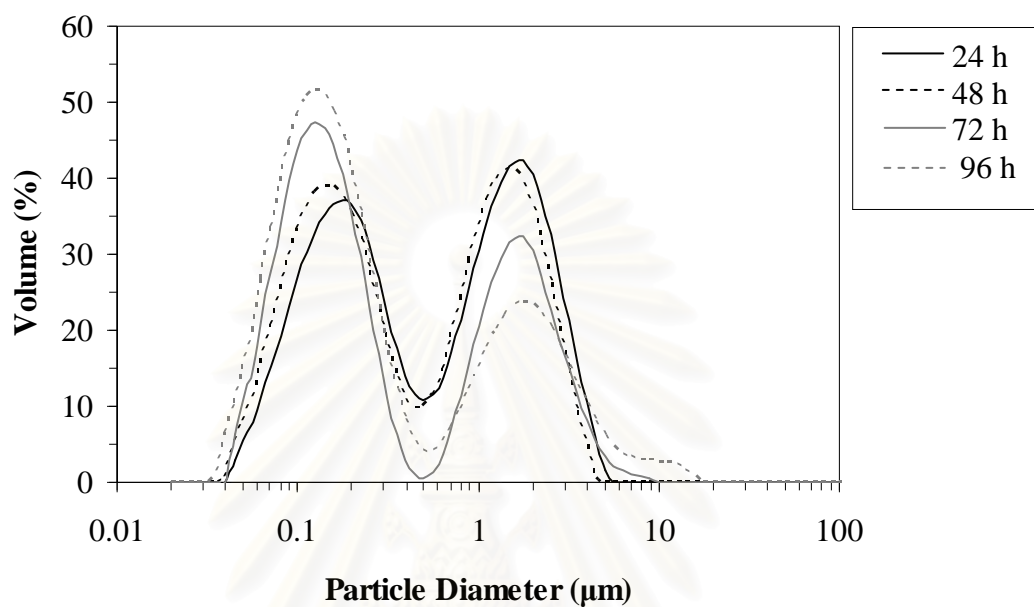
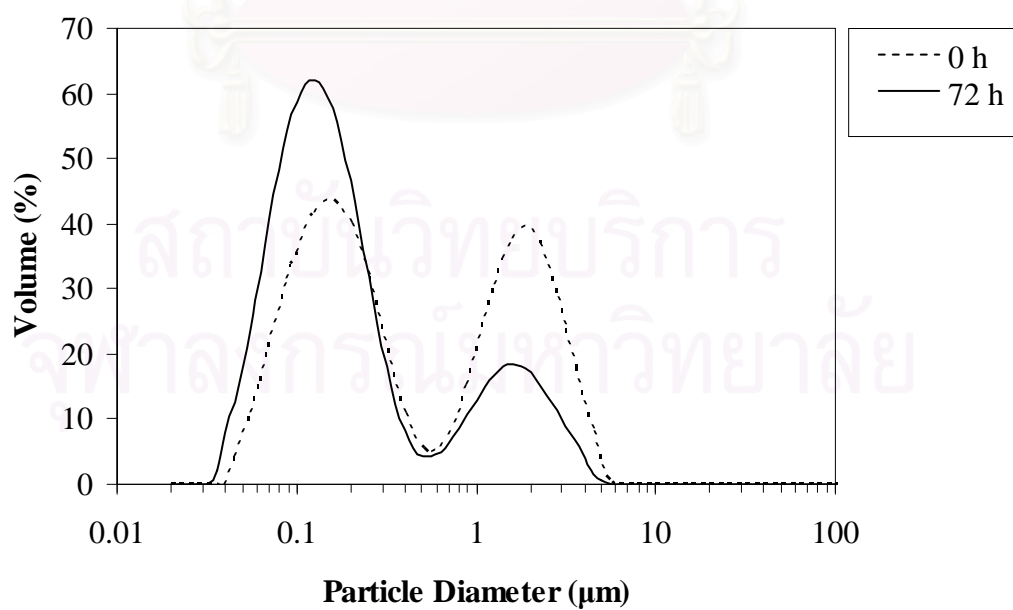
Figure 4.34 SEM images of the commercial powder before milled (a), the commercial powder which is milled for 72 h (b), the synthesized powder before milled (C) and the synthesized powder which is milled for 72 h (d).

Table 4.4 Median diameter of the calcined powder after ball milled for various period of time.

Milling time (h)	Median diameter (μm)
0	0.65
24	0.58
48	0.43
72	0.26
96	0.21

Table 4.5 Median diameter of commercial YAG powders before and after milling.

Milling time (h)	Median diameter (μm)
0	0.317
72	0.164

**Figure 4.35** Particle size distributions of the synthesized powder calcined at 1200°C and milled for various periods of time.**Figure 4.36** Particle size distributions of the commercial YAG powder before milling and after milling for 72 h.

It is found that the longer milling time, the lower the median diameter (Table 4.4). Nevertheless, the powders still have bimodal size distribution, regardless of the milling time. When the milling time is increased, the particles size distribution curves shift toward the smaller size and the amount of larger particles size is decreased while the amount of smaller particles is increased, as the result of the large secondary particles softly agglomerated are broken up to smaller particles. Comparison between the commercial YAG powder and the synthesized powder (Table 4.5) reveals that the median diameter before milling of the commercial YAG powder is smaller than the synthesized powder. Yet, the particle size distribution curve of commercial YAG powder also splits into bimodal distribution in the same range as the synthesized powder. After milled for the same milling time (72 h), it is observed that the median diameter of the commercial YAG powder is smaller than the synthesized powder. Moreover, it shows the higher fraction of smaller particles than the synthesized powder milled for either 72 or 96 h. It is indicated that most of the commercial YAG powder is under soft agglomeration which can be easily broken up by milling. In contrast, most of the synthesized powder is formed by hard agglomeration, i.e. sintering between primary particle, which can not be broken by milling.

After milling, the powder is fabricated into pellet according to the procedures described in Chapter III. The bulk density and relative density of the sintering specimen fabricated from powder prepared by various conditions are reported in Table 4.6. The relative density as a function of sintering temperature is also shown in Figure 4.37.

สถาบันวิทยบริการ
จุฬาลงกรณ์มหาวิทยาลัย

Table 4.6 Density of the sintered YAG specimen.

Powder synthesis conditions	Sintering in air at 1550°C		Sintering in air at 1600°C		Sintering in air at 1650°C	
	Bulk density (g/cm ⁻³)	Relative density (%)	Bulk density (g/cm ⁻³)	Relative density (%)	Bulk density (g/cm ⁻³)	Relative density (%)
commercial YAG powder	4.24	94.12	4.31	95.82	4.32	96.06
standard synthesis and calcined at 1200°C	4.07	90.50	4.13	91.78	4.17	92.57
synthesis at pH 7 and calcined at 1000°C	4.04	89.74	4.10	91.00	4.15	92.26
standard synthesis and calcined by putting the powder into the furnace abruptly at 1200°C	3.95	87.75	4.09	91.04	4.1	91.16

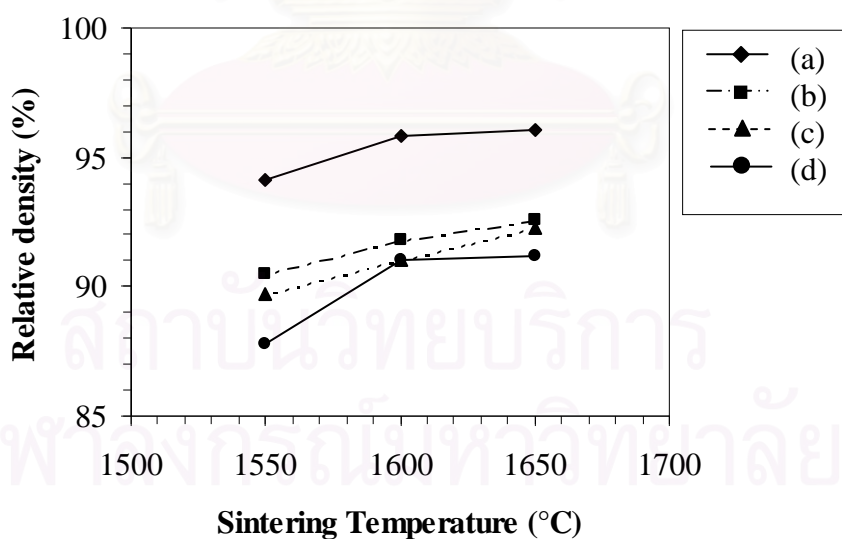


Figure 4.37 The relative density of YAG specimen, which is fabricated from YAG commercial powder (a), the powder synthesized by standard approach and calcined at 1200°C for 120 minutes (b), the powder synthesized at pH 7 and calcined at 1000°C for 120 minutes (c) and the powder synthesized by standard approach and calcined by putting the powder into the furnace at high temperature at 1200°C for 30 minutes (d).

As shown in Table 4.6 and Figure 4.37, density of the sintered specimen depends upon the sintering temperature. The increase in the sintering temperature results in the increased density of specimen. It can be seen that the density of the specimen fabricated from the commercial powder is higher than other samples. This is attributed to higher fraction of small particles with in the commercial powder. The grain size and SEM micrographs depicting microstructures of the specimen fabricated from commercial powder and synthesized powder after sintering for 5 h at 1650°C are shown in Table 4.7 and Figure 4.38.

From Table 4.7, grain size of the specimens are around 1.5-2.5 μm . It is found that the commercial powder specimen has the average grain size larger than other samples, although the grain structures is more uniform with smaller fraction of pore inside the specimen than the specimen fabricated from the synthesized powders. Moreover, the density of all specimen fabricated from the synthesized powders are lower than 95% of the theoretical density after sintering at 1650°C for 5 h in air, since all powder synthesized in this work contain certain level of agglomeration as well as the presence of larger particles, which may results in entrapped pores within the specimen. In order to increase the density of the specimen fabricated from the synthesized powder higher than 95% of the theoretical density, the powder was sintered under vacuum at 1650°C for 5 h. The resulting density of all specimens reaches the value higher than 95 % which is consistent with the previous finding in the literature [37].

Table 4.7 Average grain size of the sintered specimens.

Powder synthesis condition	Average grain size (μm)
commercial YAG powder	2.53
standard synthesis and calcined at 1200°C for 120 minutes	1.87
synthesis at pH 7 and calcined at 1000°C for 120 minutes	1.59
standard synthesis and calcined by putting the powder into the furnace abruptly at 1200°C	2.04

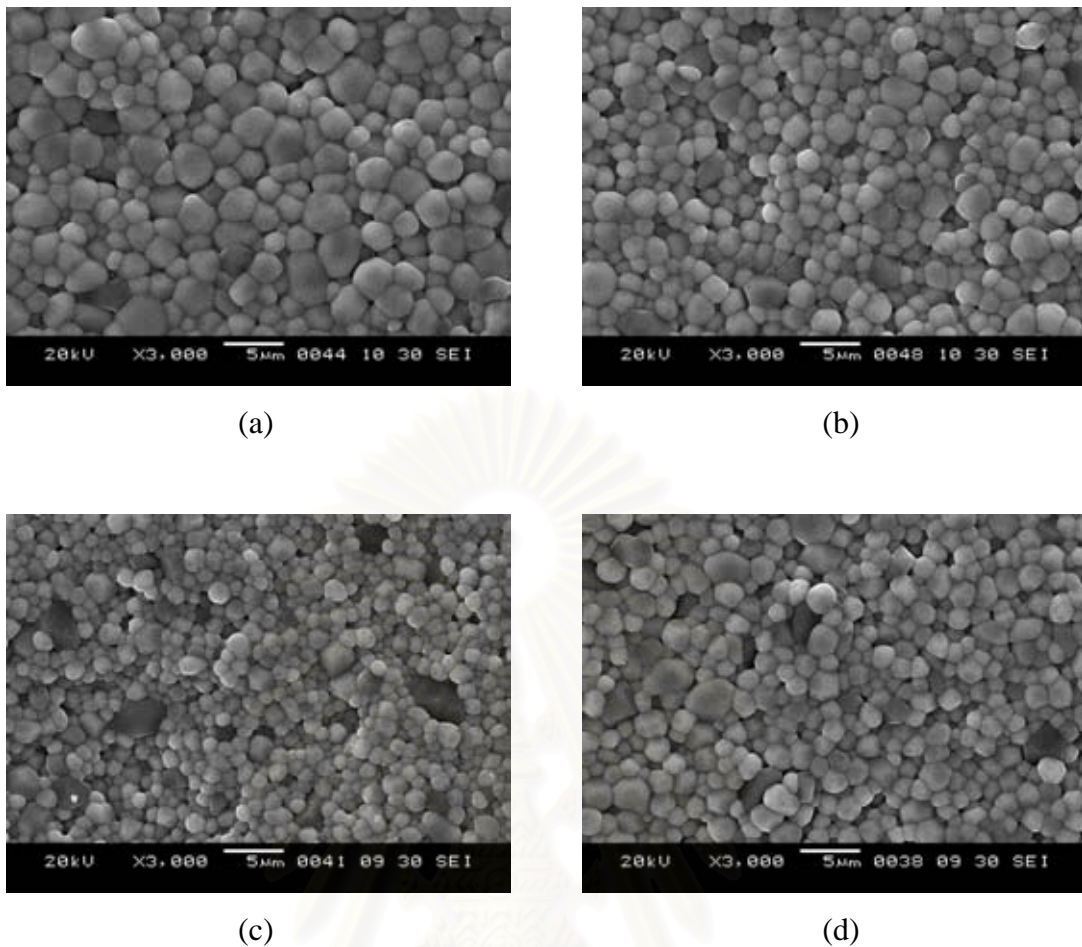


Figure 4.38 Microstructures of YAG specimen which is fabricated from YAG commercial powder (a), the powder synthesized by standard approach and calcined at 1200°C for 120 minutes (b), the powder synthesized at pH 7 and calcined at 1000°C for 120 minutes (c) and the powder synthesized by standard approach and calcined by putting the powder into the furnace at high temperature at 1200°C for 30 minutes (d).

สถาบันวิทยบริการ
จุฬาลงกรณ์มหาวิทยาลัย

CHAPTER V

CONCLUSIONS AND RECOMMENDATIONS

5.1 Conclusions

In this work, YAG powder was prepared by precipitation method. Effects of yttrium-to-aluminium ratio, reaction temperature, pH of the reaction, precipitation processes and variation of calcination time on phase formation, structure and morphology of YAG powder were investigated. Moreover, the effects of various factors such as concentration of precursors, speed of mixing and dropping rate on particle size distribution of powder synthesized by the precipitation method were also investigated. The conclusions of the study can be drawn as follows:

1. YAG nanocrystals size can be successfully synthesized by the precipitation method.
2. When the molar ratio of Y:Al is lower than the stoichiometric ratio of 3:5, it requires higher energy to form YAG phase. With the Y:Al molar ratio increased to the level higher than the stoichiometric ratio, the YAG phase forms at the same temperature as in case of the sample with stoichiometric ratio.
3. The decomposition of reactants by high reaction temperature has the effect on the formation of intermediate after calcination.
4. Controlling pH at 7 during the precipitation process is very important for obtaining pure YAG phase without any intermediate phase.
5. For multi-cation materials, the reverse strike process has the advantage of better cation homogeneity in the precursor than normal strike process.

6. The secondary particles are formed by the sintering of small primary particles. This effect is increasing with the calcination time.
7. Speed of mixing, dropping rate and concentration of precursors affect both size and size distribution of the obtained powder.
8. Bulk density of the specimen depends on size and size distribution of powder.

5.2 Recommendations

1. The mechanism of the transformation of the intermediate phase to YAG phase should be further studied in detail.
2. The sintering under vacuum to increase the density of the specimen should be investigated.



สถาบันวิทยบริการ
จุฬาลงกรณ์มหาวิทยาลัย

REFERENCES

- [1] Abell, J.S., I.R. Harris, B. Cockayne and B. Lent, An Investigation of Phase Stability in the $Y_2O_3-Al_2O_3$ System. Journal of Materials Science 9 (1974): 527-537.
- [2] Warshaw, I. and R. Roy, Stable and Metastable Equilibria in the Systems $Y_2O_3-Al_2O_3$ and $Gd_2O_3-Fe_2O_3$. Journal of the American Ceramic Society 42 (1959): 434-438.
- [3] Uehara, N. and K. Ueda, Ultra stabilized Nd:YAG lasers by laser diode pumping. The Review of Laser Engineering 21 (1993): 590.
- [4] Yokoyama, T., Bullatin of the Ceramic Society of Japan 23 (1988): 461.
- [5] Zumdahl and S. S., Chemical Principles. 4th ed. 2005, New York: Houghton Mifflin Company.
- [6] Ikesue, A., I. Furusato and K. Kamata, Fabrication of Polycrystalline, Transparent YAG Ceramics by a Solid-State Reaction Method. Journal of the American Ceramic Society 78 (1995): 225-228.
- [7] Ikesue, A., K. Yoshida, T. Yamamoto and I. Yamaga, Optical Scattering Centers in Polycrystalline Nd:YAG Laser. Journal of the American Ceramic Society 80 (1997): 1571-1522.
- [8] Sekita, M., H. Haneda, T. Yanagitani and S. Shirasaki, Induced emission cross section of Nd:Y₃Al₅O₁₂ ceramics. Journal of Applied Physics 67 (1990): 453-458.
- [9] With, G.d. and H.J.A.v. Dijk, Translucent Y₃Al₅O₁₂ ceramics. Materials research bulletin 19 (1984): 1669-1674.
- [10] Ikesue, A., T. Kinoshita, K. Kamata and K. Yoshida, Fabrication and Optical Properties of High-Performance Polycrystalline Nd:YAG Ceramics for Solid-State Lasers Journal of the American Ceramic Society 78 (1995): 1033-1040.
- [11] Sim, S.M., K.A. Keller and T.I. Mah, Phase Formation in Yttrium Aluminum Garnet Powders Synthesized by Chemical Methods. Journal of Materials Science 35 (2000): 713-717.
- [12] Li, J., Y. Pan, J. Zhang, L. Huang and J. Guo, Journal of the Chinese Ceramic Society 31 (2003): 490-493.

- [13] Li, J.-G., T. Ikegami, J.-H. Lee, T. Mori and Y. Yajima, Co-precipitation synthesis and sintering of yttrium aluminum garnet (YAG) powders : the effect of precipitant. Journal of the European Ceramic Society 20 (2000): 2395-2405.
- [14] Li, X., H. Liu, Jiyang Wang, X. Zhang and H. Cui, Preparation and properties of YAG nano-sized powder from different precipitating agent. Optical Materials 25 (2004): 407.
- [15] Hreniak, D. and W. Streck, Synthesis and optical properties of Nd³⁺ doped Y₃Al₅O₁₂ nanoceramics. Journal of Alloys and Compounds 341 (2002): 183-186.
- [16] Veith, M., S. Mathur, A. Kareiva, M. Jilavi, M. Zimmer and V. Huch, Low temperature synthesis of nanocrystalline Y₃Al₅O₁₂ (YAG) and Ce-doped Y₃Al₅O₁₂ via different sol-gel methods. Journal of Materials Chemistry 9 (1999): 3069.
- [17] Hakuta, Y., K. Seino, H. Ura, T. Adschiri, H. Takizawa and K. Arai, Production of Phosphor (YAG:Tb) Fine Particles by Hydrothermal Synthesis in Supercritical Water. Journal of Materials Chemistry 9 (1999): 2671-2673.
- [18] Hakuta, Y., T. Haganuma, K. Sue, T. Adschiri and K. Arai, Continuous production of phosphor YAG : Tb nanoparticles by hydrothermal synthesis in supercritical water. Materials Research Bulletin 38 (2003): 1257-1265.
- [19] Takamori, T. and L.D. David, Controlled Nucleation for Hydrothermal Growth of Yttrium-Aluminum Garnet Powders. American Ceramic Society Bulletin 65 (1986): 1282-1286.
- [20] Inoue, M., H. Otsu and H. Kominami, Synthesis of yttrium aluminum garnet by the glycothermal method. Journal of the American Ceramic Society 74 (1991): 1452-1454.
- [21] Li, X., H. Liu, et al., Rapid synthesis of YAG nano-sized powders by a novel method. Materials Letters 58 (2004): 2377-2380.
- [22] Zhang, X., H. Liu, W. He, J. Wang, X. Li and R.I. Boughton, Synthesis of monodisperse and spherical YAG nanopowder by a mixed solvothermal method. Journal of Alloys and Compounds 372 (2004): 300-303.

- [23] Cockayne, B., The Uses and Enigmas of the $\text{Al}_2\text{O}_3\text{-Y}_2\text{O}_3$ Phase System. Journal of the Less-Common Metals 114 (1985): 199-206.
- [24] Olds, L.E. and H.E. Otto, Phase Diagrams for Ceramicists. American Ceramics Society (1987): Fig. 311.
- [25] Toropov, N.A., I.A. Bondar, F.Y. Galakhov, X.S. Nikogosyan and N.V. Vinogradova, Phase Diagrams for Ceramists. American Ceramic Society (1987): Fig. 2344.
- [26] Carda, J., M.A. Tena, G. Monros, V. Esteve, M.M. Reventos and J.M. Amigo, A Rietveld Study of the Cation Substitution between Uvarovite and Yttrium-Aluminum Synthetic Garnets, Obtained by Sol-Gel Method. Crystal Research and Technology 29 (1994): 387-391.
- [27] Yamane, H., M. Omori and T. Hirai, Thermogravimetry and Rietveld Analysis for the High-Temperature X-ray Powder Diffraction Pattern of $\text{Y}_4\text{Al}_2\text{O}_9$. Journal of Materials Science Letters 14 (1995): 470-473.
- [28] Hess, N.J., G.D. Maupin, L.A. Chick, D.S. Sunberg, D.E. McCreedy and T.R. Armstrong, Synthesis and Crystallization of Yttrium-Aluminium Garnet and Related Compounds. Journal of Materials Science 29 (1994): 1873-1878.
- [29] Chen, P.-L. and I.-W. Chen, Reactive Cerium (IV) Oxidase Powders by the Homogeneous Precipitation Method. Journal of the American Ceramic Society 76 (1993): 1577-1583.
- [30] Ertl, G., H. Knozinger and J. Weitkamp, Preparation of Solid Catalysts. 1997: Wiley-VCH.
- [31] Muangsombut, B., Effects of metal doping and seed introduction on phase transformation of alumina prepared by precipitation method Master Thesis: Chulalongkorn University (2005).
- [32] Chiang, C.C., M.S. Tsai, C.S. Hsiao and M.H. Hona, Synthesis of YAG:Ce phosphor via different aluminum sources and precipitation processes. Journal of Alloys and Compounds 416 (2006): 265-269.
- [33] Li, X., Q. Li, J. Wang, S. Yang and H. Liu, Synthesis of Nd^{3+} doped nanocrystalline yttrium aluminum garnet (YAG) powders leading to transparent ceramic. Optical Materials 29 (2007): 528-531.
- [34] Dorre, E. and H. Hubner., Alumina, Processing, Properties, and Applications. 1984: Springer-Verlag.

- [35] Kingery, W.D, H.K. Bowen and D.R. Uhlmann, Introduction to ceramics. 1976: Wiley-VCH.
- [36] William, E., L.D. Phil and W.M.R. PhD, Ceramic Microstructures property control by processing. 1994: Mcgraw-Hill College.
- [37] Wen, L., X. Sun, Z. Xiu, S. Chen and C.-T. Tsai, Synthesis of nanocrystalline yttria powder and fabrication of transparent YAG ceramics Journal of the European Ceramic Society 24 (2004): 2681-2688.
- [38] J. Su , Q.L. Zhang, C.J. Gu, D.L. Sun, Z.B. Wang, H.L. Qiu, A.H. Wang and S.T. Yin, Preparation and characterization of $Y_3Al_5O_{12}$ (YAG) nanopowder by co-precipitation method. Materials Research Bulletin 40 (2005): 1279-1285.
- [39] Chen, Z.-H., Y. Yang, Z.-G. Hu, J.-T. Li and S.-L. Hec, Synthesis of highly sinterable YAG nanopowders by a modified co-precipitation method. Journal of Alloys and Compounds 433 (2007): 328-331.
- [40] Yen-Pei, F., S. Tsaob, and H. Chen-Ti, Preparation of $Y_3Al_5O_{12}:Cr$ powders by microwave-induced combustion process and their luminescent properties. Journal of Alloys and Compounds 395(2005): 227-230.
- [41] Li , X., Q. Li, J. Wang and S. Yang, Effect of process parameters on the synthesis of YAG nano-crystallite in supercritical solvent. Journal of Alloys and Compounds 421(2006): 298-320.
- [42] Yamaguchi, O., Takeoka, K., Hirota, K., Takano, H. and Hayashida, A., Formation of alkoxy-derived yttrium aluminium oxides. Journal of Materials Science Letters 27(1992):1261-1264.



APPENDICES

สถาบันวิทยบริการ
จุฬาลงกรณ์มหาวิทยาลัย

APPENDIX A

CALCULATION OF CONCENTRATION OF BOTH REACTANTS IN PRECIPITATION METHOD

In this study, precipitate has been produced by the reaction of ammonium aluminium sulfate (AAS) and yttrium nitrate ($Y(NO_3)_3$) with various molar ratio of Y:Al (ions solution) and ammonium hydrogencarbonate solution (AHC solution). The YAG powder was prepared with different concentration ratio of AAS to AHC.

Calculation of the amount of ammonium hydrogencarbonate (AHC), ammonium aluminum sulfate (AAS) and yttrium nitrate for precipitate preparation

Ammonium aluminum sulfate (AAS), yttrium nitrate and ammonium hydrogencarbonate (AHC) are used as reactants to prepare precipitate.

1. Ammonium aluminum sulfate ($NH_4Al(SO_4)_2 \cdot 12H_2O$) has an molecular weight of 237.18 g/mol (not included molecule of water)
2. Yttrium (III) nitrate hexahydrate ($Y(NO_3)_3 \cdot 6H_2O$) has an molecular weight of 274.92 g/mol (not included molecule of water)
3. Ammonium hydrogencarbonate (NH_4HCO_3) has an molecular weight of 79.06 g/mol.

Example : Calculation concentration of AAS solution to AHC solution equal to 0.2 : 2.0 mol/l and molar ratio of AAS solution to AHC solution is 0.05 : 0.2 , which is equal to 1:4 as mentioned before, and the molar ratio for Y : Al of 3:5 are as following :

AAS solution 0.05 mol consists of :

$$\text{AAS } 0.05 \times 237.18 = 11.859 \text{ g}$$

To get concentration 0.2 mol/l

$$\text{Distilled water} = 250 \text{ cm}^3$$

Molar ratio for Y : Al of 3:5 consists of :

Yttrium nitrate = $0.03 \times 274.92 = 8.2475 \text{ g}$

Adding to AAS solution

AHC solution 0.2 mol consists of :

AHC $0.2 \times 79.06 = 15.812 \text{ g}$

To get concentration 2.0 mol/l

Distilled water = 100 cm^3



สถาบันวิทยบริการ
จุฬาลงกรณ์มหาวิทยาลัย

APPENDIX B

CALCULATION OF THE CRYSTALLITE SIZE

Calculation of the crystallite size by Debye-Scherrer equation

The crystallite size was calculated from the half-height width of the diffraction peak of XRD pattern using the Debye-Scherrer equation.

From Scherrer equation:

$$D = \frac{K\lambda}{\beta \cos \theta} \quad (\text{B.1})$$

- where
- D = Crystallite size, Å
 - K = Crystallite-shape factor = 0.9
 - λ = X-ray wavelength, 1.5418 Å for CuK α
 - θ = Observed peak angle, degree
 - β = X-ray diffraction broadening, radian

The X-ray diffraction broadening (β) is the pure width of a powder diffraction free from all broadening due to the experimental equipment. α -Alumina is used as a standard sample to observe the instrumental broadening since its crystallite size is larger than 2000 Å. The X-ray diffraction broadening (β) can be obtained by using Warren's formula.

From Warren's formula:

$$\beta = \sqrt{B_M^2 - B_S^2} \quad (\text{B.2})$$

- Where
- B_M = The measured peak width in radians at half peak height.
 - B_S = The corresponding width of the standard material.

Example: Calculation of the crystallite size of α -alumina

$$\begin{aligned} \text{The half-height width of 012 diffraction peak} &= 0.25^\circ \text{ (from the figure B.1)} \\ &= \left(\frac{2\pi}{360}\right) \cdot (0.26) \\ &= 0.0045 \text{ radian} \end{aligned}$$

The corresponding half-height width of peak of α -alumina (from the B_s value at the 2θ of 25.88° in figure B.2) = 0.0038 radian

$$\begin{aligned} \text{The pure width, } \beta &= \sqrt{B_M^2 - B_S^2} \\ &= \sqrt{0.0045^2 - 0.0038^2} \\ &= 0.0024 \text{ radian} \end{aligned}$$

$$B = 0.0024 \text{ radian}$$

$$2\theta = 25.88^\circ$$

$$\theta = 12.94$$

$$\lambda = 1.5418 \text{ \AA}$$

$$\text{The crystallite size} = \frac{0.9 \times 1.5418}{0.0024 \cos 12.94} = 590 \text{ \AA} = 59 \text{ nm}$$

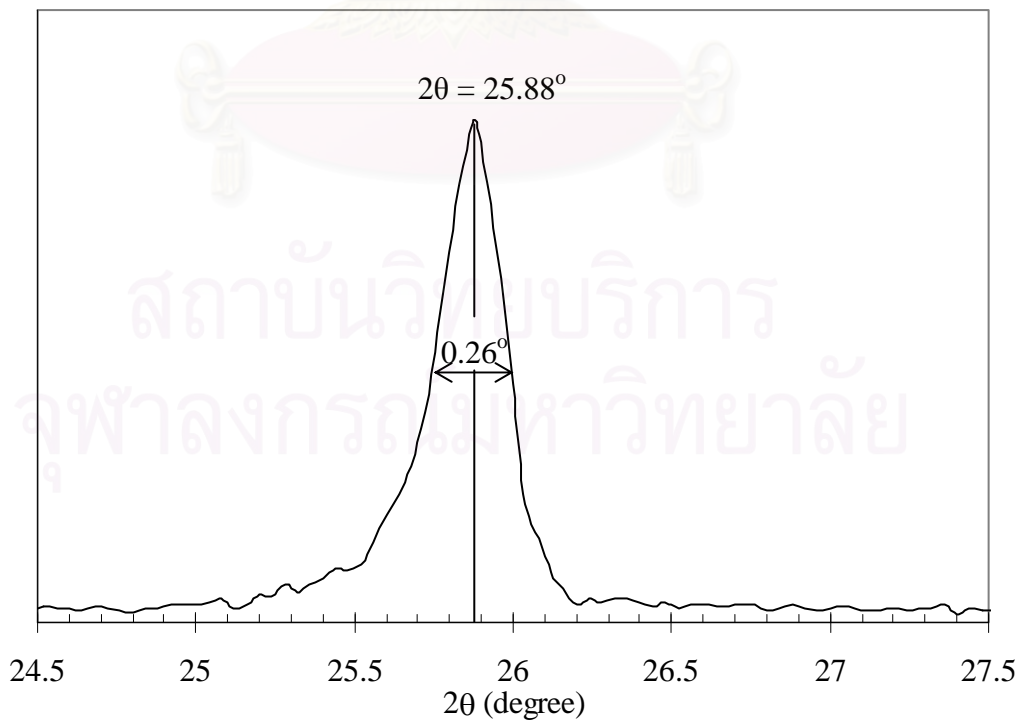


Figure B.1 The observation peak of α -alumina for calculating the crystallite size.

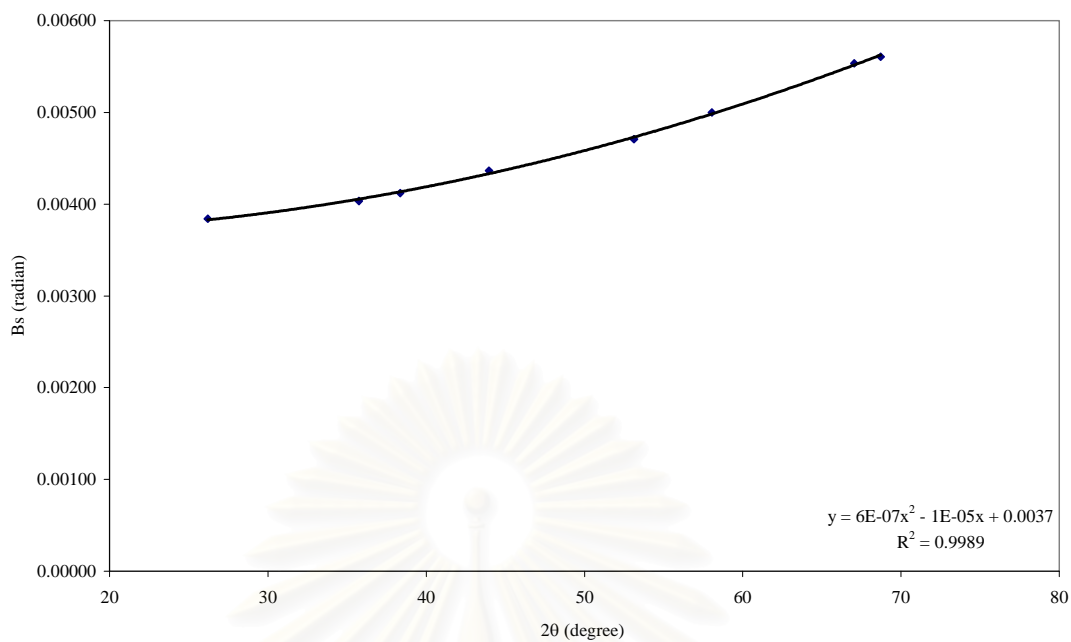


Figure B.2 The graph indicating that value of the line broadening attribute to the experimental equipment from the α -alumina standard.

สถาบันวิทยบริการ
จุฬาลงกรณ์มหาวิทยาลัย

APPENDIX C

CONDITIONS FOR BALL MILL AND DISPERSION OF POWDER

Ball mill

The particles size can be reduced a by breaking some soft agglomeration of powders by using polypropylene bottle and high purity alumina balls.

Place high purity alumina ball 362 g or half of bottle, YAG powder, and ethanol solution 100 cc into the polypropylene bottle which has volume 250 cc. Mill this bottle with rotating speed 150 rpm at desired time. After milling with ball mill, filter the solution of powder and dry in the oven at 110°C for 24 h.

Dispersion of powder

Before measuring a particle size distribution of calcined powder, all powders should to be dispersed by following steps :

1. Preparation of dispersion solution with concentration 0.2 wt% by dissolving NaHMP (Sodium Hexa Methaphosphate) 0.2 g in distilled water 99.8 g.
2. Use this solution 20 cc for 0.2 g of powder, then mix this solution with magnetic stirrer for 30 minutes.

After mixing by magnetic stirrer, pour the solution into a bottle and sealed with para-film and place it into ultrasonic apparatus for 30 minutes before measuring their particle size distribution by using Laser Particle Size Distribution Analyzer.

APPENDIX D

DENSITY

Bulk density

The bulk density of specimens was measured according to Archimedes' method. The air in open pores of specimen was removed by applying vacuum for 30 min and then water was poured onto specimens until submerged in water. Water was further forced into the opened pores by applying vacuum for 2 h. The dry weight W_d were measured and used to calculate the bulk density using equation (D.1) following ASTM standard (Designation : C830-93).

$$\text{Bulk density} = \frac{W_d}{W_{\text{sat}} - W_{\text{sus}}} \rho \quad (\text{D.1})$$

Where ρ is water density at the measurement temperature (0.996512 g/cm³ at 27°C)

Theoretical density

The theoretical density of sintered pellets was calculated from real density using the following equation ;

$$\text{Theoretical density} = \frac{W_{\text{total}}}{W_a / \rho_a + W_b / \rho_b + \dots} \quad (\text{D.2})$$

Where W_{total} is total weight of used components.
 W_a, W_b are weights of component, a and b, respectively.
 ρ_a, ρ_b are real densities of component, a and b, respectively.
 a, b,..... are used components.

In this experiment, the theoretical densities of pure YAG = 4.5 g/cm³ was used for calculation.

Relative density

The relative density of the sintered specimens was calculated from its bulk density and theoretical density using the following equation :

$$\text{Relative density} = \frac{\text{Bulk density}}{\text{Theoretical density}} \quad (\text{D.3})$$

$$\text{And \% of theoretical density} = \text{Relative density} \times 100$$



สถาบันวิทยบริการ
จุฬาลงกรณ์มหาวิทยาลัย

APPENDIX E

PARTICLE SIZE DISTRIBUTION

In section 4.3, the effect of preparation conditions on the particle size distributions of powder calcined at 1200°C for 2 h was investigated. The concerned factors included the speed of mixing, the rate of addition of ions solution into the reaction system, the concentration of both reactants and milling time. These particle size distributions were obtained by the Laser particle size distribution analyzer. The values reported in Section 4.3 are volume-basis size distributions. For those based on number of particles are shown in Table E.1-E.5 and Figure E.1-E.5, respectively.

The median diameter calculated under number-basis of the product varies in the range of 0.060-0.080 μm which are consistent with the results of TEM micrographs. The results indicate the same phenomena reported in Section 4.2 and Section 4.3. The higher the speed of mixing, the smaller the median diameter of the product appears. On the other hand, the lower the addition rate, the smaller the particles become. The median diameter increases with both the increase in the concentration of the ions solution. In addition to the prolonged milling time, the lower the median diameter appears. Nevertheless, unlike the volume-basis, the particle size distribution curves under number-basis are unimodal. This is attributed to the fact that the size distribution under volume-basis are accounted to the volume occupied by for each particle but the size distribution under number basis are accounted for the number of particles.

Table E.1 Median diameter of the calcined product prepared by using various stirring speeds, base on number-basis.

Stirring speed (rpm)	Median diameter (μm)
100	0.067
300	0.066
500	0.063

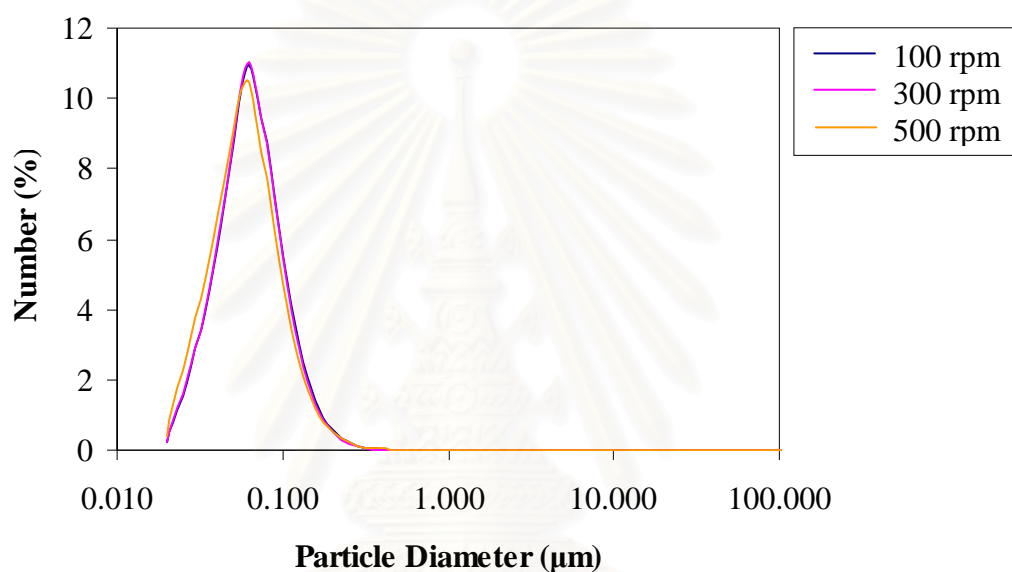


Figure E.1 The particle size distributions, base on number-basis, of the powder prepared via the standard synthesis procedure using various speed of mixing and subsequently calcined at 1200°C .

สถาบันวิทยบริการ
จุฬาลงกรณ์มหาวิทยาลัย

Table E.2 Median diameter of the calcined products prepared by using various rates of addition, base on number-basis.

Adding rate (ml/min)	Median diameter (μm)
5	0.063
10	0.066
15	0.067
pour directly	0.074

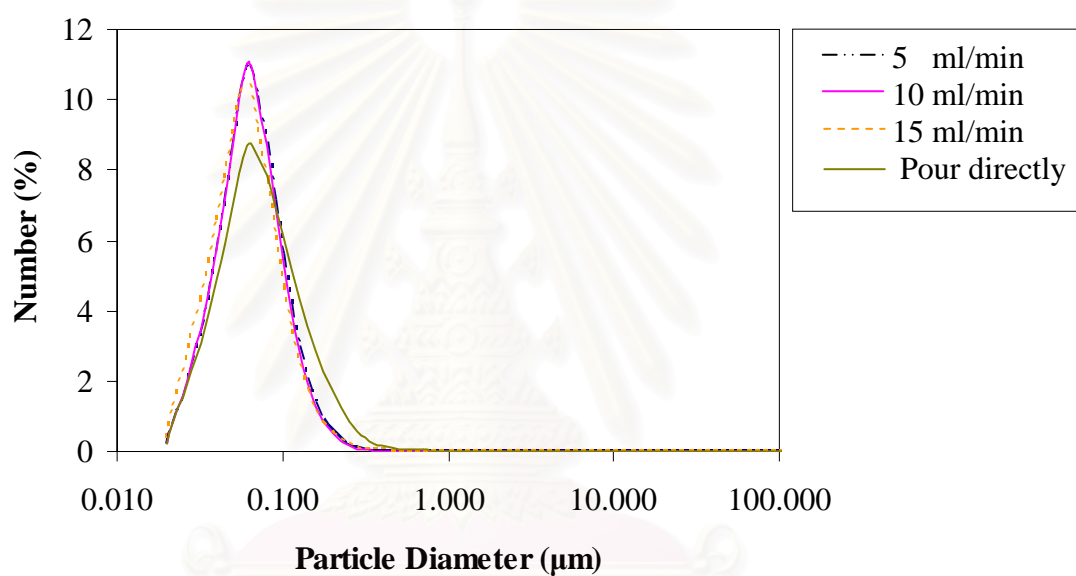


Figure E.2 The particle size distributions, base on number-basis, of the powder prepared via the standard synthesis procedure using various rate of addition and subsequently calcined at 1200°C.

Table E.3 Median diameter of calcined powder prepared via the standard synthesis procedure using various concentrations of reactants, base on number-basis.

Concentration of AHC solution	Median diameter at various concentration of ion solution (μm)		
	0.1 M	0.2 M	0.3 M
1 M	0.063	0.065	0.069
2 M	0.062	0.063	0.068

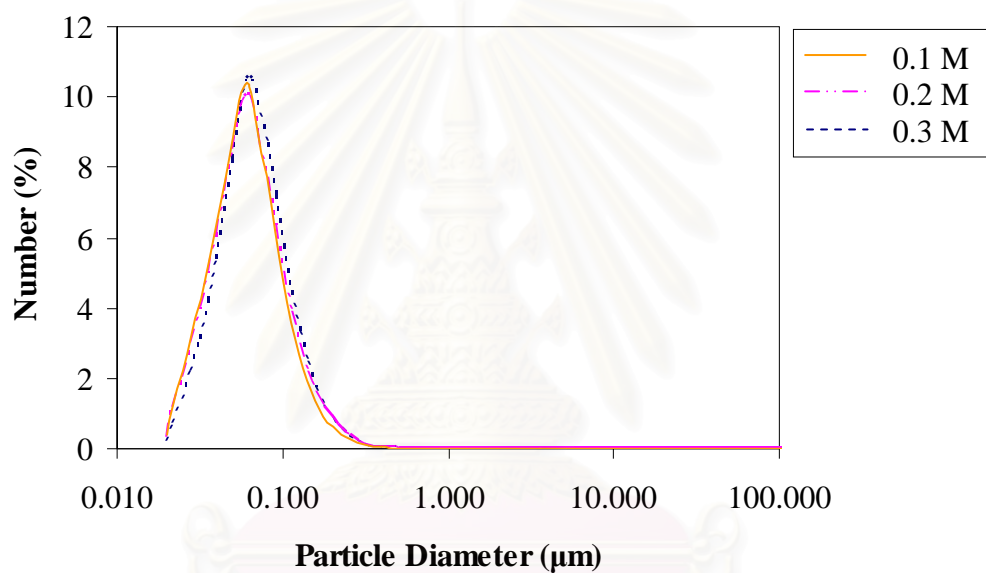


Figure E.3 The particle size distributions, base on number-basis, of the powder prepared via the standard synthesis procedure using 1 M of AHC solution and ions solution at various concentrations.

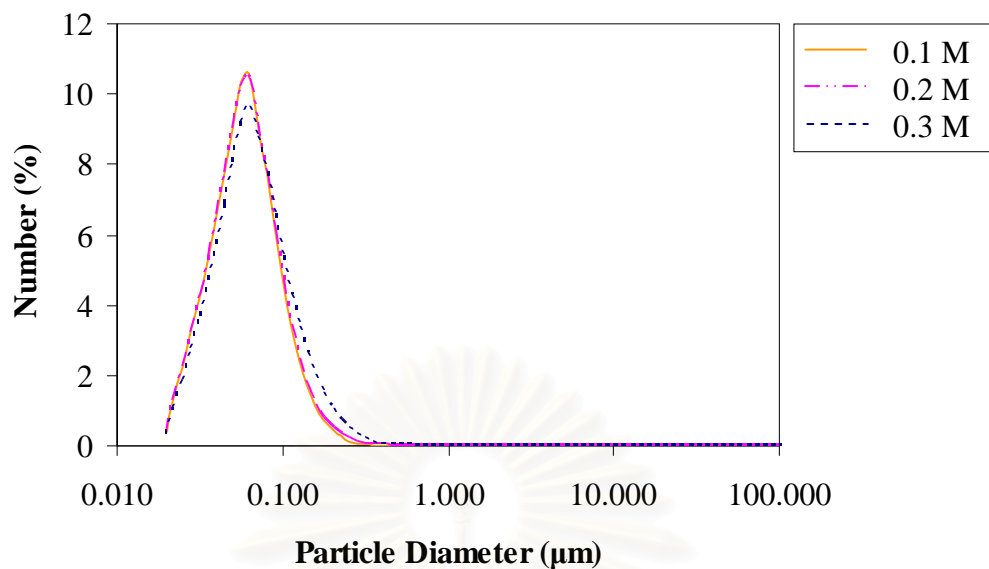


Figure E.4 The particle size distributions, base on number-basis, of the powder prepared via the standard synthesis procedure using 2 M of AHC solution and ions solution at various concentrations.

Table E.4 Median diameter of the calcined powder after ball milled for various period of time, base on number-basis.

Milling time (h)	Median diameter (μm)
24	0.072
48	0.070
72	0.065
96	0.062

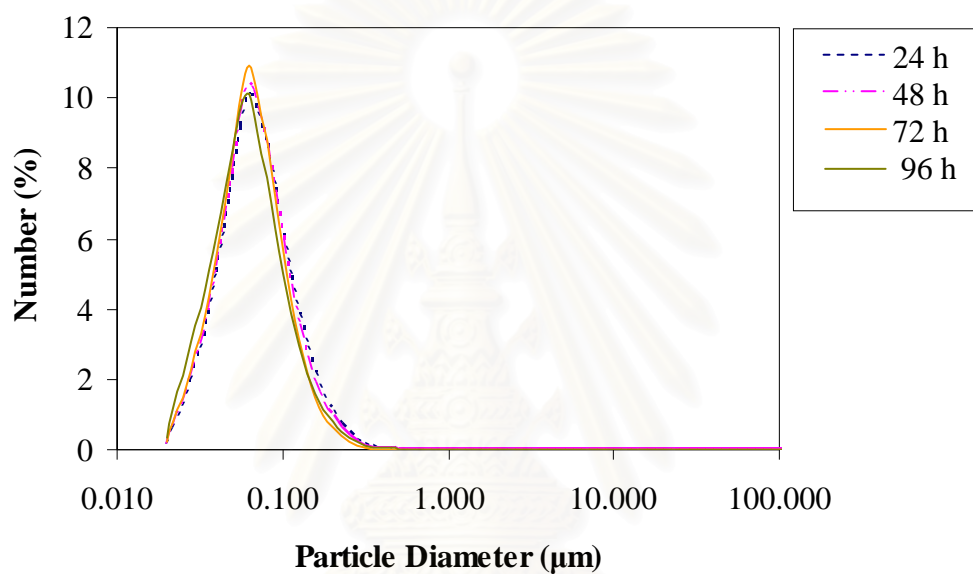


Figure E.5 Particle size distributions, base on number-basis, of the synthesized powder calcined at 1200°C and milled for various periods of time.

สถาบันวิทยบริการ
จุฬาลงกรณ์มหาวิทยาลัย

APPENDIX F**LIST OF PUBLICATIONS**

1. Pornan Wannarong, Thanakorn Wasanapiarnpong and Varong Pavarajarn. “Synthesis of nanocrystallite yttrium aluminium garnet by precipitation method”, The 17th Thailand Chemical Engineering and Applied Chemistry Conference, Thailand, October 29-30, 2007



สถาบันวิทยบริการ
จุฬาลงกรณ์มหาวิทยาลัย

การสังเคราะห์อิทเทรียมอะลูมิเนียมคาร์เนตที่มีผลึกขนาดนาโนด้วยวิธีตกตะกอน

พรพรรณ หว่านณรงค์¹, ธนากร วาสนาเพียรพงศ์² และ วรงค์ ปวรจารย์*

1) ภาควิชาวิศวกรรมเคมี คณะวิศวกรรมศาสตร์ จุฬาลงกรณ์มหาวิทยาลัย เขตพญาไท กรุงเทพฯ 10330

2) ภาควิชาวัสดุศาสตร์ คณะวิทยาศาสตร์ จุฬาลงกรณ์มหาวิทยาลัย เขตพญาไท กรุงเทพฯ 10330

1. บทนำ

อิทเทรียมอะลูมิเนียมคาร์เนต (YAG, $Y_3Al_5O_{12}$) มีโครงสร้างผลึกแบบ cubic garnet โดยที่ YAG ชนิดผลึกเดี่ยวนั้นได้ถูกนำมาใช้เป็นตัวกลางด้านเลเซอร์กันอย่างกว้างขวาง แต่เนื่องจากมีราคาแพงและยากที่จะผลิตให้มีขนาดใหญ่ ดังนั้นจึงมีการคาดการณ์ว่าเซรามิก YAG ชนิดผลึกโพลี (polycrystalline) จะถูกนำมาใช้แทนที่ เนื่องจากมีคุณสมบัติทางด้านการมองเห็น สามารถทนความร้อนได้ที่อุณหภูมิสูง แต่มีต้นทุนการในผลิตที่ต่ำ ดังนั้นเพื่อให้ได้ YAG เซรามิกที่มีความโปร่งแสง จึงมีความสำคัญที่จะต้องสังเคราะห์อนุภาค YAG ให้มีขนาดในระดับนาโนเมตรที่มีการกระจายตัวของอนุภาคในช่วงแคบและปราศจากการเกาะกลุ่มกันของอนุภาค (agglomeration)

ผง YAG สามารถสังเคราะห์ได้หลายวิธี เช่น ปฏิกริยาของแข็ง (solid-state reaction), ไฮโดรเทอร์มอล (hydrothermal synthesis), โซล เจล (sol-gel) และ การตกตะกอนร่วม (co-precipitation) โดยเมื่อทำการเปรียบเทียบในแต่ละวิธีจะพบว่า การตกตะกอนร่วมเป็นวิธีที่สามารถทำได้ง่าย สามารถผลิตสารได้ในปริมาณที่มาก มีการปนเปื้อนน้อย และไม่ต้องใช้อุณหภูมิและความดันที่สูงในระหว่างการเกิดปฏิกริยา

ในงานวิจัยครั้งนี้ได้ทำการสังเคราะห์อิทเทรียมอะลูมิเนียมคาร์เนตที่มีผลึกขนาดนาโนโดยวิธีตกตะกอน และศึกษาปัจจัยต่างๆระหว่างการสังเคราะห์ ที่มีผลต่อผงอิทเทรียมอะลูมิเนียมคาร์เนตที่สังเคราะห์ได้ เพื่อให้มีคุณสมบัติที่เหมาะสมต่อการนำไปผลิตเป็นเซรามิกที่มีความโปร่งใสต่อไป

2. อุปกรณ์และวิธีการทดลอง

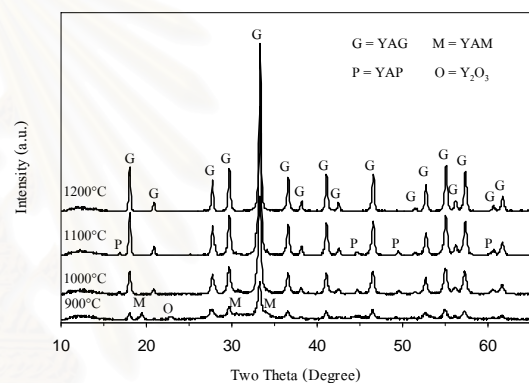
เตรียมสารละลายไอออน (Ions solution) จากแอมโมเนียมอะลูมิเนียมซัลเฟต $NH_4Al(SO_4)_2$ และ อิทเทรียมไนเตรด $Y(NO_3)_3$ โดยละลายในน้ำกลั่น ที่อัตราส่วนของอิทเทรียมต่ออะลูมิเนียมต่างๆ กัน และเตรียมสารละลายตกตะกอน (precipitant) จากแอมโมเนียมไฮดรอกไซด์ที่ละลายในน้ำกลั่น ทำการหยดสารละลายไอออนลงในสารละลายตกตะกอนด้วยอัตราคงที่ตลอดการหยด ปั่นกวนเป็นเวลา 30 นาที เพื่อให้เกิดปฏิกริยาที่สมบูรณ์ นำตะกอนที่ได้ไปล้างด้วยน้ำกลั่นและเมทานอล เพื่อล้างไอออนของไนเตรด หรือ แอมโมเนียมออก จากนั้นนำไปอบให้แห้งที่อุณหภูมิ 110 องศาเซลเซียส เป็นเวลา 24 ชั่วโมง และทำการเผาที่อุณหภูมิ 900, 1000, 1100 และ 1200 องศาเซลเซียส เป็นเวลา 2 ชั่วโมง ด้วยอัตรา 10 องศาเซลเซียสต่อนาที

ผงอิทเทรียมอะลูมิเนียมคาร์เนตที่สังเคราะห์ได้จะถูกวิเคราะห์ด้วยเทคนิคการกระเจิงรังสีเอ็กซ์ (X-ray diffraction, XRD) กล้องจุลทรรศน์อิเล็กตรอนแบบส่องกราด (Scanning electron microscopy,

SEM) การวิเคราะห์สมบัติทางความร้อน (Thermogravimetric analysis, TGA) และการวิเคราะห์ด้วยเทคนิคเอฟที-ไออาร์สเปกโทรสโกปี (Infrared spectroscopy, IR)

3. ผลการทดลองและวิจารณ์ผล

งานวิจัยนี้ได้แสดงให้เห็นว่าผงอิทเทรียมอะลูมิเนียมคาร์เนตที่มีผลึกขนาดนาโนนั้น สามารถสังเคราะห์ได้จากกระบวนการตกตะกอนร่วม

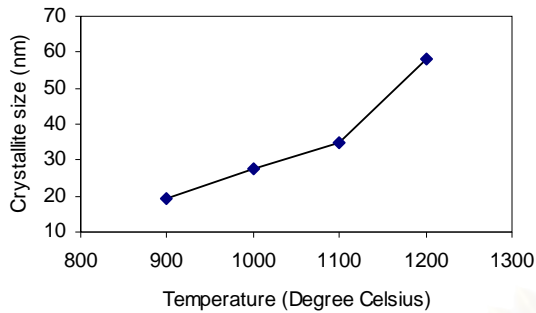


รูป 1 ผลจากการวิเคราะห์ด้วยการกระเจิงรังสีเอ็กซ์ของผงที่ได้หลังจากทำการเผาที่อุณหภูมิต่างๆกันตั้งแต่ 900, 1000, 1100 และ 1200 องศาเซลเซียส เป็นเวลา 2 ชั่วโมง ด้วยอัตรา 10 องศาเซลเซียสต่อนาที ที่อัตราส่วนระหว่างอิทเทรียมต่ออะลูมิเนียมเป็น 3:5

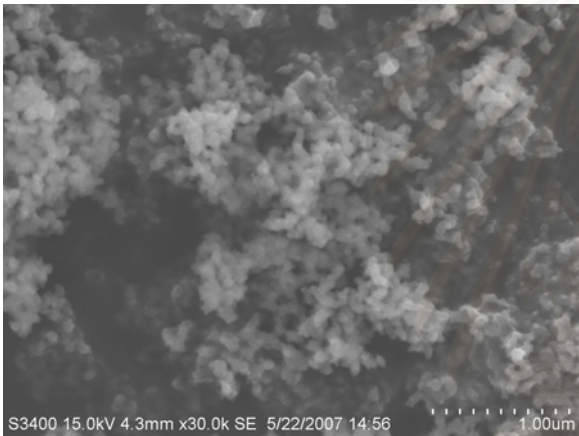
เมื่อทำการวิเคราะห์ผงของตะกอนที่สังเคราะห์ได้ก่อนนำไปเผาด้วยเทคนิค XRD จะพบว่าตะกอนที่ได้นั้นเป็นสารอสถาบัน แต่เมื่อนำตะกอนดังกล่าวไปเผาที่อุณหภูมิต่างๆ จะเห็นได้จากรูปที่ 1 ว่ากราฟจะเริ่มมียอดแหลมที่เด่นชัดที่อุณหภูมิตั้งแต่ 900 องศาเซลเซียสเป็นต้นไป แสดงว่าผลิตภัณฑ์ยังคงรูปอสถาบันอยู่จนถึง 900 องศาเซลเซียส นอกจากนั้นยังพบว่าเกิดเป็นสารประกอบของอิทเทรียมอะลูมิเนียมที่อุณหภูมิตั้งแต่ 1000 องศาเซลเซียส ซึ่งเป็นไปตามผลการวิเคราะห์ด้วยเทคนิคเอฟที-ไออาร์สเปกโทรสโกปี เนื่องจากพบว่ามียอดแหลมของกราฟที่บ่งบอกว่ามีพันธะระหว่างออกซิเจนกับโลหะอยู่ และเมื่อพิจารณากราฟจากการกระเจิงรังสีเอ็กซ์พบว่าความสูงของแต่ละยอดกราฟพิกขึ้นเมื่ออุณหภูมิในการเผาพิกขึ้น แสดงให้เห็นว่าที่อุณหภูมิสูงขึ้นอนุภาคที่ได้จะมีความเป็นผลึกมากขึ้น และขนาดของผลึกเดี่ยวจะมีขนาดที่ใหญ่ขึ้น ซึ่งสามารถคำนวณได้จากสมการของเชอร์เรอ (Scherrer equation) ดังแสดงไว้ในรูปที่ 2 ทั้งนี้เนื่องจากอนุภาคเกิดการ

* corresponding author; varong.p@eng.chula.ac.th

ผนึ่งตัว (Sintering) เข้าด้วยกันดียิ่งขึ้นเมื่ออุณหภูมิในการเผามีค่าสูงขึ้น ทำให้ได้อนุภาคมีขนาดใหญ่มากขึ้น



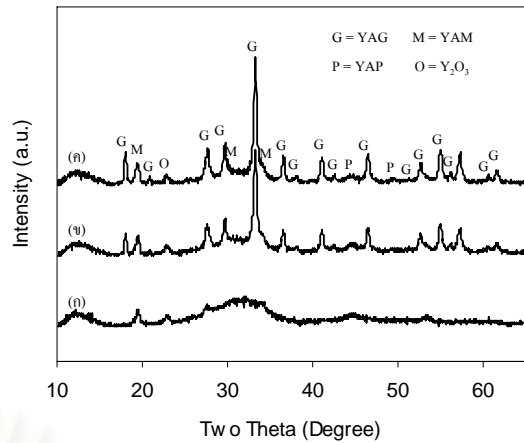
รูป 2 ขนาดของผลึกเดี่ยวของอนุภาคที่สังเคราะห์ได้ที่อุณหภูมิการเผาต่างกัน ซึ่งคำนวณได้จากสมการของเชอร์เรอ



รูป 3 ภาพถ่ายจากกล้องจุลทรรศน์อิเล็กตรอนแบบส่องกราด (Scanning electron microscopy, SEM) ของอนุภาคอิทเทรียมอะลูมิเนียมการ์เน็ต หลังจากการเผาที่อุณหภูมิ 1200 องศาเซลเซียส

จากรูปที่ 3 อนุภาคอิทเทรียมอะลูมิเนียมการ์เน็ตหลังจากการเผาที่อุณหภูมิ 1200 องศาเซลเซียส เป็นเวลา 2 ชั่วโมง พบว่าจะมีขนาดอยู่ในช่วงระหว่าง 80-120 นาโนเมตร และเมื่อทำการเปรียบเทียบกันระหว่าง ขนาดของอนุภาคที่ได้จากภาพถ่ายจากกล้องจุลทรรศน์อิเล็กตรอนแบบส่องกราดกับขนาดของผลึกเดี่ยวที่คำนวณได้จากสมการของเชอร์เรอ พบว่าขนาดอนุภาคที่ได้จากภาพถ่ายจากกล้องจุลทรรศน์อิเล็กตรอนแบบส่องกราดมีขนาดใหญ่กว่าขนาดที่ได้จากการคำนวณ ซึ่งแสดงให้เห็นว่าอนุภาคที่ทำการสังเคราะห์ได้มีลักษณะเป็นอนุภาคนิวคลีไอ นอกจากนั้นอนุภาคที่สังเคราะห์ได้พบว่ามีลักษณะของรูปร่างที่ไม่แตกต่างกัน และยังมีเกาะกัน (agglomeration) ของแต่ละอนุภาคอยู่

จากรูปที่ 4 เมื่อทำการเปลี่ยนแปลงอัตราส่วนโดยโมลระหว่างอิทเทรียมต่ออะลูมิเนียมเป็น 2:5, 3:5 และ 4:5 พบว่าเมื่อเผาที่อุณหภูมิ



รูป 4 ผลจากการวิเคราะห์ด้วยการกระเจิงรังสีเอ็กซ์ (X-ray diffraction, XRD) ของผงที่ได้หลังจากทำการเผาที่อุณหภูมิ 900 องศาเซลเซียส ที่อัตราส่วนระหว่างอิทเทรียมต่ออะลูมิเนียมเป็น (ก)2:5, (ข) 3:5 และ (ค)4:5

เท่ากับที่ 900 องศาเซลเซียส ผลึกเดี่ยวที่ได้จากการตั้งต้นที่มีอัตราส่วนของอิทเทรียมต่ออะลูมิเนียมเป็น 2:5 จะมีค่าความเป็นผลึกที่ต่ำ แต่เมื่อทำการเพิ่มอัตราส่วนของอิทเทรียมต่ออะลูมิเนียมมากขึ้น อนุภาคที่ได้มีความเป็นผลึกที่เด่นชัดมากยิ่งขึ้น โดยผลึกจะประกอบไปด้วยรูปของอิทเทรียมอะลูมิเนียมการ์เน็ต นอกจากนี้ก็ยังพบว่ามีผลึกในรูปของ YAM และ YAP ปะปนอยู่ด้วย และจะหายไปเมื่อเพิ่มอุณหภูมิในการเผามากขึ้น

4. สรุปผลการทดลอง

จากการทดลองพบว่าอิทเทรียมอะลูมิเนียมการ์เน็ตขนาดนาโนชนิดหลายผลึกสามารถทำการสังเคราะห์ได้ด้วยวิธีคอกเคอชั่นร่วม และพบว่าจะเป็นสารประกอบของ อิทเทรียมอะลูมิเนียมที่อุณหภูมิตั้งแต่ 1000 องศาเซลเซียส โดยที่อุณหภูมิในการเผาที่สูงขึ้นจะทำให้อนุภาคที่ได้มีขนาดใหญ่ขึ้น ขนาดของอนุภาคที่ได้มีขนาดอยู่ในช่วง 80-120 นาโนเมตร และเมื่ออัตราส่วนของอิทเทรียมต่ออะลูมิเนียมมากขึ้นจะเกิดเป็นผลึกรูปอิทเทรียมอะลูมิเนียมการ์เน็ตได้ที่อุณหภูมิจากการเผาที่ต่ำกว่าที่ใช้อัตราส่วนของอิทเทรียมต่ออะลูมิเนียมน้อยกว่า

5. เอกสารอ้างอิง

Li, J.-G., T. Ikegami, J.-H. Lee, T. Mori, and Y. Yajima, Journal of the European Ceramic Society 2000. 20: p. 2395-2405.
 Li, X., H. Liu, JiyangWang, X. Zhang, and H. Cui, Optical Materials, 2004. 25: p. 407.
 Chiang, C.C., M.S. Tsai, C.S. Hsiao, and M.H. Hona, Journal of Alloys and Compounds, 2006. 416: p. 265-269.

VITAE

Miss Pornpan Wannarong was born in Bangkok, Thailand, on December 3, 1984. She received bachelor's degree in Chemical Engineering from the department of Chemical Engineering, Faculty of Engineering, Chulalongkorn University, Bangkok Thailand on April, 2006.



สถาบันวิทยบริการ
จุฬาลงกรณ์มหาวิทยาลัย